THE CHARGE STATE OF THE IONS PRODUCED BY A SADDLE FIELD ION SOURCE

by

Essam Ahmed Mahmoud

(B.Sc., M.Sc.)

A thesis submitted to the University of Aston in Birmingham for the degree of Doctor of Philosophy

Department of Physics

January 1982

"THE CHARGE STATE OF THE IONS PRODUCED BY A SADDLE FIELD ION SOURCE"

Essam Ahmed Mahmoud

Doctor of Philosophy

1982

SUMMARY

The work described in this thesis is concerned with an analysis of the charge state and energy of the ions produced by a saddle field ion source and its application to the measurement of the sputtering yield.

A review of the literature concerned with the production of ions is given together with a discussion of the fundamental processes and parameters involved.

A magnetic analyser has been developed to measure the charge state of the ions produced by a water cooled source for hydrogen, helium, neon, nitrogen, oxygen and argon. The highest charge state observed in any significant proportion was the argon Ar^{3+} ion and the ratio of Ar^{2+} to Ar^{+} was found to increase from 0.05 to 0.16 as the pressure increases from 4 to 14×10^{-5} mbar.

The energy of the ions has been inferred from the charge spectra and directly measured using a retarding field analyser. It has been found that the energy of the ions is directly proportional to their charge state and thus all the ions must be formed in the same region in the source. This suggests that the higher charge states are produced by a single electron impact process, which is supported by the fact that the proportions of the observed quantities of Ar^{3+}, Ar^{2+} and Ar^{+} and the respective ionisation cross-sections for a single impact process are in reasonable agreement.

The analyser has been modified to measure the sputtering yield of gold for the argon ions, Ar^{+} and Ar^{2+} and the yield was found to increase from 4 to 11 atoms per ion as the ion energy increases from 3 to 13.5 keV. However it has been shown that for ions of the same energy, the yield is independent of the charge state of the ions, which is in agreement with the momentum transfer theory for the sputtering process.

KEY WORDS: Ion source, ionisation, charge state, analyser, sputtering.

ACKNOWLEDGMENTS

I would like to thank Dr. R.K. Fitch for supervising and directing this work, for his continuous guidance and help throughout the period of this work.

My thanks are also due to Professor S.E. Hunt, Head of the Department of Physics, for providing the facilities in his Department, to Professor T. Mulvey for helpful advice and to Dr. J.A. Archer-Hall for his help with the design of the electro-magnet.

I am grateful to the technical staff of the Physics Department for their help and in particular to Mr. A McKenzie, in the Vacuum Physics laboratory.

Finally, I would like to thank the Ministry of Education of Iraq for providing financial support during this work.

CONTENTS

	Page
SUMMARY	i
ACKNOWLEDGMENTS	ii
CONTENTS	iii
LIST OF TABLES	vi
LIST OF FIGURES	vii
LIST OF SYMBOLS	xi
CHAPTER 1 PRODUCTION OF MULTICHARGED IONS	
1.1 Introduction	1
1.2 Fundamental parameters and processes	3
1.2.1 Ionisation potentials	3
1.2.2 Ionisation cross-sections by electron collisions	4
1.2.3 Fundamental processes	9
1.3 Multiple charged ion sources (MCIS)	15
1.3.1 The Duoplasmatron	16
1.3.2 The Duopigatron	17
1.3.3 Penning Ionisation Gauge discharge	18
1.3.4 Magnetron ion source	22
1.3.5 Radio frequency ion source	22
CHAPTER 2 SADDLE FIELD ION SOURCES	
2.1 Introduction	24
2.2 Design and properties of the spherical source	27
2.3 Application of saddle field ion sources	29

Page

CHAPTER 3 DESCRIPTION OF THE ION SOURCE, VACUUM SYSTEM, MONITORING FACILITIES AND SOURCE CHARACTERISTICS

3.1 The ion source 33

3.2 Performance of the water cooled source 34

3.3 Vacuum system and experimental procedure 36

3.4 Electrical circuit and beam monitoring facilities 38

3.5 Characteristics of the ion source 42

CHAPTER 4 ANALYSIS OF THE IONIC CHARGE STATE

4.1 Introduction 47

4.2 Description of the analyser 48

4.2.1 The analyser tube 48

4.2.2 Einzel lens 51

4.2.3 Electro-magnet 54

4.2.4 Recording of the spectra 59

4.3 Calibration of the spectra 59

4.4 Ion spectra for various gases 64

4.5 Analysis for the spectra for argon 78

CHAPTER 5 MEASUREMENT OF THE ENERGY FOR ARGON

5.1 Introduction 86

5.2 Ion energy measurement 86

5.2.1 Indirect method 86

5.2.2 Direct method 87

5.3 Discussion 94

Page

CHAPTER 6 MEASUREMENT OF THE SPUTTERING YIELD OF GOLD FOR Ar^+ AND Ar^{2+} IONS

6.1 Introduction 96

6.2 Measurement of the yield 98

6.2.1 Method 98

6.2.2 Calibration of the ion beam 99

6.2.3 Production of the films and measurement of their thickness 102

6.3 Results and discussion 103

CHAPTER 7 CONCLUSIONS, DISCUSSION AND SUGGESTIONS FOR FURTHER WORK 109

REFERENCES 112

PUBLICATIONS 126

LIST OF TABLES

Table	Title	Page
1.1	The values of $\sigma_{(n)}$ (cm^2) for E = 2 keV for Kr^{n+} and Xe^{n+}	7
1.2	Ionisation energies in eV for different charge states of neon, krypton and xenon	10
1.3	Electron energies E_e in eV and ionisation cross-sections in πa_o^2 units at the respective maximum cross-section for neon	12
1.4	Typical discharge parameters for multiply charged ion production	21
3.1	Variation of plate current with pressure for different materials, I_A = 2mA	41
4.1	A selection of the values of P_{21} and P_{31} when the chamber pressure is constant	80
4.2	A selection of the values of P_{21} and P_{31} when the anode voltage is constant	83
5.1	Values of the ratio of energy for different charge states	87
6.1(a)	Values of the measured parameters and calculated yield of gold for Ar^+ ions in the energy range 3.0 to 6.75 keV	105
6.1(b)	Values of the measured parameters and calculated yield of gold for Ar^{2+} ions in the energy range 6.0 to 13.5 keV	106

LIST OF FIGURES

Figure No.	Title	Page No.
1.1	Total ionisation cross-sections for argon and zenon	6
1.2	Partial cross-sections for the production of ions with charge 1 up to 7 for electron incident on argon	7
1.3	A conceptual Auger cascade leading to Xe^{20+} after ejection of K-shell electron	14
1.4	Schematic diagram of a duoplasmatron	17
1.5	Schematic diagram of a duopigatron	18
1.6	Schematic diagram of the PIG-type ion source	20
1.7	Particle current yield for charge state z relative to yield z = 1 obtained with typical gas discharge ion sources for Xenon	22
2.1	Diagram showing (a) stable and (b) unstable electron trajectories	25
2.2	Ion beam escaping through an aperture in the cathode cylinder	26
2.3	Schematic diagram of the spherical source - B11 fine beam source	28
2.4	Potential distribution in the spherical source	28
2.5	Ion energy spectrum for the spherical source for argon	29
3.1	Schematic diagram of the water jacket	34
3.2	Schematic diagram of the vacuum system	35
3.3	Calibration of ionisation gauge against Penning gauge using nitrogen	37

Figure No.	Title	Page No.
3.4	Schematic diagram of the ion source and electrical circuitry	39
3.5	Schematic diagram of the Faraday cup	42
3.6(a)	Variation of anode voltage, V_A, with chamber pressure, P_c, using argon	44
3.6(b)	Variation of ion beam current, I_B, with chamber pressure, P_c, using argon	45
4.1	Schematic diagram of the experimental arrangement showing the ion source, Einzel lens, magnetic analyser and ion detector	47
4.2	Photograph of the analyser tube and demounted flange supporting the Faraday cup	49
4.3	Comparison of pressures in the analyser tube and in the main experimental chamber	50
4.4	The Einzel lens, (a) PF_1 and PF_2 are the principal foci, PP_1 and PP_2 are the principal planes, f_1, f_2 are the focal lengths, and F_1, F_2 are the mid-focal lengths. (b) Potential field	51
4.5	Focal characteristics of an Einzel lens	53
4.6	Calibration of the electro-magnet	57
4.7	Spectra for argon (a) without the slit and (b) with the slit	58
4.8	Relationship between i_m and B^2	61
4.9	A typical spectrum for argon	62
4.10	$m/_{ze}$ vs. B^2 for various gases at different voltages	63
4.11	Argon spectra with the Einzel lens voltage varying from 0.8 to 4.5 kV	65

Figure No.	Title	Page No.
4.12	The variation of i_F with V_i using argon with a 1.5mm diameter aperture in the Faraday cup	66
4.13(a)	Argon spectra at V_A = 6.0 kV	67
4.13(b)	Argon spectra at $P_c = 7.9 \times 10^{-5}$ mbar	68
4.13(c)	Argon spectra at I_A = 2.0 mA	69
4.14(a)	Nitrogen spectra at V_A = 6.0 kV	71
4.14(b)	Nitrogen spectra at $P_c = 2.0 \times 10^{-5}$ mbar	72
4.14(c)	Nitrogen spectra at I_A = 2.0 mA	73
4.15(a)	Hydrogen spectra at $P_c = 10^{-5}$ mbar	74
4.15(b)	Helium spectra at $P_c = 5 \times 10^{-6}$ mbar	75
4.15(c)	Neon spectra at $P_c = 8 \times 10^{-6}$ mbar	76
4.15(d)	Oxygen spectra at $P_c = 4 \times 10^{-6}$ mbar	77
4.16	Variation of P_{21} and P_{31} as a function of chamber pressure	85
5.1	A schematic diagram of the retarding field energy analyser	88
5.2	Ion current against the retarding voltage for (a) Ar^+ and (b) Ar^{2+} for V_A = 5.3 kV	90
5.3	Ion current against the retarding voltage for (a) Ar^+ and (b) Ar^{2+} for V_A = 8.0 kV	91
5.4	Ion energy spectra for (a) Ar^+ and (b) Ar^{2+} for V_A = 5.3 kV	92
5.5	Ion energy spectrum for (a) Ar^+ and (b) Ar^{2+} for V_A = 8.0 kV	93
6.1	Variation of the ion beam current for Ar^+ with area for different anode voltages	100

Figure No.	Title	Page No.
6.2	Variation of the ion beam current for Ar^{2+} with area for different anode voltages	101
6.3	Illustration of the formation of the interference pattern	103
6.4	The sputtering yield for the argon ions Ar^{+} and Ar^{2+} as a function of ion energy	107

LIST OF SYMBOLS

Symbol	Meaning
eU	Ionisation potential (IP)
z,n	Charge state
σ	Ionisation cross-section (ICS)
$(I_i)_T$	Total ion current
I_e	Electron beam density
n_o	Neutral density
σ_T	Total ionisation cross-section (TICS)
E_e	Electron energy
E_m	Optimum energy
E_{th}	Threshold energy
$\sigma_{(n)}$	Partial ionisation cross-section (PICS)
f_1,f_2	Parameters (as in page 11)
K	Number of electrons (as in page 14)
$\bar{r}$	Mean radius of the outer shells of the atom
v	Velocity of the ejected K electron
h	Planck's constant
K	Cathode (as in page 17)
A	Anode (as in page 17)
MCIS	Multiple charged ion source
PIG	Penning Ionisation Gauge
A.E.M.	Auger electron microscopy

E.S.C.A.	Electron Spectroscopy of Chemical Analysis
S_E	Effective speed of the diffusion pump
P_s	Source pressure
P_c	Chamber pressure
C	Conductance
R	Ratio of the source pressure and chamber pressure
P_e	Equilibrium pressure
A	Area of the two exit apertures(as in page 38)
M	Molecular weight (as in page 38)
V	Volume of the experimental chamber (as in page 38)
V_A	Anode voltage
I_A	Discharge current
I_B	Ion beam current
V_i	Voltage on the inner electrode of the Einzel lens
V_o	Voltage on the outer electrodes of the Einzel lens
R_i	Radius of intermediate electrode of the Einzel lens
R_o	Radius of outer electrodes of the Einzel lens
S	Spacing between the tubes Einzel lens
L_i	Intermediate tube length of the Einzel lens
f	Focal length of an Einzel lens
C_f	Spherical aberration
F	Force on the electron due to a magnetic field
B	Magnetic field
i_F	Faraday cup current

I_m	Monitor current
i_m	Electro-magnet current
v	Velocity of the electron
e	Electron charge
T	Tesla
r	Radius of curvature of the particles
m	Mass of the particle (as in page 59)
P_{n1}	Percentage of the higher charge state, n is the charge state in terms of the single charged ions
K	Constant (as in page 87)
M_1, M_2	Atomic masses (as in page 97)
T_m	Energy transfer
d	Density
S	Sputtering yield
A	Sputtered area (as in page 103)
t	Film thickness
N_o	Avogadro's number
T	Sputtering time (as in page 103)
G_R	Retarding grid
G_s	Shield grid

CHAPTER 1

PRODUCTION OF MULTICHARGED IONS

1.1 Introduction

In recent years there has been considerable interest in this Department, and Ion Tech Ltd., and at the National Physical Laboratory, concerning the use of saddle field ion sources, in which long electron paths can be obtained without the use of a magnetic field or thermionic source of electrons. This can be achieved using a radial electrostatic field formed between two anodes enclosed by a cathode cylinder, such that the electrons can travel in long oscillatory paths between the anodes and thus increase the probability of ionisation. This operating principle arose from the idea of McIlraith (1) for a charged particle oscillator. Two forms of this source are now available, one employing cylindrical and the other spherical geometry. Both sources operate at low pressures without a magnetic field and they do not require any extraction electrodes because the ions are self-extracted.

The cylindrical source was first described by Fitch et al (2 to 5) which produces a wide ion beam with a fairly broad energy spread (6). The spherical source was devised by Franks (7) and the characteristics of the source were published by Franks and Ghander (8), and it produces a very fine ion beam of a narrower energy spread (6) than the cylindrical source.

Furthermore, a considerable amount of research work has been undertaken on these sources concerned with important information such as the source characteristics, beam intensities, operating modes, ion energy, source efficiency and beam composition. However, criticism

can be made of many of the previous measurements because of the lack of information regarding the charge state of the ions produced by these sources. Only in the case of the cylindrical source has this been very briefly studied by Ghander (9), and even here there is a complete lack of information as to how the multicharged ions are formed and precisely how they vary for different gases as a function of pressure.

These implications are extremely important. For example, in the estimation of the neutral current it is necessary to know the numbers of ions rather than the total charge collected by the Faraday cup. Similarly when this source is being used for measurement of the sputtering yield it is again necessary to know the total number of bombarding ions.

It is thus essential that, if further progress is to be made with these sources, a quantitative study of the beam composition is required in terms of the charge state of the ions. This has been the main object of the work described in this thesis in which the charge state has been determined for various gases. In addition the system which has been developed, has been modified to measure the energy of the ions and also to study the influence of the ionic charge state on the sputtering yield.

Although it is clear that it is important to know the charge state of the ions produced by the saddle field ion sources, it is obviously pointless starting an extensive research programme with this aim in view if there is not reasonable evidence that one might expect there to be a significant fraction of higher charge states. Thus it is essential to consider in general terms what parameters are most favourable for the production of multicharged ions, in relation to other existing sources to try to predict whether these conditions are met by the saddle-field ion sources.

In order to optimise the design and operation of an ion source it is necessary to have an understanding of the factors which determine the likelihood of the various collisional processes which in turn determine the effective yield of ions of the required species. Thus in this Chapter a brief account will be given of the mechanism of the production of multicharged ions, making references to particular sources.

1.2 Fundamental parameters and processes

Several parameters can be identified that have an effect on the multiply charged ions:

1.2.1 Ionization potentials

An atom is composed of a central nucleus of positive charge (+ Ze), surrounded by a cloud of electrons, the whole charge of which is -Ze. These electrons are grouped in consecutive shells, referred to as the K-shell (2 electrons), L-shell (8 electrons), M-shell (16 electrons), N-shell (32 electrons) and so on.

Each shell is divided into sub-shells (s, p, d, f .....). For example, an Argon atom, in its ground state, can be represented by the symbols,

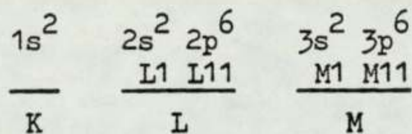

The M_{11} sub-shell is full, but the M-shell is not complete. An electron belonging to an external shell is only weakly bound to the positive nucleus, owing to the screening effect of the internal shells, and low energy is sufficient to eject it to the continuum and to transform it into a "free electron". For such an electron the corresponding ionization potential (IP) is of the order of a few eV; IP's are higher for bound electrons belonging to the internal shells,

and increase progressively from external shells to the K-shell; for heavy atoms, energies of tens or hundreds of keV are necessary to ionize a K-shell electron. In a similar shell, IP's of the different electrons are close together; from a shell to the other (the external shell being empty), discontinuities appear in the IP scale.

Determination of the ionization potential has been the object of a great number of theoretical studies, whose relative complexity increases with the atomic charge number. Different approximate expressions are now available in specialized papers, e.g. Carlson et al (10). In parallel to the development of theoretical methods, a great number of IP values have been measured in more sophisticated experiments. Unfortunately, as far as highly multicharged ions are concerned ($n > 10$), the interest of these experiments is limited, for several reasons:

(a) IP's are seldom accessible in electron collision experiments, owing to the rapid decrease of the ion current, I^{n+}, to be measured when n increases.

(b) Ionization thresholds are often very difficult to obtain, because of the presence in the collision chamber of excited (or metastable) atoms and ions which are ionized at energies less than the threshold (11).

(c) The energy domain around the threshold is not of major interest, because ionization cross-sections have negligible values; electrons with energies 2 to 10 times the IP have to be used in ion sources, in order to obtain high values of the ionization cross-section (ICS).

1.2.2 <u>Ionization cross-sections by electron collisions</u>

(a) <u>Total cross-section</u>

In a typical experiment, an electron beam crosses a collision

chamber in which a neutral gas (or vapour) is injected and the total ion current $(I_i)_T$ is collected.

$$(I_i)_T = I_e \, L \, n_o \, \sigma_T$$

where, I_e = electron beam density

L = interaction length

n_o = neutral density

σ_T = total ionization cross-section

It seems relatively easy to measure σ_T, but experimenters have to know precisely many factors which might cause systematic errors in an absolute measurement. These factors are checked in a paper by Okuno et al (12) and very precise values of σ_T are given for rare gases and for H_2, D_2, O_2, N_2, Mg, for electron energies $0 < E < 2$ keV. Experimental results obtained may be found in a survey paper by Kieffer and Dunn (13). Curves giving the variation of σ_T as a function of electron energy, E_e, have always the same shape as shown in figures 1.1 (a) and (b) (12, 11).

These curves show a rapid increase above the threshold, a maximum located at an optimum energy $E_m \simeq 2\text{-}3 \; E_{th.}$, and then a slow decrease following the approximately Law $\sigma_T \sim E^{-1}$. The maximum values of σ_T are between 0.8 and $2\text{-}3 \times 10^{-16}$ cm^2, depending on the element.

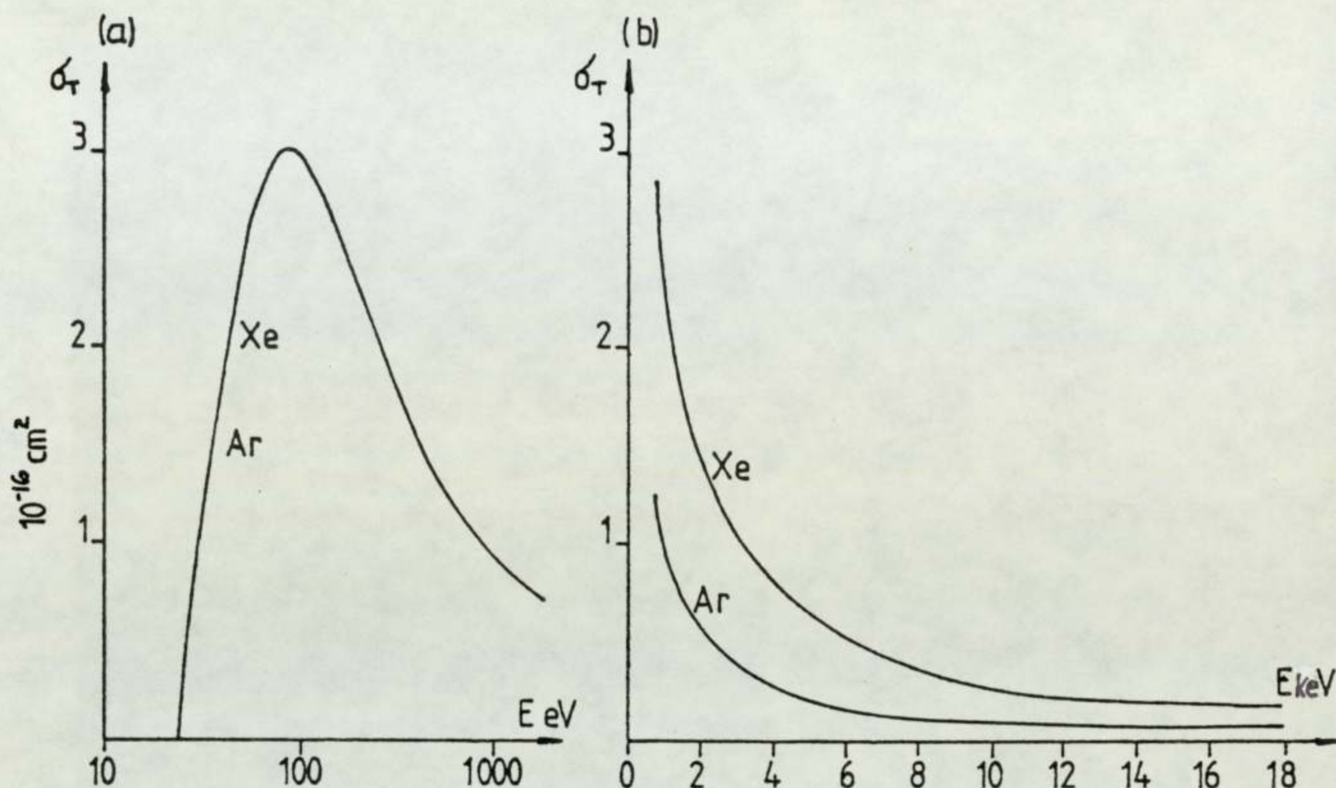

Figure 1.1 Total ionization cross-sections for argon and zenon

(b) Partial ionization cross-section (PICS) for single collision:

Precise measurements of PICS are more difficult than those of σ_T, for the different kinds of ions have to be extracted from the collision chamber, accelerated in an electrostatic system, analysed in a magnetic spectrometer, finally collected and their corresponding current measured by an appropriate technique.

When the partial ionization cross-section for monocharged ions are accurately known it is then sufficient to determine the relative proportion of other ions, by measurement of the ratios I^{2+}/I^{+} ......, I^{n+}/I^{+}.

A great deal of data for relative values of ionization cross-section will be found in papers published by specialized Laboratories located in Amsterdam (14), Orsay (15), Tokyo (16) and Pittsburgh (17).

Figure 1.2 shows, as an example (28) experimental curves giving partial ionization cross-section $\sigma_{(n)}$ for Argon ions in the domain $1 < n < 8$ and electron energies $0.5 < E_e < 4$ keV. The maximum value of $\sigma_{(n)}$ decreases rapidly when n increases.

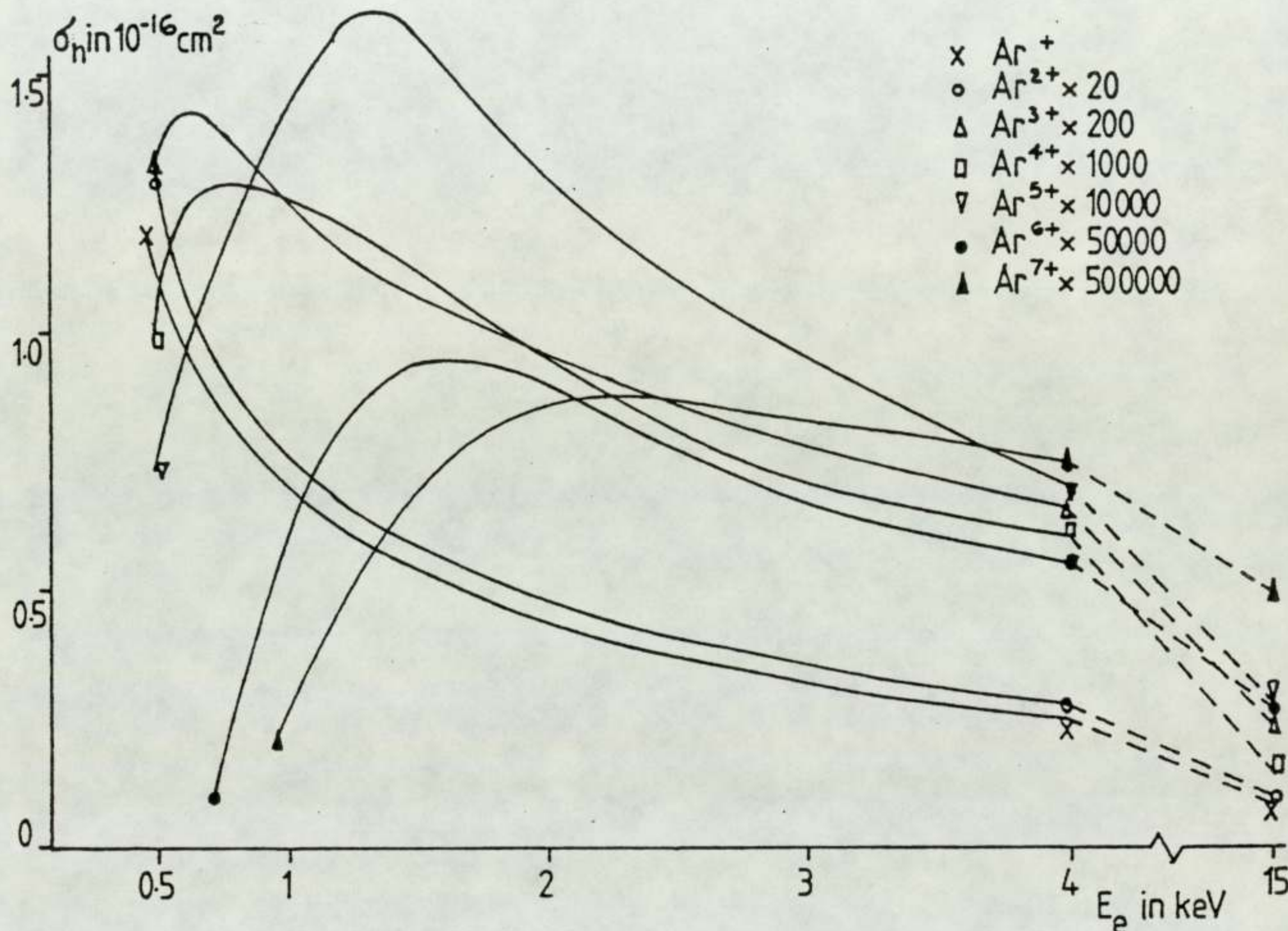

Figure 1.2 Partial cross sections for the production of ions with charge 1 + up to 7 + for electrons incident on argon

Table 1.1 gives as an example of some values of $\sigma_{(n)}$ (cm^2) for E = 2 keV for Kr^{n+} and Xe^{n+} (14).

Table 1.1

	n = 1	2	3	4	5	6
Kr	4.3×10^{-17}	5.8×10^{-18}	4.5×10^{-18}	1.3×10^{-18}	4.5×10^{-18}	1.7×10^{-19}
Xe	3.68×10^{-17}	13.6×10^{-18}	8.8×10^{-18}	4.4×10^{-18}	14.7×10^{-19}	7.3×10^{-19}

For comparison, the total ionization cross-sections, σ_T, at the same energy are σ_T (Kr) $\simeq 7.7 \times 10^{-17}$ cm^2 and σ_T (Xe) $\simeq 12 \times 10^{-17}$ cm^2.

(c) Ionization cross-section for successive collision

Suppose that we are able to maintain for a long time a cloud of ions in an electromagnetic trap, bombarded continuously by an electron beam of relatively low energy (few 100 eV).

Each ion suffers several successive ionizing collisions, each of them ejecting one electron, then

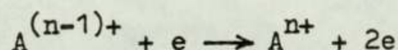

$$A^{(n-1)+} + e \longrightarrow A^{n+} + 2e$$

The IP of an ion of charge (n-1)+ is relatively low, compared to the IP corresponding to the single collision, represented by

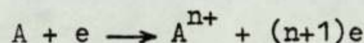

$$A + e \longrightarrow A^{n+} + (n+1)e$$

Despite a weaker electron energy in the source, very high charge states may be obtained: all electrons having a binding energy less than E_e can be ejected by step-wise ionization.

Experiments in sources using an ion trap performed by Redhead et al (18, 19) have shown the possibility to produce ions Xe^{10+}, Cs^{10+}, Ba^{10+} with an electron beam of 250 eV energy. It is difficult in this type of source to measure quantitative ionization cross-sections by successive impact because of a large number of charge discrimination mechanisms in the extraction system and of ionization of metastable atom and excited ions (17). Therefore, relative current ratios $I^{(n+)}/I^{+}$ are measured and one deduces from these experiments that the cross-sections for successive ionizations have values of the order of 10^{-16} cm^2 for $n < 2$ and decrease only slowly as n increases, e.g. value of $\sigma = 10^{-18}$ cm^2 for $N^{5+} \longrightarrow N^{6+}$, 1000 times greater than the single collision ionization cross-section (19).

(d) Theoretical predictions concerning ICS

Experiments in which values of ionization cross-section are measured cannot be used for highly charged ions. For this reason, a great deal of theoretical work has been devoted to the computation of cross-section (20, 21).

For successive collisions, an approximate formula of Beth (22) allows the calculation of $\sigma_{(n \rightarrow n+1)}$

$$\sigma_{n \rightarrow n+1} = \frac{1.6 \times 10^{-14}}{eU_{n \rightarrow n+1} \cdot E_e} \cdot \ln \frac{E_e}{eU_{n \rightarrow n+1}}$$

The above formula gives values which are about ten times lower than the experimental values. This deviation may be easily explained. For an electron energy, E_e, all electrons of atomic shells such as

$$eU_{n-j \rightarrow n} < E_e \quad \text{and for} \quad j > 1$$

may be ejected in the collision, and the total ionization cross-section is a result of a summation on all partial ionization cross-sections.

In the case of single collision cross-sections for electron energy $E_e \gg eU_n$, ejection of two or more electrons by the impinging electrons may occur by two different processes:

(i) direct ejection of external electrons, and

(ii) ejection of one electron from an internal shell, followed by a re-arrangement of all shells and ejection of a number of supplementary electrons. Variation of $\sigma_{(n)}$ as a function of E_e are different in both cases.

1.2.3 Fundamental processes

A multiple charged ion in charge state n can be generated by

electron impact processes of the following type:

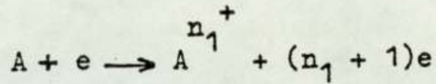

$$A + e \longrightarrow A^{n_1^+} + (n_1 + 1)e$$

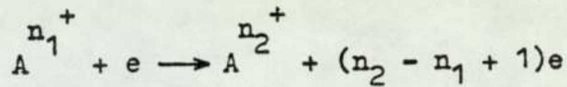

$$A^{n_1^+} + e \longrightarrow A^{n_2^+} + (n_2 - n_1 + 1)e$$

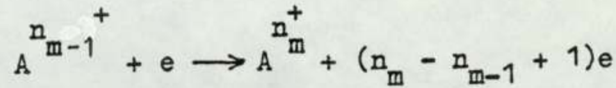

$$A^{n_{m-1}^+} + e \longrightarrow A^{n_m^+} + (n_m - n_{m-1} + 1)e$$

Where $o < n_1 < n_2 < \cdots < n_{m-1} < n_m$ and m denotes the number of ionizing electron-ion collisions.

As stated earlier there are two fundamental processes for multiple-charged ion production, one is the successive ionization production process which produce multiple-charged ions by stripping electrons off one by one, and the other is the direct ionization process which produces them by releasing electrons at one stroke through the Auger effect (23).

In both cases the same total ionization energy must be applied in order to produce the desired ion; only the energy of the impact electrons of these two processes has to be very much different, especially for larger values of n. Table 1.2 shows this situation for neon, krypton and xenon (24, 25).

<u>Table 1.2</u>

Ionization energies in eV for different charge states n of neon, krypton and xenon (a) formed by a single electron impact; (b) formed by successive electron impacts.

	a) b)	$0 \to 1^+$	0 / 1^+ $\to 2^+$	0 / 2^+ $\to 3^+$	0 / 3^+ $\to 4^+$	0 / 4^+ $\to 5^+$	0 / 5^+ $\to 6^+$	0 / 6^+ $\to 7^+$	0 / 7^+ $\to 8^+$	0 / 8^- $\to 9^+$
Ne	a)	21.6	62.7	126.2	223.4	350	508	715		
	b)	21.6	41.1	63.5	97.2	126.4	158	207		-
Kr	a)	14	38.6	75.5	128	192.7	271.2	382	508	742
	b)	14	24.6	36.9	52.5	64.7	78.5	111	126	234
Xe	a)	12.1	33.3	65.4	110.4	167.4	256	358	484	702
	b)	12.1	21.2	32.1	45	57	89	102	126	218

Unfortunately the multiple-charged ion yield by single electron impact is very poor even for the heaviest elements. The reason is that with increase in charge state the ionization probability decreases.

A better yield of multiple-charged ions is achieved by successive impacts as soon as higher and higher electron current densities are applied and thereby the ionization constant of the discharge approaches 100%. Thus the multiple-charged ions are not formed by a single electron impact of a low probability but by successive impacts of much higher total probability. The multiple charged ion yield is then of the same order as the yield of single charged ions (24).

The ionization potentials $eU_{n,n+1}$ for the release of an outermost electron from an n-fold charge ion are known for all elements either from spectroscopic measurements or theoretical studies (26, 27). Cross-sections, $\sigma_{o,n,}$ for single impact ionization for neutral atoms have been published especially for the rare gases (28). Few experimental cross sections, $\sigma_{n,n+1}$, exist for the ionization of ions by electron impact in case of successive ionization (29). The cross-sections $\sigma_{n,n+1}$ can be calculated from semiempirical formulae. In one of these formula, Drawin (30) gives the following expression for the partial cross-section, $\sigma^{m}_{n,n+1}$, for ionization of an electron in subshell m as,

$$\sigma^{m}_{n,n+1} = \sum_{m} \sigma^{m}_{n,n+1} = A\,\sigma^{0}_{n,n+1}$$

$$= Af_1 \frac{1}{E_e} \left[\frac{1}{eU_{n,n+1}} - \frac{1}{E_e} \right] \ln \left[f_2 \frac{E_e}{eU_{n,n+1}} \right] \quad .....$$

where $\sigma^{0}_{n,n+1}$ denotes the partial cross-section for the ionization of an outermost electron and A is assumed to be constant. The

parameter f_2 was chosen to be 1.25 and the value of Af_1 was determined from a fit to the measured cross-section $\sigma^{exp}_{0,1}$. Thus the resulting cross-section formula is only dependent on the known ionization potential and the electron impact energy, (31).

A comparison of the electron energies and the ionization cross-sections at the respective maximum cross-section for Ne^{2+} is given in Table 1.3.

Table 1.3

Electron energies E_e in eV and ionization cross-sections in πa_0^2 units at the respective maximum cross-section for neon

		$0 \rightarrow 1+$	$1+ \rightarrow 2+$	$0 \rightarrow 2+$
Ne	E_e	≈ 170	≈ 200	≈ 300
	σ	≈ 0.9	≈ 0.35	≈ 0.053

Recently the cross-section for transitions $4^+ \rightarrow 5^+$, $5^+ \rightarrow 6^+$ and $6^+ \rightarrow 7^+$ for carbon, nitrogen and oxygen respectively, have been reported by Dontes (32) to be of the order of $0.011\,\pi a_0^2$, while in comparison the cross-section for $Ne^{0 \rightarrow 3^+}$ is $0.004\,\pi a_0^2$ (13). These examples show the superiority of successive impacts for multiple-charged ion production.

In gas discharges neither of the two processes outlined above takes place exclusively, but usually one of them is the dominant process. If, however, the ionization energy for the step $n-1 \rightarrow n$ exceeds the single impact energy for transition $q \rightarrow q'$ where

$$eU_{n-1,n} > eU_{q,q'} \text{ and } n > q' > q+1$$

then superpositions of both processes, usually called composed-step processes, occur. The basic requirement for this process is that the containment time of the particles to be ionized inside the discharge must be sufficiently long in relation to the corresponding cross-section (33). For example in the case of uranium ion production by composed step processes, the charge state n = +38 corresponds to a total ionization time of 0.1 second (32).

It should be added that for lower electron energies, multiple-charged ions can be formed by excitation of metastable states, followed by ionising collisions. At higher electron energies other processes, such as Auger (34) and electron shake-off (35), lead to ionization.

Auger process

Ionization may take place by Auger process in which a vacancy in one of the inner shells (K) is filled by an electron coming from an external shell (L). If the energy given up by the transition $L \rightarrow K$ is greater than the binding energy of a second electron of the L-shell, this second electron is ejected; at the same time, the ion which is doubly charged, possesses two vacancies in its L-shell. Both L-vacancies can themselves be filled by Auger transition (from M-shell), so that four vacancies are produced and so on - the vacancies multiplying as they proceed outward through the electronic structure. At the same time, the probability for an Auger process has to be greater than that for a radiative process, in which the vacancy is filled by an external electron with emission of a fluorescence X-ray. The probability for such a radiative transition increase with Z and decreases rapidly as the vacancies proceed outward (36). A good example of successive Auger events is the creation of Xe^{20+} as shown in figure 1.3 (37).

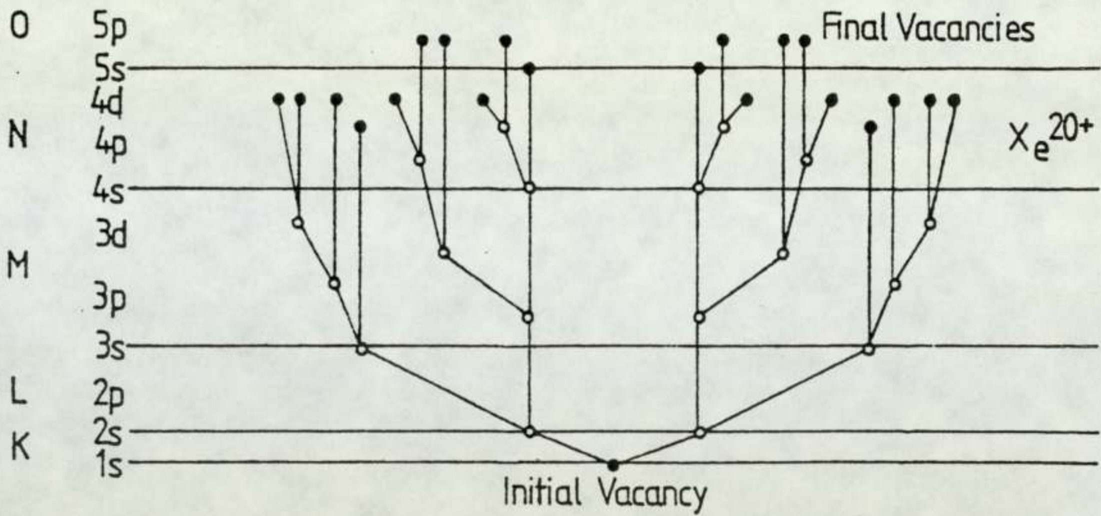

Figure 1.3 A conceptual Auger cascade leading to Xe^{20+} after ejection of a K-shell electron

Electron shake-off

Auger transitions do not completely account for the observed abundance of the various ions, and, in some cases, considerably more ionization is observed. Most of additional ionization can be explained by an "electron shake-off process".

If the ejection of the inner shell electron is rapid enough, the bound electrons, which have orbital velocities small compared to that of the ejected electron, suffer a "sudden perturbation" due to a sudden change in effective charge and screening constants and may undergo a transition to excited states or to the continuum as a result of atomic readjustment. This "sudden perturbation" approximation is roughly valid when,

$$eU_{nk}\tau h \leqslant 1$$

τ is of the order of $\frac{\bar{r}}{V}$

where $\bar{r}$ = mean radius of the outer shells

V = velocity of the ejected K electron.

Probabilities for ejection of supplementary electrons have been

calculated (35) for Ne in which a K-ionization is followed by an Auger (K$\rightarrow$LL) process, the L-electron being ejected at high velocity. Electron shake-off would be responsible for 15% Ne^{3+} ions, 3% of Ne^{4+} ions and 0.5% of Ne^{5+} ions. Okudaira (38) demonstrated that multiple charged ions with $n > 5$ are abundantly produced by Auger processes.

The probability for electron shake-off is independent of the energy of the impact electron when $E_e \gg eU$ (39). If we consider that a sudden vacancy in the K-shell has an equivalent effect on the external shells as the emission of a β-particle by a radioactive nucleus the probability for an ionization by shake-off in all shells varies as Z^{-2} and increases from L to M (O,P,....) shells being maximum for the external shells (40).

In conclusion, Auger cascades and shake-off phenomena play an important role for the production of highly charged ions of large Z.

1.3 Multiple charged ion sources (MCIS)

Any process which imparts to an atom an energy greater than the first ionization potential can produce positive ions. Usually a group of ions, electrons and unionised atoms (neutrals) will exist together, and this is referred to as a plasma when the number of ions and electrons are equal. The early work on ion beams probably began with the work of Thomson who developed an ion source operating at high voltage which produced ions of large energy spread and since then attempts have been made to develop new ion sources with less spread of energy and lower power consumption.

Ion sources are becoming extensively applied in various fields of science and technology. The basic function of an ion source is to produce an ion beam of the required intensity and energy at a suitable gas pressure. For example in sputtering processes, which is

the removal of atoms during ion bombardment, quantitative information is required concerning the effect of the nature and energy of the incident ion and the angle of incidence. It is also preferable that the ion current density should be high and the mean free path of ions and sputtered atom large compared with the dimensions of the vessel. Furthermore, the energy spread of the incident beam must be small and the ionization condition should be such as to minimise the production of multiple charged states. In addition, the development of high-intensity ion sources and the use of highly sensitive detectors for the sputtered particles made it necessary for most investigations to be performed outside the gas discharge.

In the following sections the principles of the most important types of ion sources will be discussed and it will become apparent that only a few of these are capable of producing reasonable currents of multicharged ions.

1.3.1 The Duoplasmatron

The low pressure arc-type Duoplasmatron discharge shown schematically in figure 1.4, is one of the best sources for high currents of not so highly charged ions. This has been developed for use as an ion source by Von Ardenne et al (41) and has since been thoroughly studied by various authors (42,43). Ions in this source originate by collision of thermally emitted electrons with atoms or molecules, and the ion beam emerges from a hole in the anode.

The Duoplasmatron is based on a low pressure discharge maintained between a cathode and an anode. This geometry is modified by an intermediate electrode introduced between these two electrodes and a magnetic field concentrated near the anode. The source normally operates at a pressure between 10^{-2} - 10^{-1} mbar. Recently it has become the most important source in use for moderately intense, 10 - 100 mA, ion beams, because it has a high output coupled with a

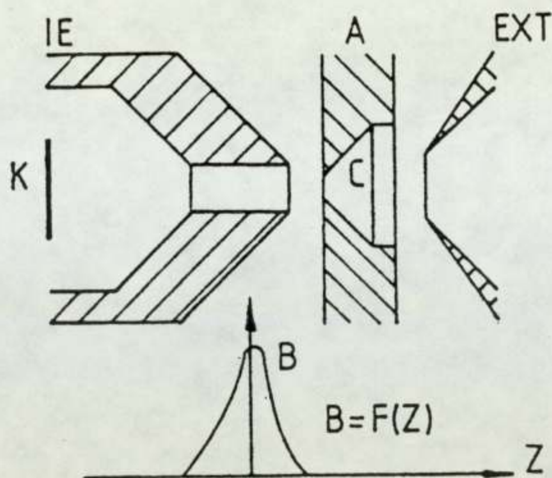

Figure 1.4 Schematic diagram of a duoplasmatron, K, cathode; A, Anode; IE, intermediate electrode; C, expansion cup; EXT, extraction electrode

high gas efficiency due to the increased containment of the electrons as a result of the applied magnetic field. It has been used extensively in high energy accelerators (Sluyters, (44)) and this source has the advantage that it can be used for both gas and solid ion production.

Von Ardenne (41) has referred to the possibility of producing multiple charged ions and Breams et al (45), Arminen (46) and Lejeune (47,48) reported investigations of yields of multiple charged ions. The most extensive examination about the yield of multiple charged ions has been carried out by Illgen (49). Detailed accounts of the discharge mechanisms of Duoplasmatron are given by Green (50) and Lejeune (51), but only details sufficient to discuss the development of the duopigatron ion source from the duoplasmatron have been given.

1.3.2 The Duopigatron

The Duopigatron ion source configuration has been developed by

Demirchanov et al (43) and Morgan et al (52) as a modification of the Duoplasmatron discharge to achieve stable discharge conditions at lower neutral gas pressures, thus larger extraction apertures could be used allowing a higher ion beam brilliance.

The resulting discharge geometry is similar to that of the Penning ionization gauge (P.I.G.) where the electrons also oscillate along axial magnetic field lines, between cathode and anti-cathode (or reflector electrode) and only reach the anode by diffusing across the magnetic field, thus increasing the probability that they can ionise a gas molecule. Figure 1.5 shows a schematic diagram of the duopigatron.

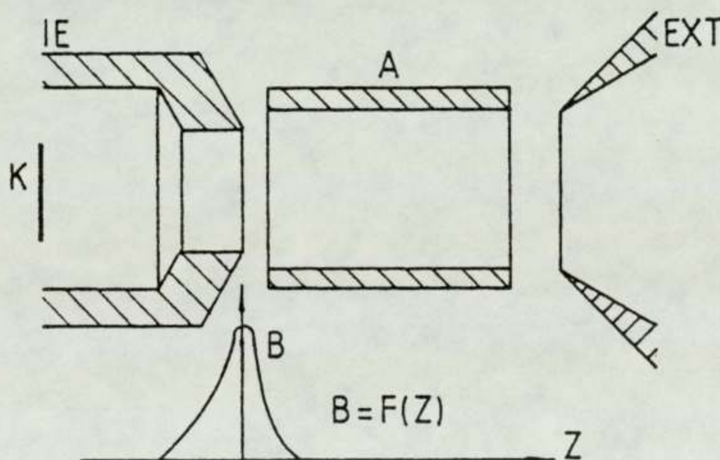

Figure 1.5 Schematic diagram of a duopigatron, K, cathode; A anode, IE, intermediate electrode, EXT, extraction electrode

A double sheath at the intermediate electrode again divides the plasma into two regions, and the term "duo" in duopigatron refers to these two plasma regions. A form of this source has been developed by Winter (53) which appears to be quite a versatile source for generation of intense beams of moderately charged ions.

1.3.3 Penning Ionization Gauge discharge

The PIG-discharge (Penning Ionization Gauge) is maintained by

primary electrons, which are emitted by the cathodes, enter the plasma and are able to oscillate between the cathodes due to the guiding action of the axially directed magnetic field. The electrons will move in the discharge, either until their energy is successively lowered because of the inelastic collisions, or because they have reached the anode due to radial diffusion.

The modes of the PIG discharge are of great variety; at neutral gas pressures below 0.1×10^{-3} mbar they are called "low pressure PIG discharges" (54,55) and at higher pressures up to 0.1 mbar "high pressure PIG discharges".

On account of the special configuration of the PIG-discharge it is especially suited for application as an ion source in the cyclotron. Satisfactory yields of multiple charged ions can only be obtained within the high pressure discharge mode, since otherwise the densities of extracted ion currents remain too low and no significant influence of successive ionization processes can take place.

Since the first work on PIG-MCIS, Bethge et al (56), extensive experiments on various PIG-configurations have been carried out. A detailed review of these activities has been given by Bennet (57).

Generally PIG-MCIS show the highest yields of highly charged ions compared to all other sources. It is not possible to overview exactly the capability of the various types of PIG-MCIS. On the other hand, great problems of technological nature exist, since at elevated discharge powers a progressive destruction of the cathodes by sputtering appears, thereby terminating the life time of the source.

A PIG-MCIS type cold-cathode source developed by Bennet et al (57) consists of an extractor electrode, magnetic coil, cooling system, anode cylinder, cathode and anti-cathode. A simplified diagram of this source is shown in figure 1.6. The "high pressure PIG-discharge" has rising current-voltage characteristics as long as the

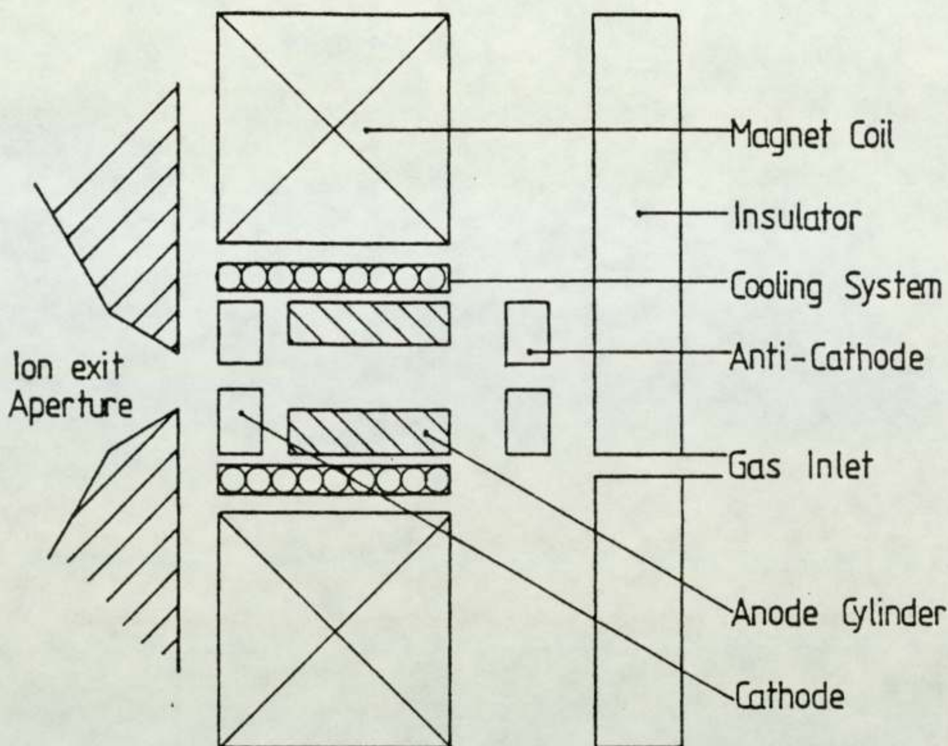

Figure 1.6 Schematic diagram of the PIG-type ion source

essential creation processes for the primary electrons are achieved by ion-induced emission at the cathodes: The characteristics become saturated for the discharge voltage over a wide current range as typically found for a glow discharge. Falling characteristics occur if the cathodes are heated by ion impact or by some external means to such an extent that they emit thermionically. A discussion of the processes influencing the discharge balance in hot cathode PIG-ion sources has been given by Green and Goble (58).

In table 1.4 a comparison is given of discharge parameters of the three sources, Duoplasmatron, Hot-cathode and Cold-cathode PIG-MCIS under typical conditions for multiple charged ion production.

The tabulated data suggests the following interpretation:

(a) Duoplasmatron ion sources; the low arc voltage corresponds to a low energy of the impact electrons. Because of the coincident high arc current it is likely that the multiple-charged ions

are formed by successive electron impacts.

(b) Cold Cathode Penning source: The high arc voltage corresponds to a high energy of the impact electrons. Because of the coincident low arc current it is likely that the multiple charged ions are formed by single impact processes.

(c) Hot cathode penning sources: The intermediate arc voltage and the intermediate arc current correspond to an electron energy and to an electron current density for which composed-step processes are likely to occur.

Table 1.4

Typical discharge parameters for multiple charged ion production

		a) Duoplasmatron	b) Cold cathode Penning	c) Hot cathode Penning
Arc coltage	U (V)	100–350	1500–3000	300–800
Arc current	I (A)	30–10	2.5–0.8	20–6
Power consumption	N (kW)	1–5	2–4	3–8
Magnetic field strength	B(kG)	0.6–3	≈ 3–5	≈ 3–8
Gas pressure	P(torr)	$\approx 5 \times 10^{-3} - 10^{-1}$	$\approx 5 \times 10^{-6} - 5 \times 10^{-5}$	$\approx 10^{-5} - 10^{-4}$
Plasma density	D (cm^{-3})	$\approx 10^{14}$	$\approx 10^{11}$	$\approx 10^{11}$
Duty factor	τ (%)	3	2	100
Lifetime	T (h)	≈ 50	≈ 60	≈ 2–20

Accordingly, the sources (a) and (c) (step processes) should outclass the source (b) (single impact) for the production of multiple charged ions. This remark is supported by the experimental results shown in figure 1.7, especially up to a charge state n = 5 for Xenon (59).

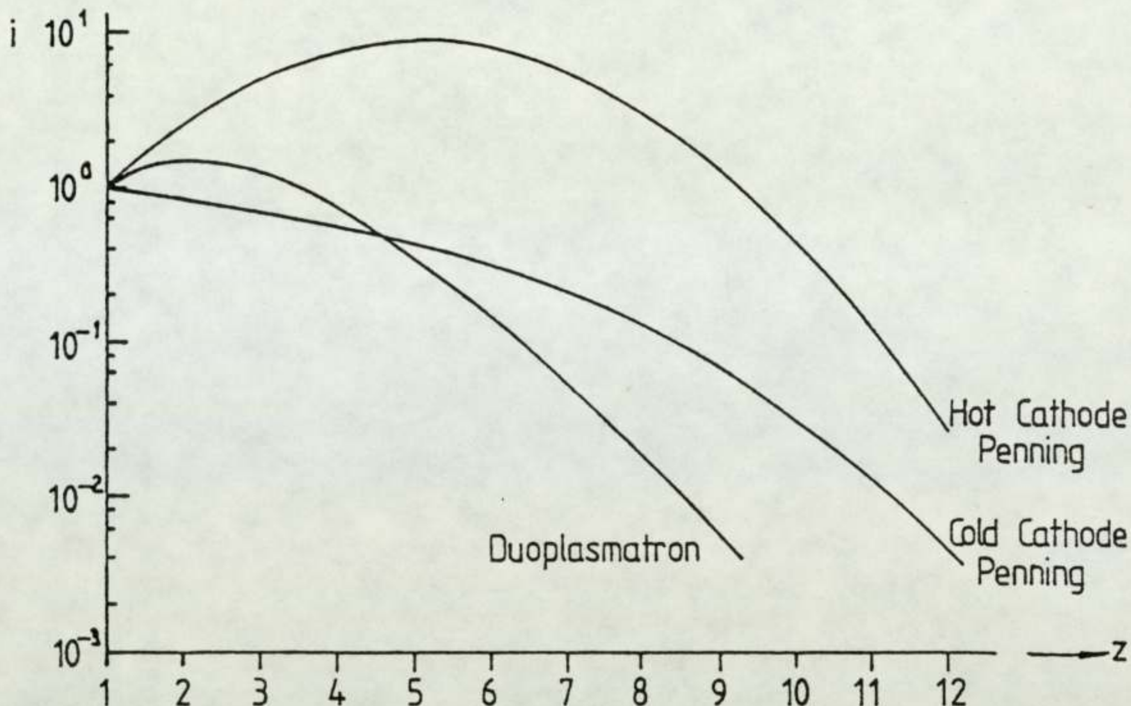

Figure 1.7 Particle current yield for charge states Z relative to yield Z = 1 obtained with typical gas discharge ion sources for xenon.

1.3.4 Magnetron-ion source

This configuration involves an anode cylinder immersed in a homogenous magnetic field with a homocentric thermionic cathode; the extraction of ions may be done either parallel or transverse to the magnetic field direction.

One investigation has been reported using Kr and Xe with discharge currents of approximate 0.5A and discharge voltages of around 250V, (B Cobic (60)). No major influence of successive ionization processes were found, since only rather low fractional rates of higher charged ions could be achieved.

1.3.5 Radio frequency-ion source

A radio frequency ion source was first used by Thonemann (61). In an R.F. ion source ionization takes place by collision produced by coupling the gas discharge tube with a radio-frequency tuned supply. It consists of a glass tube surrounded by a radio frequency coil.

The source produces gas ions better than solid ions. In order to constrain the ions near to the exit aperture, a magnetic field is used and the electric field from the positive potential of a few kV on the anode moves the ions towards the exit aperture. Eubank et al (62) developed this source and constructed an R.F. source up to 15 mA of hydrogen ion current. The R.F. ion source can produce about 10 mA of ion current with 20-100 eV energy spread at 10^{-2} - 10^{-3} mbar.

The generation of He^{2+} ions in an r.f. ion source was given by Valyi (63). The energy of the electrons in such discharges is rather low and it is necessary to use correspondingly high frequency to ensure more collision between the electrons and neutral particles. The most favourable results have been obtained at low gas pressure ($< 10^{-2}$ mbar) yielding a fractional rate of He^{2+} ions of about 2%.

It is thus clear from the previous discussion that there are several important parameters and processes which determine the production of multicharged ions. A review of the literature has also indicated that the hot cathode Penning ion source produces a greater yield of highly charged ions than most other sources commonly in use. This is primarily because in this device the operating voltage is low and thus the electron energy is near to the maximum of the ionization cross-section curve.

In addition, the electron and ion containment time is large, and thus the source provides favourable conditions for the production of highly charged ions by the process of successive electron impacts.

In the following Chapter a detailed discussion of the saddle field ion sources will be given and this will include an estimate of the likely yield of multicharged ions from these sources.

CHAPTER 2

SADDLE FIELD ION SOURCES

2.1 Introduction

In hot cathode ion sources, where the electrons are produced by thermionic emission, the life of the cathode is a limiting factor and the construction of the device is also complicated by the use of the heated cathode. For this reason many investigators prefer cold cathode ion sources. These sources operate essentially on the principle of the Penning ionization gauge in which a self-maintained discharge can be operated at low pressures typically in the range 10^{-4} to 10^{-3} mbar. It generally consists of a ring-shaped anode and two plane cathodes placed at each end of the anode. The electrons which fly on a nearly helical trajectory under the action of the electric field generated between the electrodes, oscillate at the same time in the direction parallel to that of an applied magnetic field which is along the discharge axis. The nature and condition of the cathode and the ion energy are important factors in the production of secondary electron emission at the cathode surface.

In many respects the saddle field ion sources are similar to that of the cold cathode Penning ion sources in that they operate at low pressures without a thermionic source of electrons. However they differ in that the long electron path lengths in the saddle field ion sources are achieved by using a particular configuration of electrostatic field, thus avoiding the use of a magnetic field which may be undesirable in certain situations.

The saddle field ion source was developed from the idea of the McIlraith (1) oscillator, which is capable of producing a self-maintained cold cathode discharge at low pressures. In 1966 McIlraith

found that if a pair of positively charged parallel wires is surrounded by a conducting cylinder, a saddle line is produced between the wires, and an electron follows an infinitely long oscillatory path between the wires. He showed theoretically that the electron path length, for example at pressure $2x10^{-5}$ mbar, is about 5 km, thus it should be possible to maintain a discharge to a pressure of the order of 10^{-8} mbar. In practice it has been shown (Rushton and Fitch (64)) that the discharge ceases at about 10^{-6} mbar due to the disturbance of the electron trajectories by stray magnetic field of the order of the earth's field.

The particle trajectories are of two types - stable and unstable - as shown in figure 2.1. In the case of a stable trajectory the oscillating particle passes between the two electrodes and in the unstable trajectories it orbits around them.

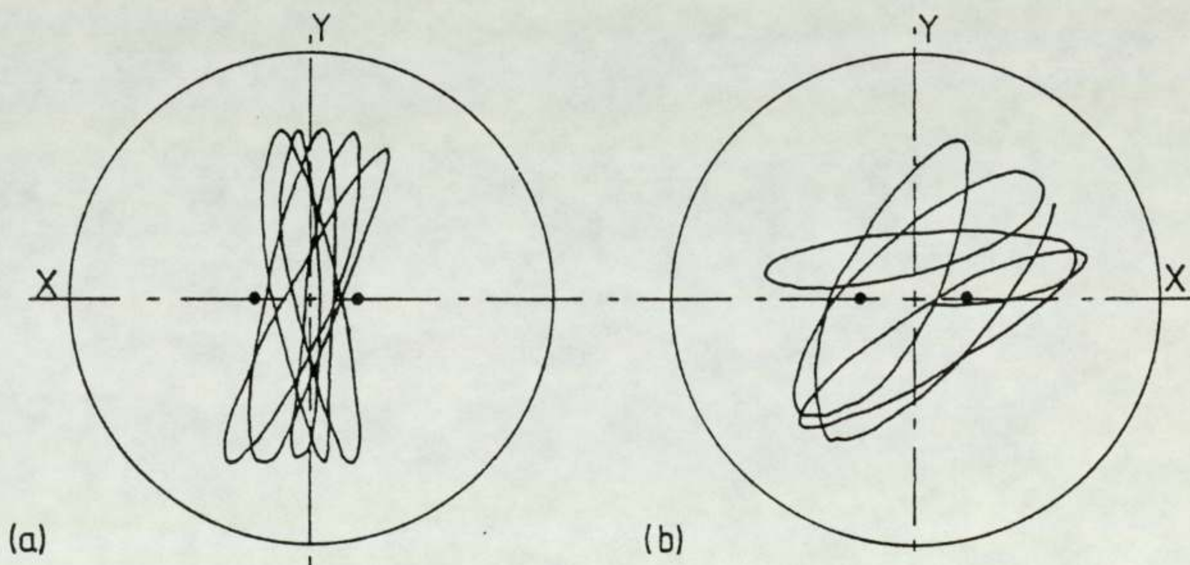

Figure 2.1 Diagram showing (a) stable and (b) unstable electron trajectories.

In the process of maintaining the discharge, electron/ion pairs are formed by collision of electrons with gas molecules. The resulting ions are accelerated to the cathode and thus produce secondary electrons which also go into oscillation and some fraction of these energetic ions can be allowed to escape through an aperture in the cathode cylinder in the form of an intense and well defined ion beam, without disturbing the discharge, (figure 2.2). This idea led to the development of the saddle field ion sources. Two forms of these sources are now available, one employing cylindrical and the other spherical geometry.

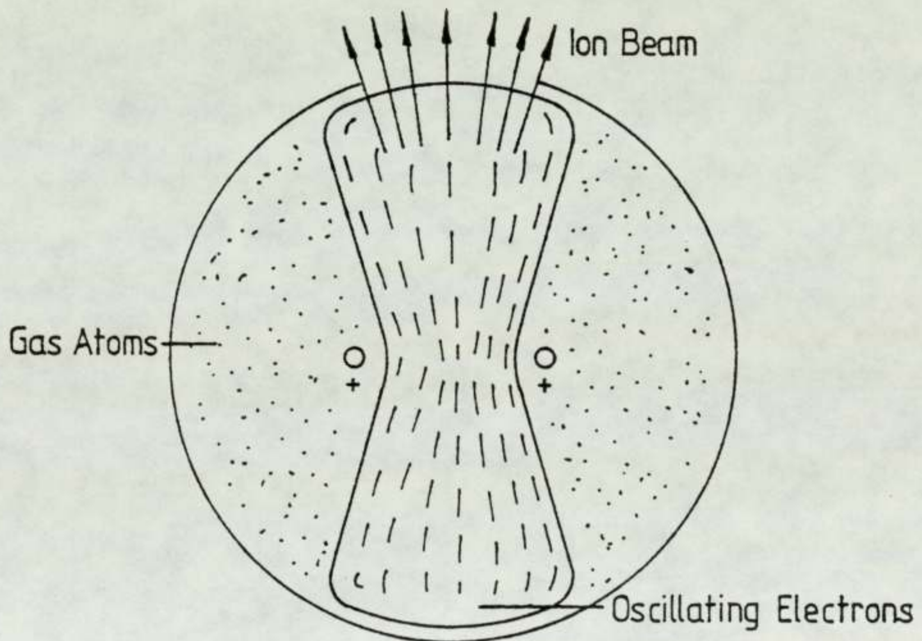

Figure 2.2 Ion beam escaping through an aperture in the cathode cylinder

Fitch and Rushton (3) used the cylindrical source to produce a beam of energetic positive ions of argon of about 100 μA cm^{-2} at a pressure of 6.6×10^{-4} mbar when operated at an anode potential of 10 kV. It consisted of a cylindrical cathode surrounding two anode wires which were symmetrically disposed about the axis of the cylinder. This source produced a wide ion beam with a fairly broad

energy spread (6).

2.2 Design and properties of the spherical source

In the cylindrical source a wide beam is obtained, where sometimes a narrow and fine beam is required. Furthermore, in the cylindrical source undesirable end plates, which are at cathode potential, are necessary to reflect the electrons along the axis of the cylinder. However, Franks (7) showed that if the cathode is made spherical and the anode rods are replaced by a ring anode, then the saddle line becomes a saddle point and the end effects are eliminated. In 1973, Franks (7) described and designed a saddle field ion source of spherical geometry by making the cathode from two aluminium hemispheres and the anode from a stainless steel annulus. In order to retain the true spherical geometry, he added two guard rings at earth potential which were placed either side of the anode. These were isolated from the anode by four ceramic insulators and the ion beam emerged through a hole in the cathode. A schematic diagram of this source is shown in figure 2.3

In this source a saddle point exists at the centre of the anode and thus it has axial symmetry. It therefore produces a very fine beam which is of narrower energy spread (6) than produced by the cylindrical source. The equipotential distribution in this source is shown in figure 2.4, which illustrates that a saddle point potential of 75% of the anode potential. The characteristics of the source were published by Franks and Ghander (8) and they showed these were affected by variation of the anode and hole diameter.

They showed that as the anode hole diameter is decreased the saddle point potential increases. They therefore determined the appropriate anode hole diameter in the same way as Rushton et al (66) had done to optimise the anode separation in the cylindrical source. Khorassany and Fitch (67) used a retarding field energy analyser to

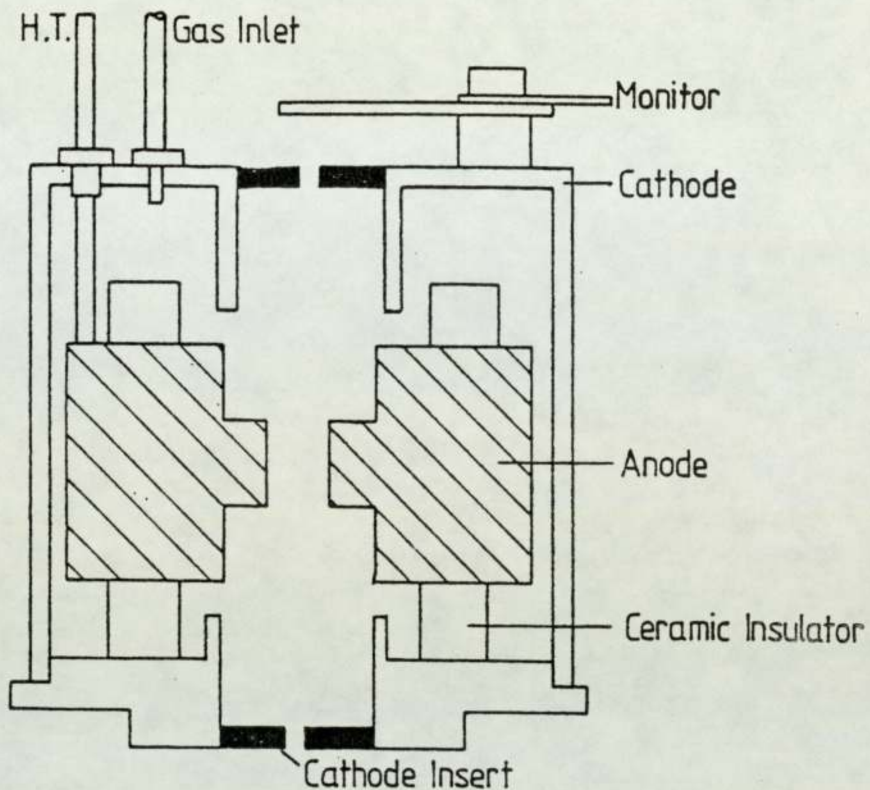

Figure 2.3 Schematic diagram of the spherical source - B11 fine beam source

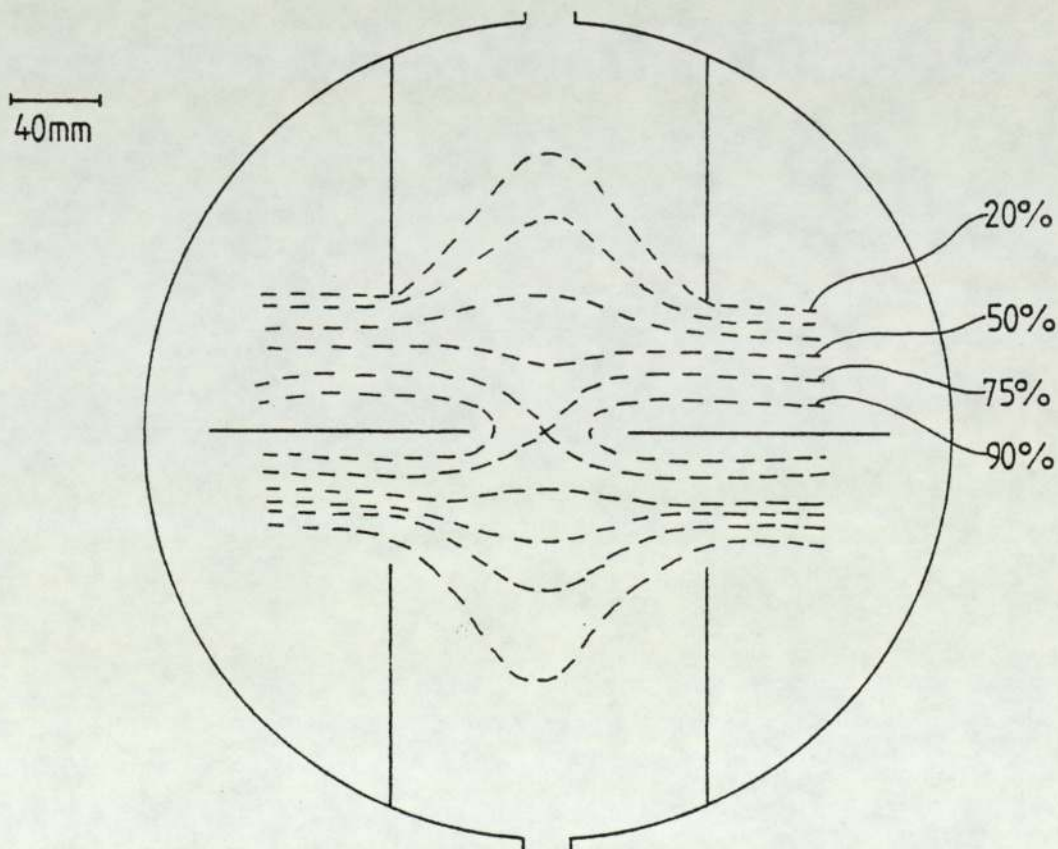

Figure 2.4 Potential distribution in the spherical source

measure the energy distribution of the ions produced by the spherical source for various gases. They found that most of the ions occur at an energy equivalent to about 75% of the anode potential with a peak half-width of about 10% of the anode potential as shown in figure 2.5.

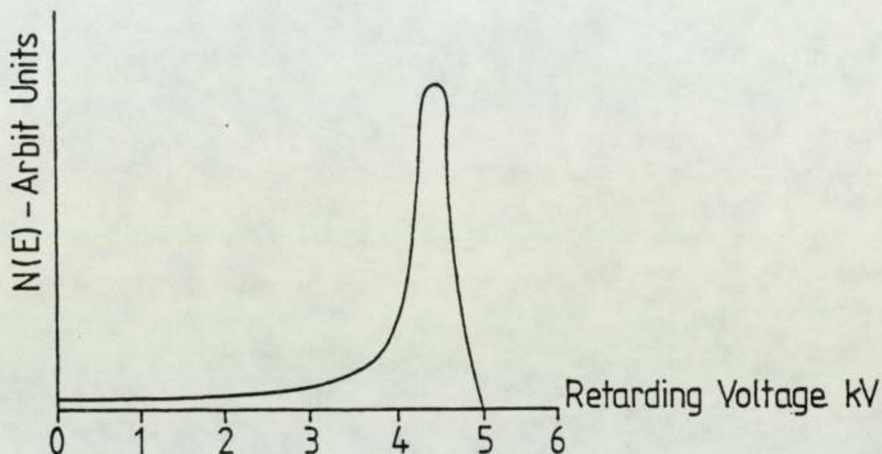

Figure 2.5 Ion energy spectrum for the spherical source for argon

Fitch et al (65) found that there is a significant proportion of energetic neutrals in the emerging beam which increases from about 20% to 70% as the chamber pressure increases and the anode voltage reduces from about 7 kV to 2 kV. It is thus possible to use this source for etching insulating materials without the need of some additional facility to neutralize the charge build-up that occurs on this type of specimen.

2.3 Applications of saddle field ion sources

The cylindrical and spherical saddle field ion sources are now in use in various applications in different aspects of vacuum science and technology. In general, the cylindrical source should be used if a wide ion beam with a broad energy spread is required, but if a fine beam of ion of narrower energy spread is necessary, then the spherical source is more suitable.

The versatility of these sources has been demonstrated during

the last few years by the range of applications that have taken place in this department and in many other laboratories throughout the world. These include ion etching studies (Barnes et al (68)), metal coating of SEM samples and shadowing of TEM samples, (Christopher et al (69)), preparation of field emitting tips (Walls et al (70)), development of surface features on copper during ion bombardment (Lewis et al (71)), and even as a source of ultraviolet radiation (Burger et al (72)).

In one study in this Department, Fitch et al (3) used a cylindrical source with argon to ion etch nickel, molybdenum, copper and acrilonitrile butadiene styrene (ABS) plastic. Ghander and Fitch (73) used a cylindrical source with a focussing electrode which increased the etching rates of copper from 0.4 to 10 μmhr^{-1} when the focussing electrode potential increased from zero to 5 kV. Fitch et al (5) used a technique in which a tungsten tip was sharpened by rotation in the ion beam, which has the advantage over other techniques in that it can be used to sharpen all types of materials.

Franks et al (8) used a spherical source with a beam current of about 2 mA cm^{-2} for ion thinning. He showed that both the cylindrical and spherical sources are compatible with ultra high vacuum equipment and may be used for cleaning surfaces prior to analysis by Auger electron microscopy (A.E.M.) or electron spectroscopy of chemical analysis (E.S.C.A.). In 1980 Franks (74) showed that this source in particular is suitable for use in an ion beam deposition system for shadowing materials for examination in the transmission electron microscope.

In another application Dhariwal and Fitch (75), introduced one of these sources into the specimen stage of a scanning electron microscope to provide a facility for in-situ ion etching. They used this technique to show the formation of artefacts such as the growth of cones and structural effects on copper samples which had been

annealed under different conditions. They found that this source was suitable for etching insulating materials and consequently were able to apply this technique to reveal the structure of various dental materials such as the dentinal tubules in the dentine of the tooth.

In a very recent paper, Ghafouri et al (76) used a similar technique to study the interface between the enamel of a restored tooth and various restorative materials.

There are several other applications currently in use in this University, for example, in the field emission laboratory the spherical source is being used to remove the oxide layer from a titanium target in high voltage vacuum breakdown studies (Mohindra (77)) and in the thin film laboratory to remove the oxide layer from aluminium samples being examined by ellipsometry (Rehal (78)).

It is thus obvious that the saddle field ion sources are being successfully used in various applications. These sources have several advantages over other sources such as their relatively simple construction and operation, freedom from thermionic filament and magnetic field and their suitability for bombardment of both conducting and non-conducting materials. However if further progress with these sources is to be made it is essential to have a better understanding of the manner in which the discharge operates and to have more reliable information about the nature and type of particles they produce.

Information which is particularly lacking in this respect is concerned with the charge state of the ions. Only in the case of the cylindrical source has this been briefly studied by Clark et al (79). However the resolution they obtained was not very satisfactory and no systematic study was made of the variation of the charge state with anode voltage, anode current and source pressure. Furthermore, no attempt was made to explain their results in terms of any fundamental

processes and parameters.

In the present work a detailed analysis of the ions produced by the spherical ion source has been made. Using the information given in Chapter 1 it is possible to estimate the proportion of higher charged states that could be expected from this source. It will be shown later that conditions in the source favour a single impact process for the production of higher charge states. Published ionisation cross-sections for this process indicate that very high charge states are unlikely and hence the proportion of doubly charged states are not expected to be more than about 20% of the singly charged ions. Thus it was considered that a relatively simple magnetic analyser would be adequate for this investigation.

CHAPTER 3

DESCRIPTION OF THE ION SOURCE, VACUUM SYSTEM, MONITORING FACILITIES AND SOURCE CHARACTERISTICS

3.1 The ion source

The spherical source used in this work was a modified form of the B11 source manufactured by Ion Tech Ltd which has been already illustrated in figure 2.3. In this device the spherical configuration is produced by using two stainless steel cylinders of diameter 10 mm and spaced equally either side of the stainless steel anode of aperture diameter 5 mm and thickness 7 mm. The ends of the two cylinders are closed with two aluminium insert cathode discs of diameter 11 mm and thickness 1.5 mm.

The field in the source is symmetrical about the central anode plane, and consequently two identical intense ion beams are allowed to escape through 1.5 mm diameter holes in each disc. One of these beams is continuously monitored during operation using a flat rectangular stainless steel plate, 10 x 20 mm, located opposite the aperture. The insert discs allow ion exit apertures of different size to be used and also make it easy to change the inserts after the apertures have been widened by ion bombardment. This was usually necessary after 20 to 30 hours of operation when it was observed that the operating conditions of the source changed. The anode assembly is isolated from the cathode body by using glazed ceramic insulators. The E.H.T lead is fitted in the stainless steel anode and the other end is mounted on the cylindrical Duralumin body through a ceramic insulator. A stainless steel pipe, 50 mm in length and 3 mm diamter, is connected to the body to admit the gas into the source.

In order to avoid the gas being injected in the form of a jet,

the end of the tube is closed and the gas is allowed to escape through a small hole in the side of the tube and diffuses into the source via the threads on the end of the tube.

3.2 Performance of the water cooled source

Previous work in this laboratory (Mahmoud (80)), had shown that if the cathode of the source is water cooled there is no change in the source characteristics but it was shown that the source is more stable and can be continuously operated at higher anode voltages for as much as 70 hours, before it is necessary to clean the source.

Cooling of the source was achieved using a detachable water jacket. The main body of the water jacket was made from solid brass, the front end of the body being counterbored to receive the ion source. The inlet and outlet pipes were silver soldered in a position such that the inlet pipe was at the bottom and the outlet at the top of the jacket. A schematic diagram of the water jacket is shown in figure 3.1.

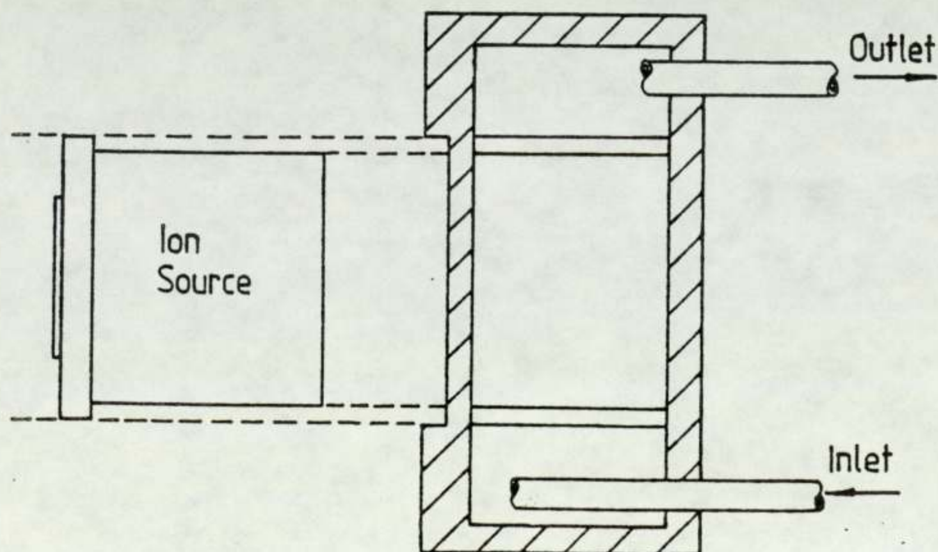

Figure 3.1 Schematic diagram of the water jacket

The cooling water was fed in and out of the vacuum chamber by coiled copper tubes, which were sufficiently flexible to make it possible to fix the source in the desired position in the vacuum chamber.

3.3 Vacuum system and experimental procedure

In all the experimental investigations, the measurements were undertaken in a conventional high vacuum system shown schematically in figure 3.2. It consists of a combination of a rotary pump and a water-cooled oil diffusion pump of rated speed 600 ls^{-1}. "Santovac" fluid was used in the oil diffusion pump and an ultimate pressure of less than 10^{-6} mbar was obtained. "Santovac 5" was used because it has a low backstreaming rate, a low vapour pressure and has unusually high thermal and oxidation stability. However in this particular application its main advantage is that, unlike silicone fluid, it does not produce insulating films during electron or ion bombardment. The figure also shows the magnetic analyser chamber attached to a 6" port in the main chamber wall, which is made of stainless steel and includes three flanges carrying ten high voltage and current lead-throughs, two glass viewing windows, a Mullard ionization gauge and a Penning gauge. The gas could be admitted into the source by a PTFE tube connected to a fine needle valve mounted in the chamber wall.

During the main part of the study of the Penning gauge was used because it is most suitable for continuous high pressure operation. However the ionization gauge was used intermittently to check that there had been no change in the sensitivity of the Penning gauge. Furthermore it is well known that the ionization gauge is more reliable and a calibration curve of the Penning gauge against ionization gauge is given in figure 3.3. Both of these gauges, of course, give the chamber pressure and when studying effects inside the ion source it is necessary to know the actual source pressure.

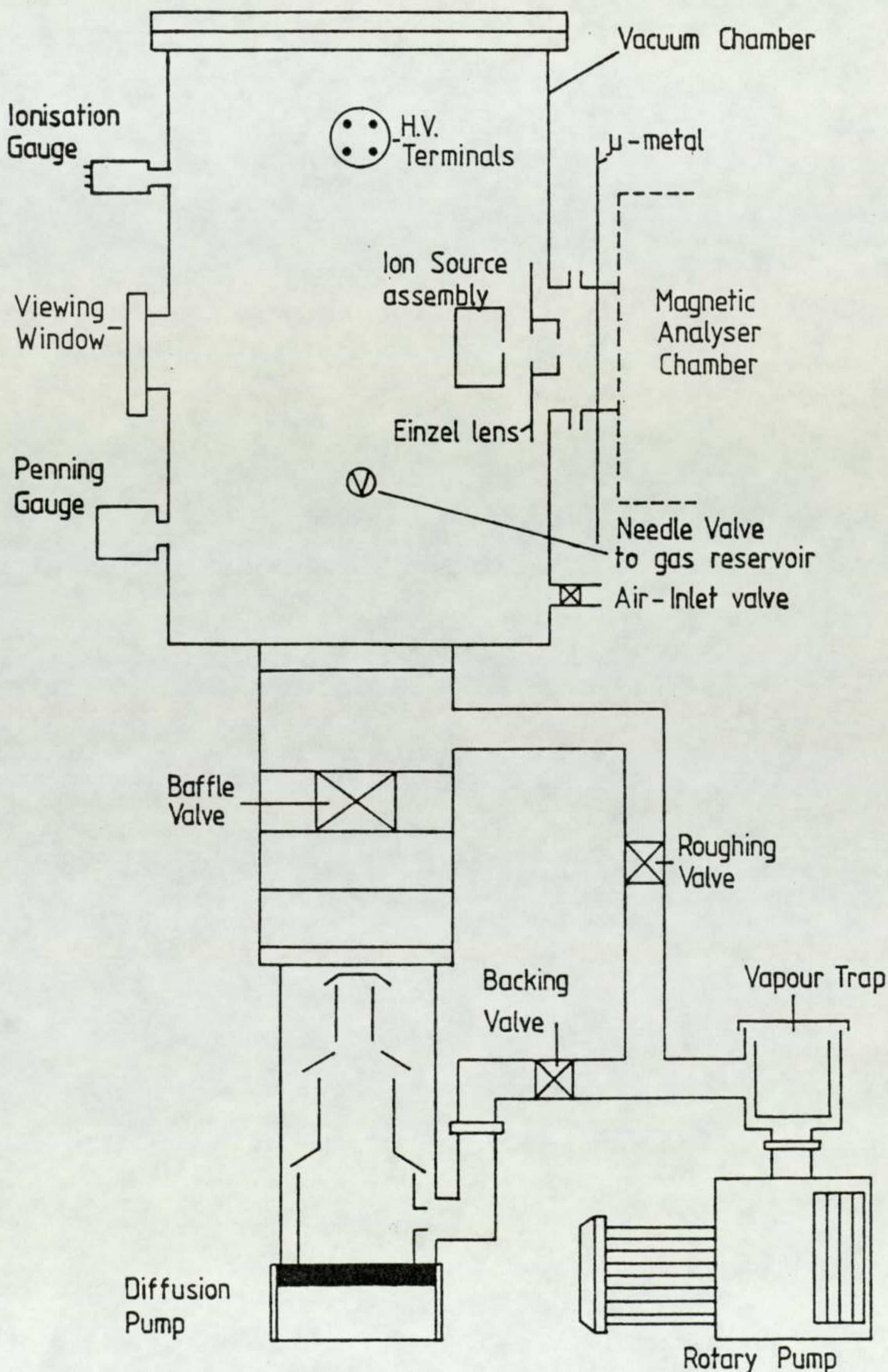

Figure 3.2 Schematic diagram of the vacuum system

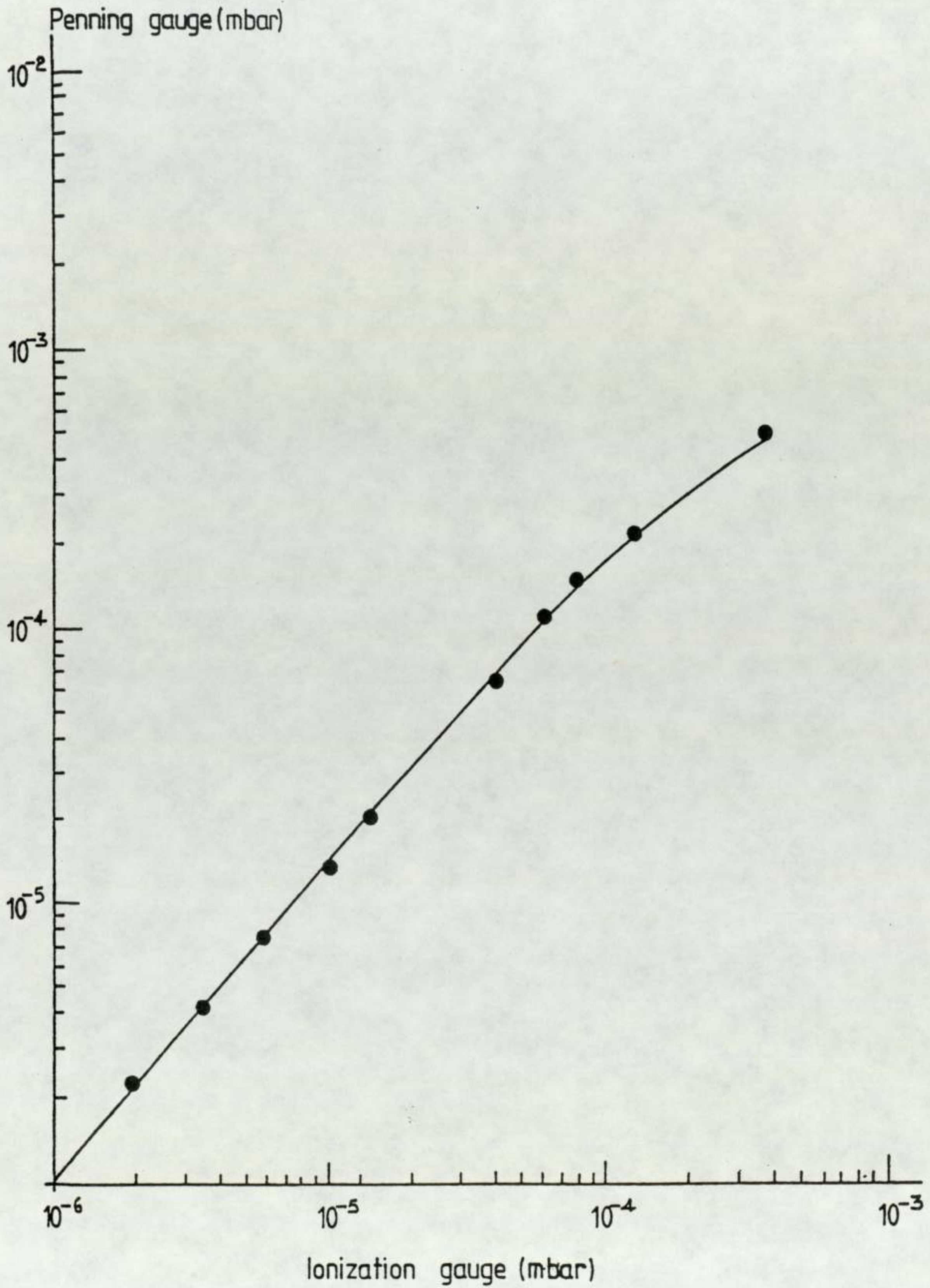

Figure 3.3 Calibration of ionization gauge against Penning gauge using nitrogen

If the effective speed of the diffusion pump is S_E, and the total conductance of the two ion exit apertures of the source is C, then it can be shown that the ratio, R, of the source pressure, p_s, to the chamber pressure, p_c, is given by:

$$R = \frac{p_s}{p_c} = \frac{S_E + C}{C}$$

The approximate value of S_E was found by the constant volume method in which the rate of rise of pressure, $\frac{dp}{dt}$, is measured for a constant leak into the system, then:

$$S_E = \frac{V}{p_e} \cdot \frac{dp}{dt}$$

where V is the volume of the chamber and, p_e, is the equilibrium pressure. For this sytem the effective speed for argon was found to be 90 ± 5 ls^{-1}.

Assuming conditions of molecular flow, C, is given by the equation,

$$C = \frac{62.5 x A}{M^{\frac{1}{2}}}$$

where A cm^2 is the area of the two apertures, and M is the molecular weight of the gas. Hence for apertures of diameter 1.5 mm, C for argon is about 0.33 ls^{-1}, and hence R is equal to 275. Thus as the effective speed of the pump was found to be constant in the range of chamber pressures used - $6x10^{-5}$ to 10^{-3} mbar - it was therefore assumed that the source pressure is always about 275 times that of the measured chamber pressure.

3.4 Electrical circuit and beam monitoring facilities

A schematic diagram of the ion source and its associated electrical circuit is shown in figure 3.4. The source is designed to operate up to about 10 kV and this was provided by a current

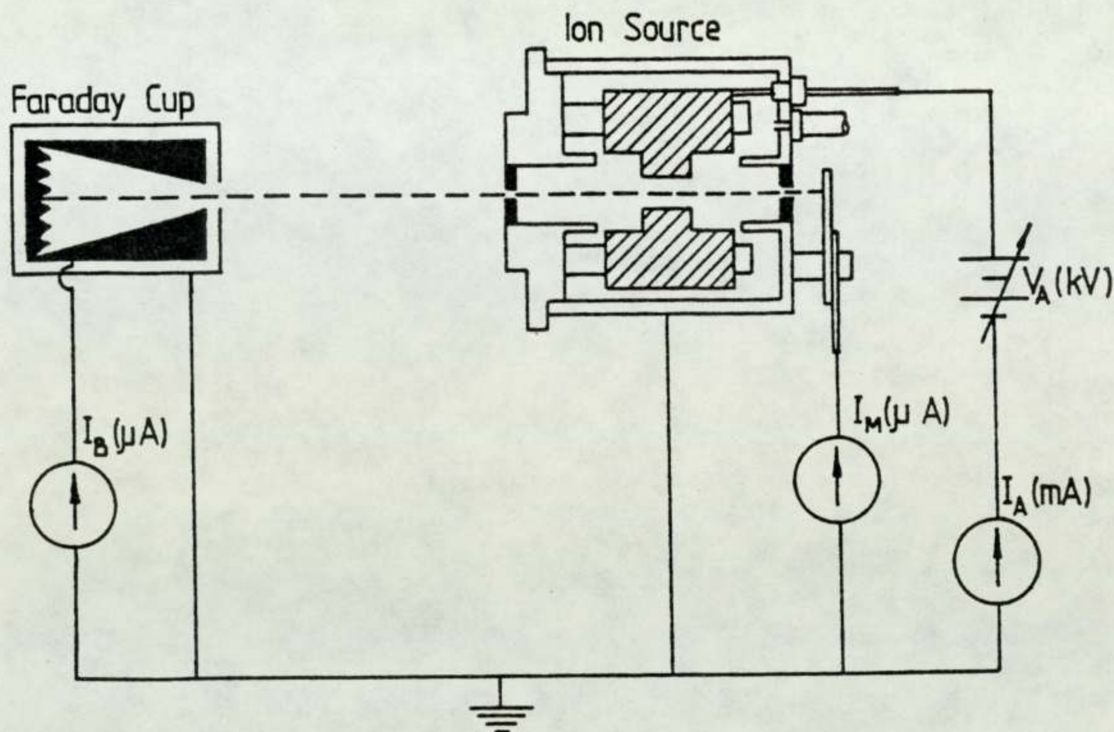

Figure 3.4 Schematic diagram of the ion source and electrical circuitry

stabilised power supply, 0 - 10 kV and 0 - 10 mA. Monitoring facilities for the anode voltage and current were built into the power supply. The ion beam from the back aperture was continuously monitored by the stainless steel plate. However this does not of course record the true ion beam current because of the escaping secondary electrons. Hence it was necessary to design and construct a collector suitable for monitoring the true ion beam current emerging from the front aperture.

The Faraday cup has been one of the primary standards in the measurement of particle fluxes. This is because it is one of the least expensive and simplest detectors to fabricate, along with it being an absolute detector. It can be used to collect both positive and negative particles (Perrin (81)), but its main disadvantages are

its low sensitivity and inability to detect neutral particles.

Tate (82) has shown that the Faraday cup should be made at least 10 times as deep as the diameter of the entrance aperture and Hasted (83) used different shapes of cup, some with an acute angle, to decrease the secondary electron emission. Magnetic fields are sometimes used to suppress the secondary electrons when the cup is being used for ion detection (Bronshtein and Denisov (84)). Alternatively this can be achieved by applying a positive bias to the Faraday cup with respect to its surrounding screen. Additional improvements include the use of fins on the base of the collector to improve the retention of the secondary electrons. Normally materials of high work function are used for the Faraday cup, because the number of secondary electrons decreases with increasing work function. A Faraday cup had previously been developed in this Laboratory by Khorassany (85). Essentially this consisted of a conical cup with an earthed screen and a few nickel plates were also welded inside the base of the cone. This cup has been quite successful in many aspects of the study of ion beams in this Department, but its main disadvantage is its overall size (125 mm length, 78 mm diameter base, 27 mm entrance aperture), which makes it impossible to use in certain situations.

A variety of smaller Faraday cups of different design have therefore been tested in an attempt to produce an efficient collector capable of retaining the secondary electrons without significantly influencing the incoming ion beam. It is clear from the previous discussion that the correct design will depend not only on its geometry, but also on the materials used in the construction, and the potentials applied to the various electrodes.

All of these effects have been considered as follows:-

(1) Choice of material:

A series of experiments were performed using three flat plate collectors - aluminium, stainless steel and nickel. The total current on each plate arising from an incident ion beam was recorded as a function of pressure and anode voltage on the source. The appropriate values are shown in Table 3.1.

Pressure mbar	V_A kV	Plate current (μA)		
		Nickel	Stainless steel	Aluminium
2.5×10^{-5}	7.2	66.8	80.5	115.7
7×10^{-5}	6.0	45.2	54.9	76.3
1.5×10^{-4}	5.1	38.5	46.4	65.8

Table 3.1 Variation of plate current with pressure for different materials, $I_A = 2$ mA

It is clear from this Table that stainless steel and nickel are much more suitable materials than aluminium. However, although nickel appears to be preferable to stainless steel, it was decided to use the latter because it is more suitable for construction.

(2) Geometrical effects:

Various geometrical designs of cup were constructed and tested including the variation of length, diameter and shape of the cup. Fins were also added to the base of the cup and an outer screen was always incorporated. The efficiency of the cup was determined by its ability to retain the secondary electrons produced by a beam of energetic neutrals. Advantage was therefore taken of the fact that the saddle field ion source produces a significant fraction of energetic neutral particles. The positive ions in the beam were extracted by an electrostatic field and the resultant current in the

cup due to the escape of the secondary electrons was recorded for various designs. A schematic diagram of the most efficient and suitable cup is shown in figure 3.5, for which it was estimated that

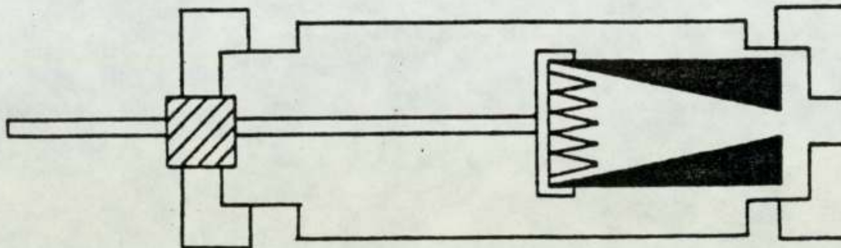

Figure 3.5 Schematic diagram of the Faraday cup

about 95% of the secondary electrons were retained.

(3) Effect of varying the potential on the cup

The performance of the cup was then studied as a function of potential difference between the screen and the cup by applying either a positive bias to the cup or a negative bias to the screen. Of course the latter has a disadvantage when detecting positive ions because a negative bias to the screen cup helps to retain secondary electrons but may also attract positive ions.

In this particular study this was considered to be negligible for small bias voltages as most of the ions are of energy greater than 500 eV. The residual current due to the incident energetic neutral particles was reduced to virtually zero with a bias voltage of about 14 V. Hence it was considered that the efficiency of the cup was nearly 100%.

3.5 Characteristics of the ion source

It has been previously stated that there are three principal modes of the source but normally it is used in the more efficient

low pressure oscillating mode where high ion beam currents can be achieved. It is therefore only in this range of operation that there is a real interest in the proportion of the charge states produced by this source. Thus the variation of ion beam current, I_B, and anode voltage, V_A, was determined as a function of pressure at constant anode currents of 1, 2 and 3 mA, and these results are shown for argon in figures 3.6a and 3.6b.

It can be seen from the figures, that as the pressure increases, both the ion current and the anode voltage decrease. The "knee" in the curve which occurs at the transition mode, which separates the oscillating and glow discharge modes, is most clearly seen in the voltage characteristics of figure 3.6(a). Advantage of this can be taken in that it makes it easy to determine the operating range of chamber pressure for the oscillating mode irrespective of the value of the pump speed, calibration of the gauge or nature of the gas. Furthermore if some fault develops in the source or the pumping system, this can be identified by a displacement of the "knee" in the characteristics.

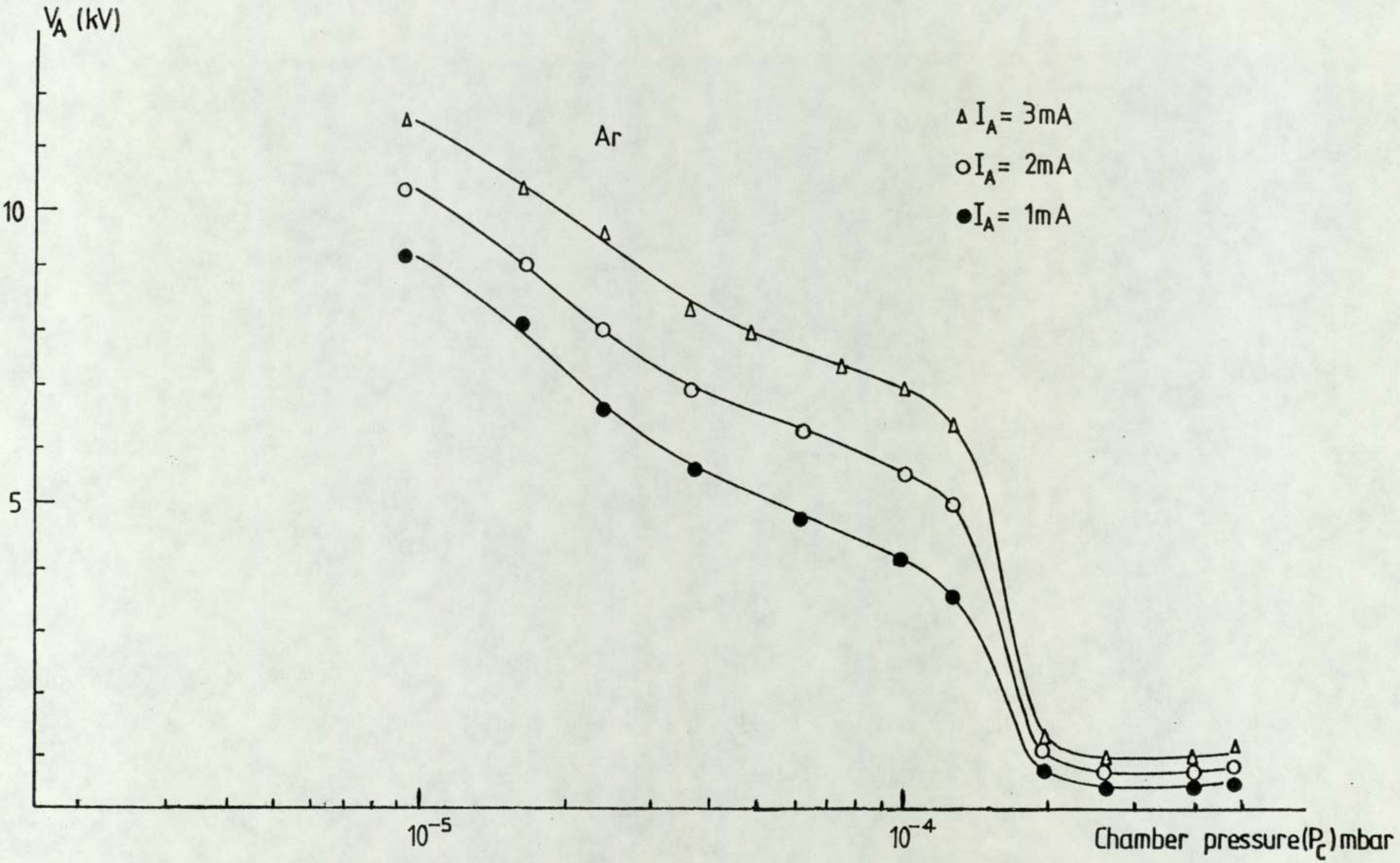

Figure 3.6(a) Variation of anode voltage, V_A with chamber pressure p_c using argon

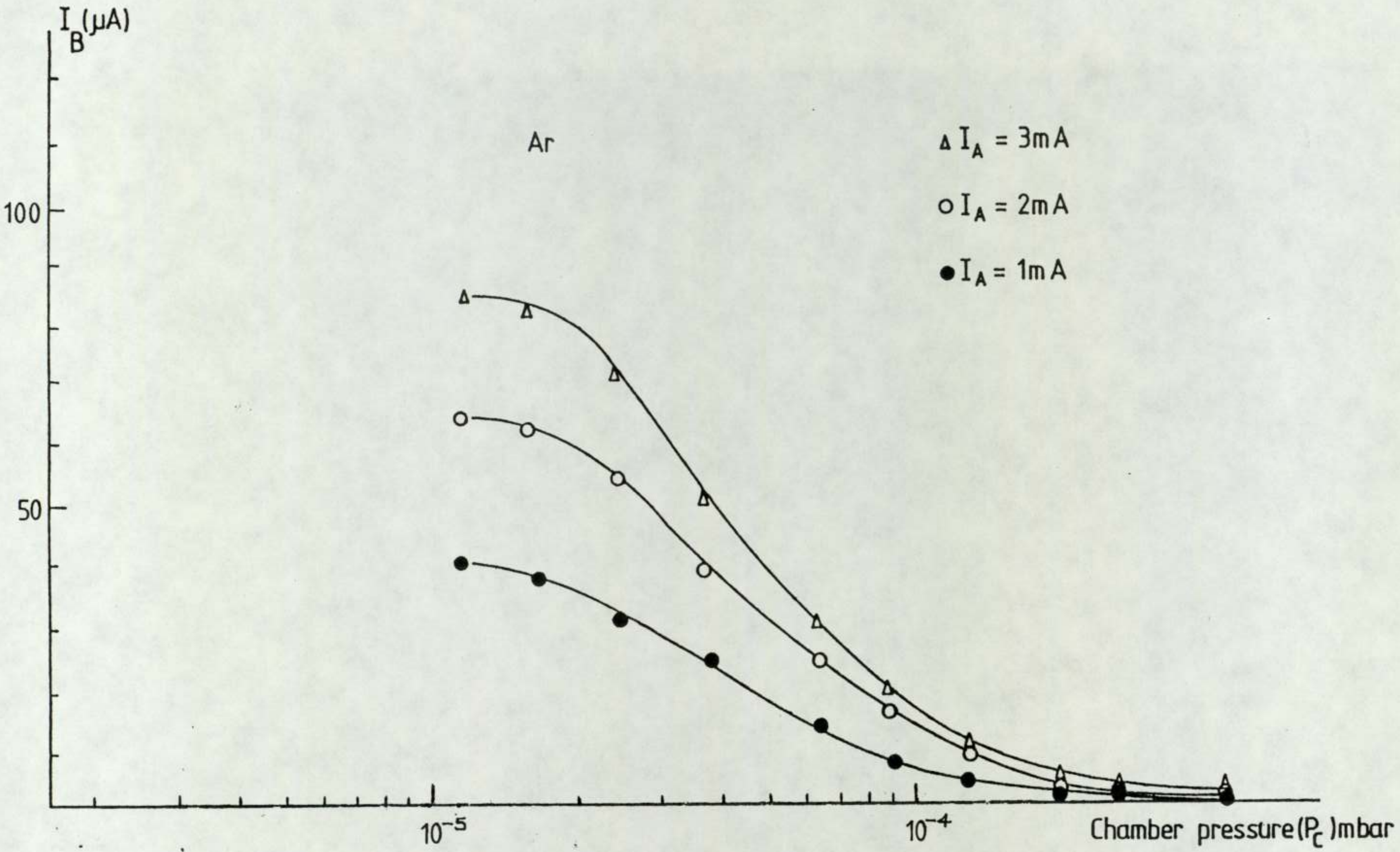

Figure 3.6(b) Variation of ion beam current, I_B with chamber pressure, p_c, using argon

CHAPTER 4

ANALYSIS OF THE IONIC CHARGE STATES

4.1 Introduction

It was recognized that the analyser necessary for separating the different charge states did not need to have a very high resolution, as the energy spread of the ions was thought to be about ± 10% (Khorassany (85)) and furthermore no studies were to be undertaken using gas mixtures.

Consideration was given to a magnetic analyser and to an electrostatic analyser such as the quadropole. However the latter was rejected on the grounds that it would be necessary to reduce the ion energy as the quadropole only accepts ions up to energies of about 100 eV. Thus a magnetic analyser appeared to be the only reasonable alternative although, as we shall see later, it has the disadvantage that it was necessary to shield the source from the magnetic field.

The analyser was designed which took into account the constraints imposed upon it by the strength of the magnetic field, the required resolution, and the energy, intensity and divergence of the ion beam. A schematic diagram of the complete analyser is given in figure 4.1 which shows the electro-magnet, ion source, collimating and focussing electrodes (Einzel lens), Faraday cup, power supplies and x-y recorder. In previous Chapters details of the ion source, vacuum system and Faraday cup have already been given and the remaining components will be discussed in this Chapter.

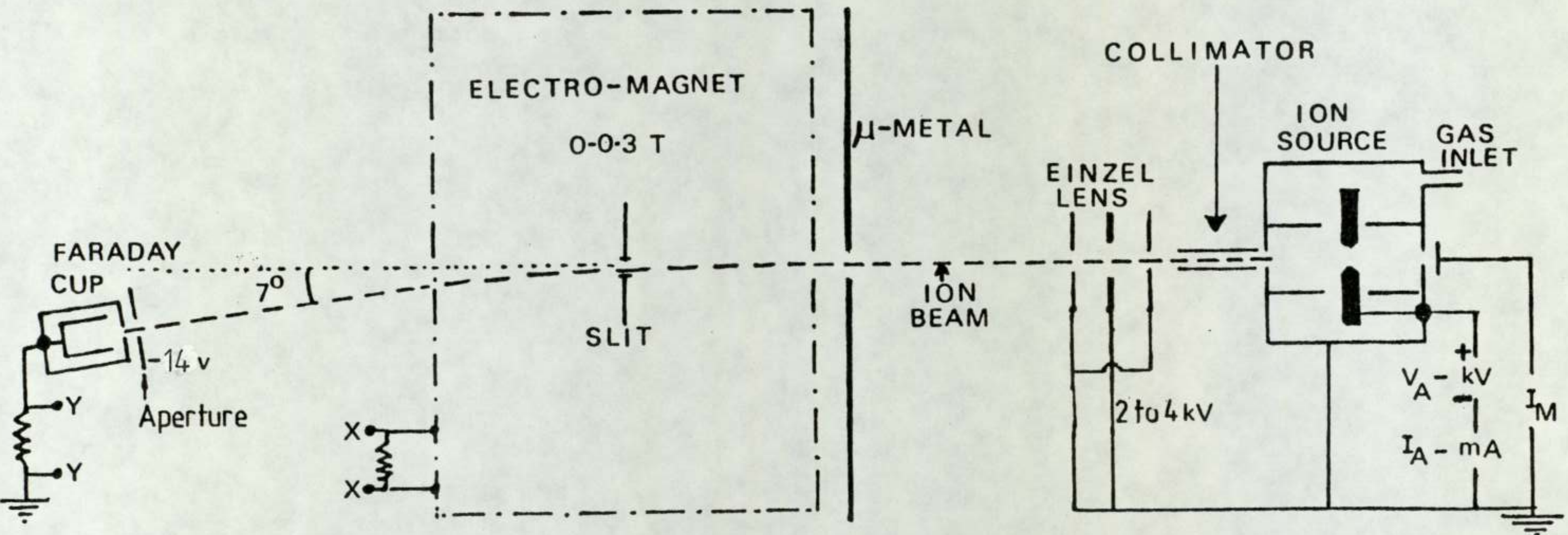

Figure 4.1 Schematic diagram of the experimental arrangement showing the ion source, Einzel lens, magnetic analyser and ion detector

4.2 Description of the analyser

4.2.1 The analyser tube

Although the main vacuum system was constructed from stainless steel, it was decided that it would be more convenient to construct the analyser tube from brass. This consisted essentially of two parts - a rectangular box section, length 13 cm, depth 8 cm and width 2.5 cm, which fitted between the two pole pieces of the magnet, and a cylindrical section of length 12 cm, diameter 14 cm. The box section was attached to the vacuum chamber by means of a 16 cm diameter flange. A similar flange was attached to the far end of the cylindrical section. This flange included a number of insulated lead throughs to support the Faraday cup and the retarding energy analyser which will be discussed in the next Chapter. A vacuum coupling was also mounted on to this flange to support an ionization gauge.

In some experiments this flange was replaced by a flat glass window when it was necessary to view such things as the focussed ion beam and the sputtering measurement to be described in Chapter 6. In all cases vacuum sealing of the flanges was achieved by neoprene O-rings. A photograph of the analyser tube and the demounted flange supporting the Faraday cup is shown in figure 4.2.

It was anticipated that due to the conductance through the analyser tube the pressure in the region of the Faraday cup would be higher than that of the main experimental chamber. Measurements were taken and the comparison of these two pressures is shown in Figure 4.3. It can be seen that the pressure in the analyser tube was about 1.8 times that in the experimental chamber. As all experiments were performed at chamber pressure less than 1.5×10^{-4} mbar, this ensured that the molecular mean free path in the analyser tube was always greater than the effective length of the tube.

Figure 4.2 Photograph of the analyser tube and demounted flange supporting the Faraday cup.

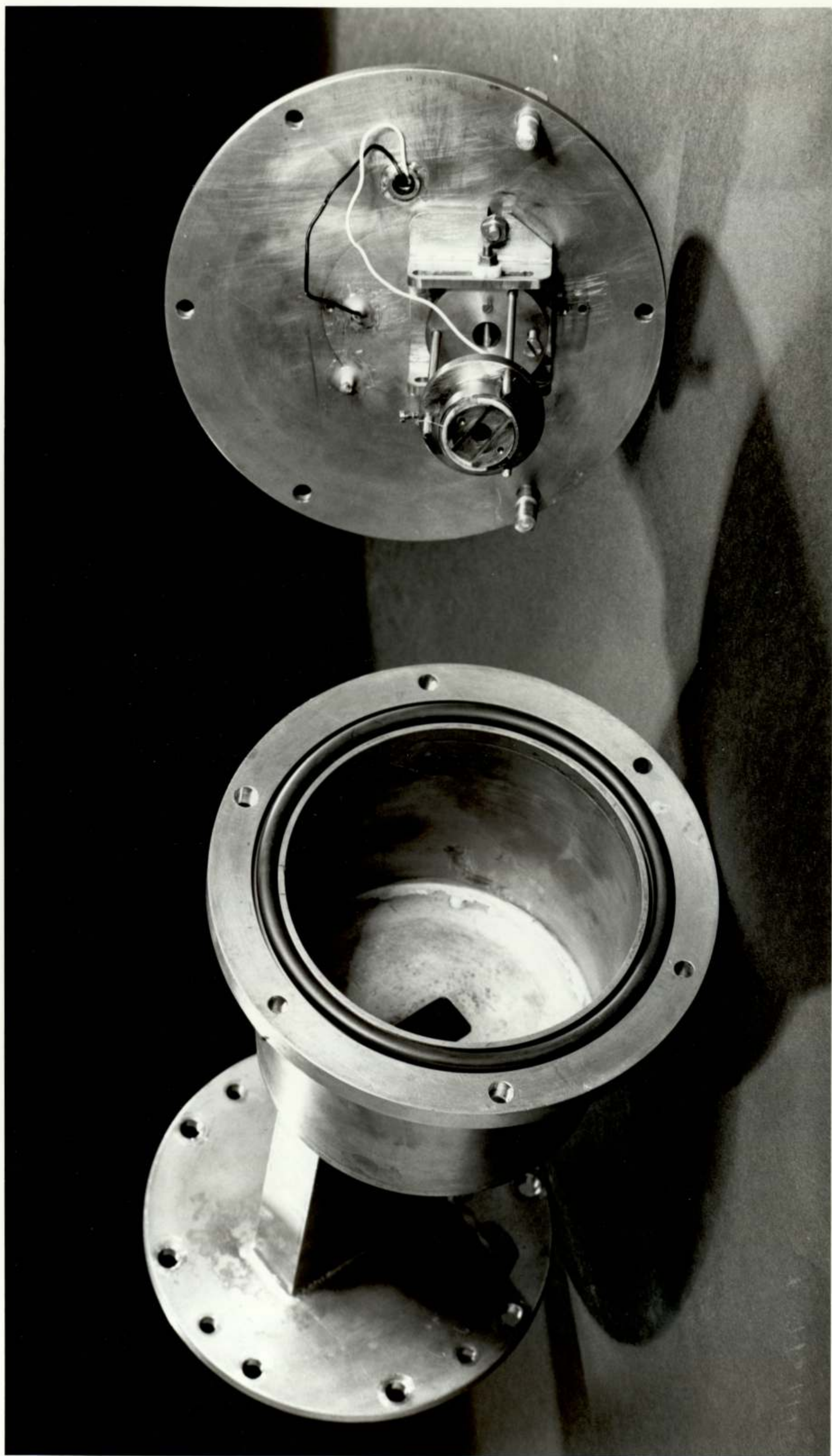

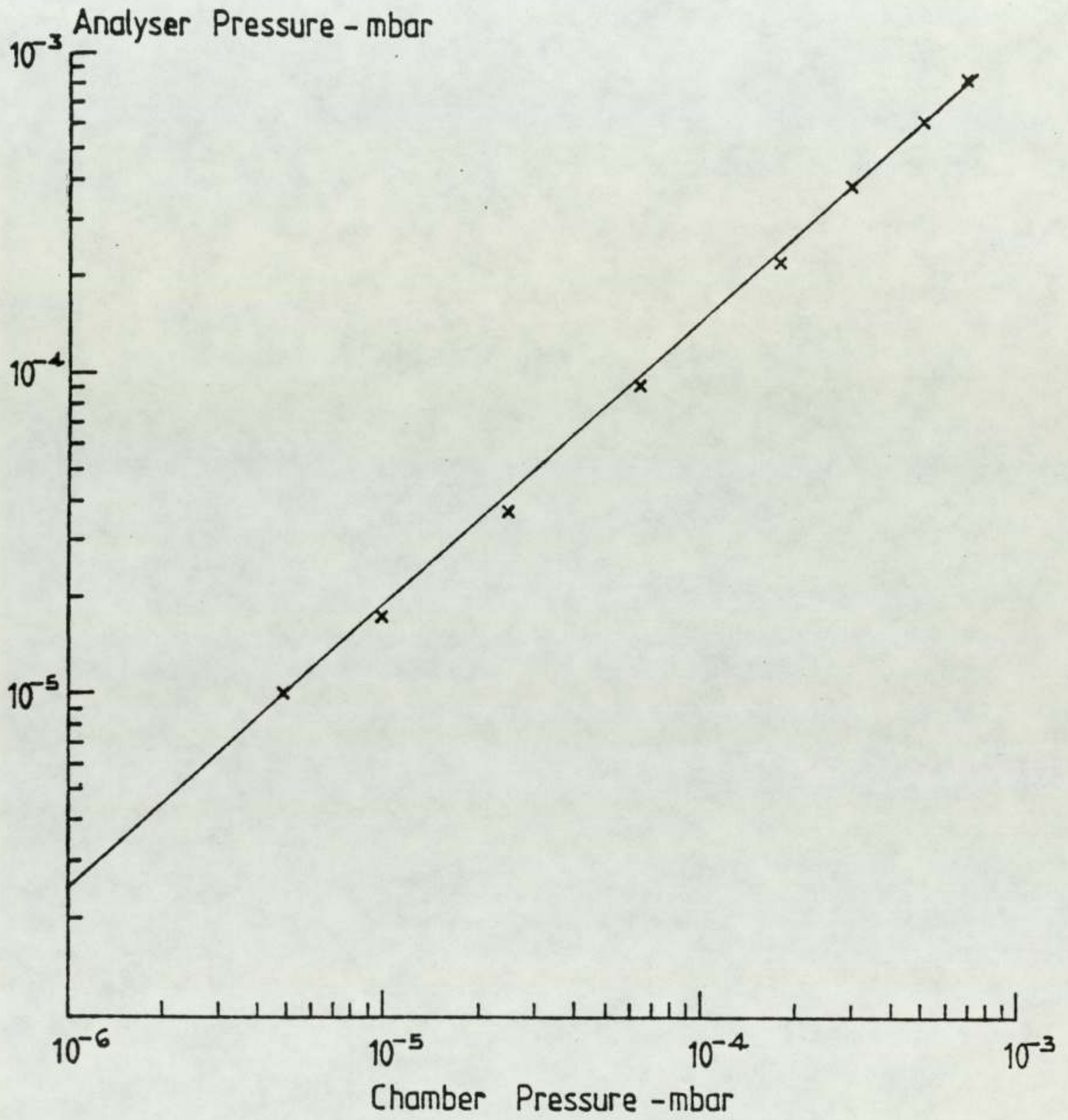

Figure 4.3 Comparison of pressures in the analyser tube and in the main experimental chamber

4.2.2 Einzel lens

The ion beam produced by the source is divergent with a half-angle of about 5° and thus in order to increase the ion current density at the Faraday cup it was necessary to focus the ion beam with an Einzel lens.

An "Einzel lens" is a type of electrostatic lens which may be realized by a three-diaphragm, or three-tube system, whose external electrodes have the same potential. Usually the potential of the intermediate electrode has such a sign that the particles are decelerated in the field between the entrance and intermediate electrode. This lens is called an "Einzel lens" because it initiates and terminates in a single value of potential as shown in figure 4.4. Ions leave this lens at the same potential at which they enter, so it is particularly appropriate in the present investigation because it provides a means for focussing the beam without changing the energy.

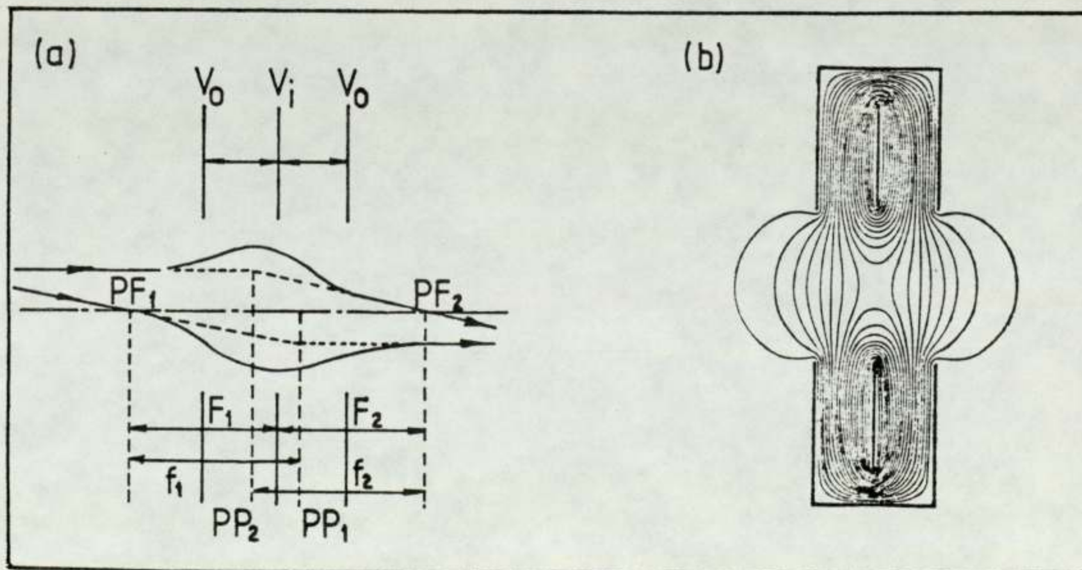

Figure 4.4 The Einzel lens, (a) PF_1 and PF_2 are the principal foci, PP_1 and PP_2 are the principal planes, f_1, f_2 are the focal lengths, and F_1, F_2 are the mid-focal lengths, (b) Potential field

Whilst the theory of the Einzel lens has been discussed extensively by many workers (e.g. Plass (86), Ramberg (87), Bachman and Ramo (88) and Harting and Read (89)), a case of practical interest arises if $V_o = 0$, the equivalent ion lens is then surrounded by media of the same refractive index at both sides. In this case the outer lens electrode is simply brought up to cathode potential, while the inner electrode may be connected to the anode of the system from which the ions are emitted. Thus only one voltage is applied to such a lens and it is frequently called a "unipotential" lens. Moreover, as the voltage ratio $^{V_i}/_{V_o}$ of this lens is always infinite, the position of its cardinal points will be largely independent of the applied voltage.

On the other hand, the focal length depends essentially on the dimensions of the intermediate electrode. If a unipotential lens is used in an apparatus where a given focal length is required, the dimensions of the electrodes must be adjusted with precision. The influence of the intermediate tube length, L_i, on the power of the Einzel lens is demonstrated in figure 4.5(a), in which the radii of all three tubes are equal and the spacing between the tubes, $S = 0.1$ tube radii. Figure 4.5(b) shows in a general way how the focal length varies with S and R_i.

Exact measurements about the cardinal points of a few selected Einzel lenses have been published by Liepmann (90). He found for instance, the focal lengths for tube lenses with three tubes of equal radius R, and with intermediate tube length $L_i = 0.68R$, to be $f = 6.20R$ and $3.84R$ for tube spacings $0.26R$ and $0.76R$ respectively. Again, for tube spacing equal to one tube radius, he found focal lengths $f = 1.94R$ and $1.72R$ with $L_i = 1.44R$ and $2R$ respectively.

The spherical aberration occurs when rays emitted from a point object on the axis do not recombine to form a point image. Spherical

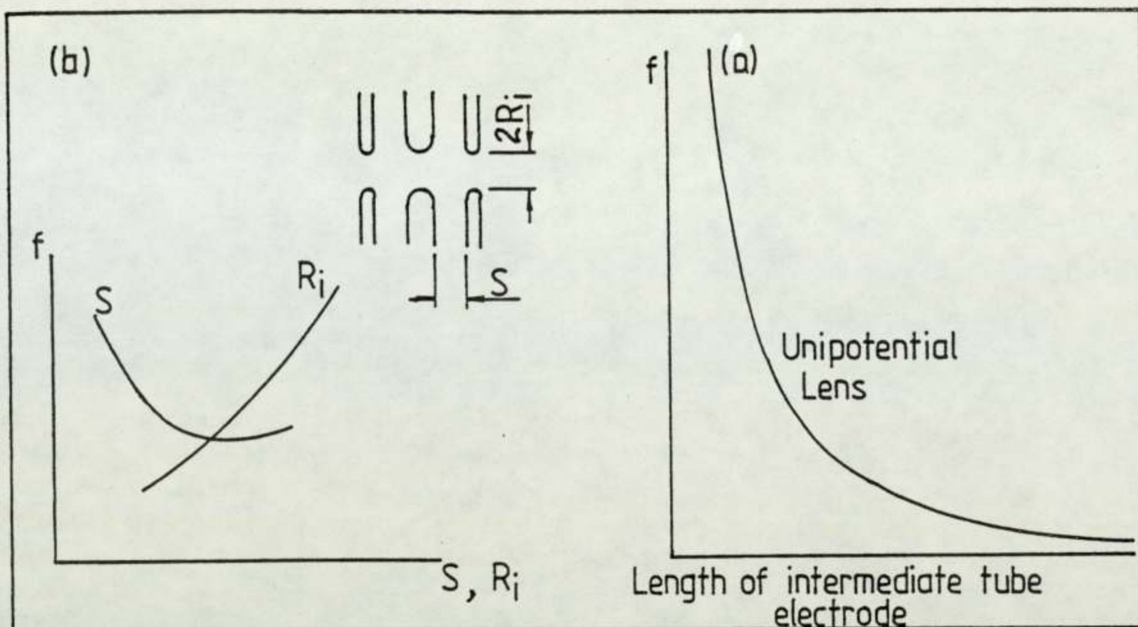

Figure 4.5 Focal characteristics of an Einzel lens

aberration of an Einzel lens has been investigated by Harting and Read (89) and Gobrecht (91), and they have shown that the aberration largely depends upon the size and shape of the electrodes. The following results are of practical interest;

(1) When the ratio of radii (R_i/R_o) is varied, the aberration measured in units of the larger radius is found to reach a minimum for equal tube radii ($R_i = R_o$).

(2) For a given object and image position, and for a given total length of the lens, the aberration coefficient decreases with increasing tube radius.

(3) The aberration decreases with increasing total length of the lens. It depends not only upon the total length but also upon the ratio of the length of inner and outer tubes.

(4) The aberration increases with increasing focal length of the lens, but it decreases with increasing image distance. Klemperer (92), gives a relation between the spherical aberration coefficient, C_f, and focal length, f, as

approximately $C_f \propto f^{2.7}$. Thus, the lens system should be designed with the shortest possible focal length in order to reduce the spherical aberration.

Many of the above factors were taken into account in the design of the present Einzel lens. It was decided to construct a uni-potential lens with the outer electrodes at the same potential as the ion source aperture and with the dimensions such that the spherical aberration was minimum. Furthermore, allowance has to be made for the restrictions imposed by the overall length and diameter permissible in the analyser chamber. This also produced some difficulty with providing suitable insulators capable of standing up to 10 kV. The electrodes were made of stainless steel and having an aperture diameter of 3.5 mm. The central electrode was of length of 5 mm and the separation between the electrodes was 3.5 mm.

The Einzel lens was then mounted onto the source using two stainless rods fixed into a supporting ring attached to the source. This ensured accurate alignment of the lens with the exit aperture of the source. In addition a short stainless steel tube, length 15 mm and internal diameter 2 mm, was mounted near to and central with the source aperture to collimate the ion beam. Preliminary tests on the focussing of the ion beam were made using a fluourescent screen but final adjustments were made by ion sputtering a gold film evaporated on to a glass substrate.

4.2.3 Electro-magnet

The influence of magnetic fields on the saddle field ion sources has already been reported by Rushton et al (66). The force on the electron of velocity, v, due to a magnetic field, B, is given by:

$$F = e\,(B \wedge v)$$

In the case of the spherical ion source, the axial velocity of the electrons, v_y, is much greater than v_x and v_z. Hence we would expect the greatest perturbation of the source to be due to the forces F_x and F_z:

$$\text{Where} \quad F_x = e\,(B_z \wedge v_y)$$

$$F_z = e\,(B_x \wedge v_y)$$

The plane (x-z) is the plane of the anode and of course this will be perpendicular to the direction of the beam and hence will be in the same direction as the strongest component of the field from the analysing magnet.

Preliminary experiments showed that perturbation of the discharge in the source arises if the field in the x-z plane exceeds 0.1 mT. In the earlier measurement of Clark et al (79) with the cylindrical source they overcame this by placing the magnet about 2 m from the source. However they were able to make use of an existing accelerator at Manchester University in which they accelerated the ions by a further 50 kV. This had the further advantage that the mass resolution was increased. However with the present work, which is only concerned with the spherical source, the energy spread of the ions is much less, and thus adequate resolution was expected without the need for further acceleration of the ions.

In designing the magnet suitable for these measurements, it was shown that, for example, the radii of curvature for both single and double charged argon ions at 5 keV were about 0.45 and 0.32 m respectively using a magnetic field of 0.15T. These conditions in the proposed analyser would give a separation between Ar^+ and Ar^{2+} of about 1 cm at a distance of 21 cm from the source. Thus in the present work a field of about 0.2T was sufficient as all the other gases to be studied are of lower mass number.

An existing electro-magnet consisting of 500 turns of resistance 7Ω was modified to include two rectangular pole pieces made from Swedish iron in order to increase the area of the magnetic field. The field between the two pole pieces, measured with a Hall probe, is shown as a function of solenoid current in figure 4.6(a). The curve shows the onset of saturation at about 0.15T but no fields were required greater than this value. The field at 3.5 amp as a function of distance from the edge of the pole pieces is given in figure 4.6(b).

The focussed ion beam enters the uniform magnetic field, B, within the rectangular pole pieces, 6x8 cm, being 2.5 cm apart. As it was planned to position the ion source at a distance of about 7 cm from the pole pieces it was necessary to reduce the field from the value of 5 mT to about 0.1 mT. This was satisfactorily achieved by using a μ-metal screen containing a small hole in line with the source aperture.

Preliminary measurements showed that the resolution was very poor and experiments were undertaken to improve this by including a horizontal slit at the centre of the analyser tube. A compromise between resolution and sensitivity was eventually achieved by using a slit of width 1.4 mm. This is illustrated in figure 4.7 which shows spectra for argon in figure 4.7(a) without and 4.7(b) with a slit.

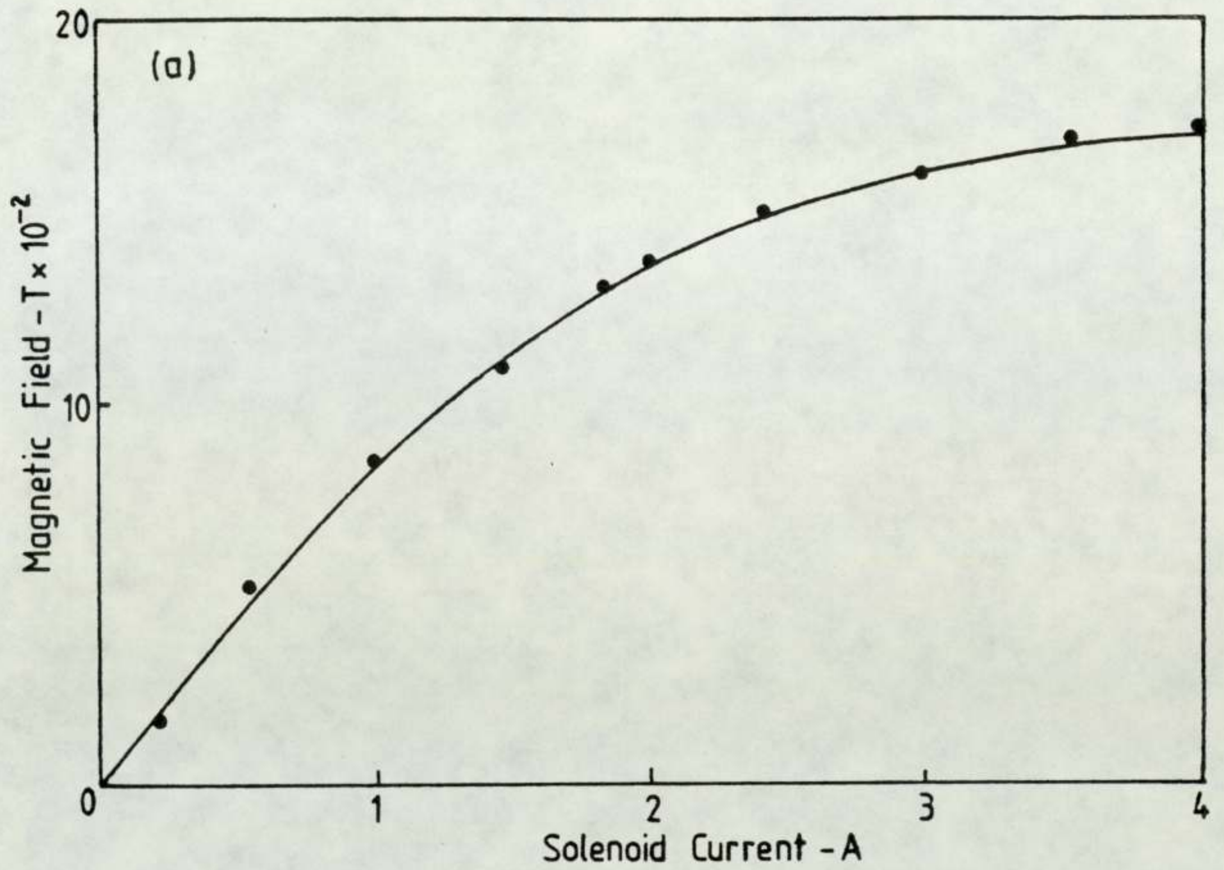

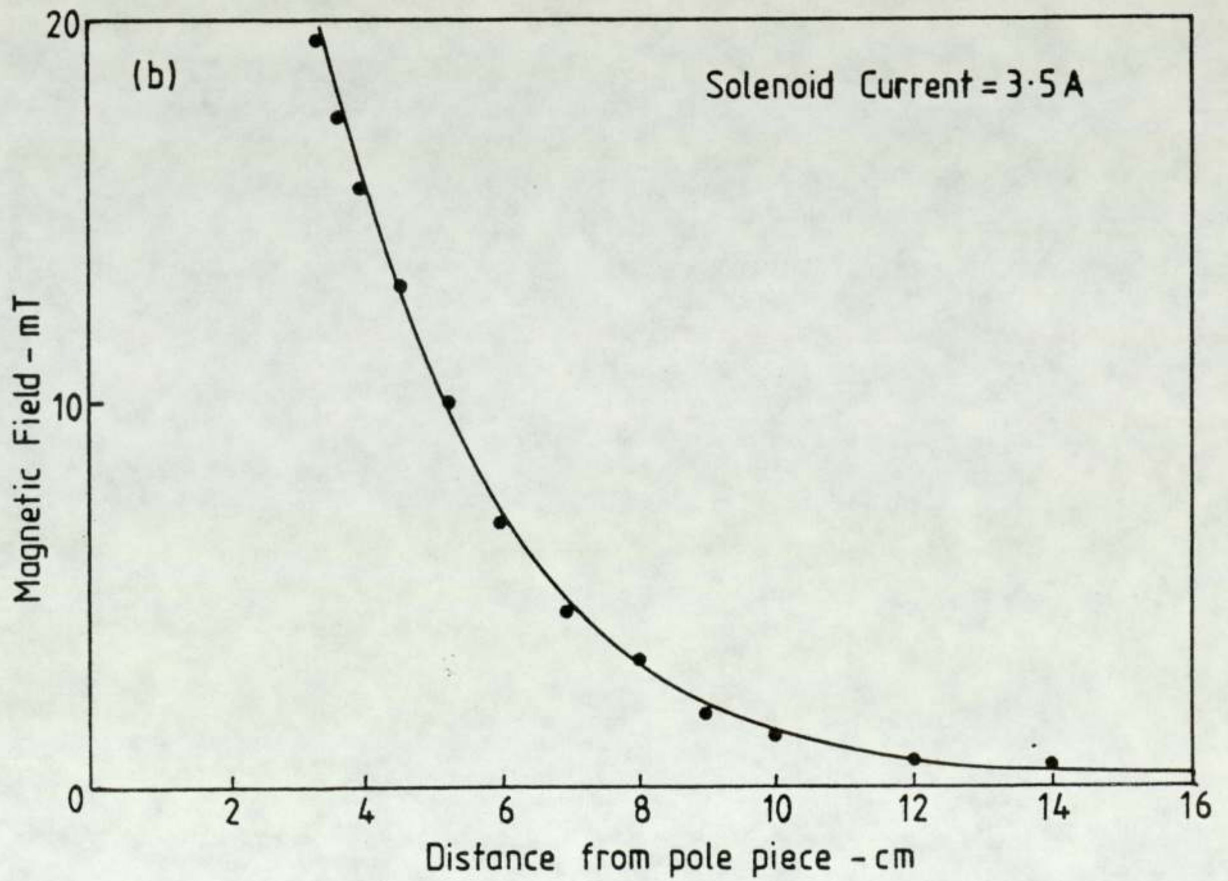

Figure 4.6 Calibration of the electro-magnet

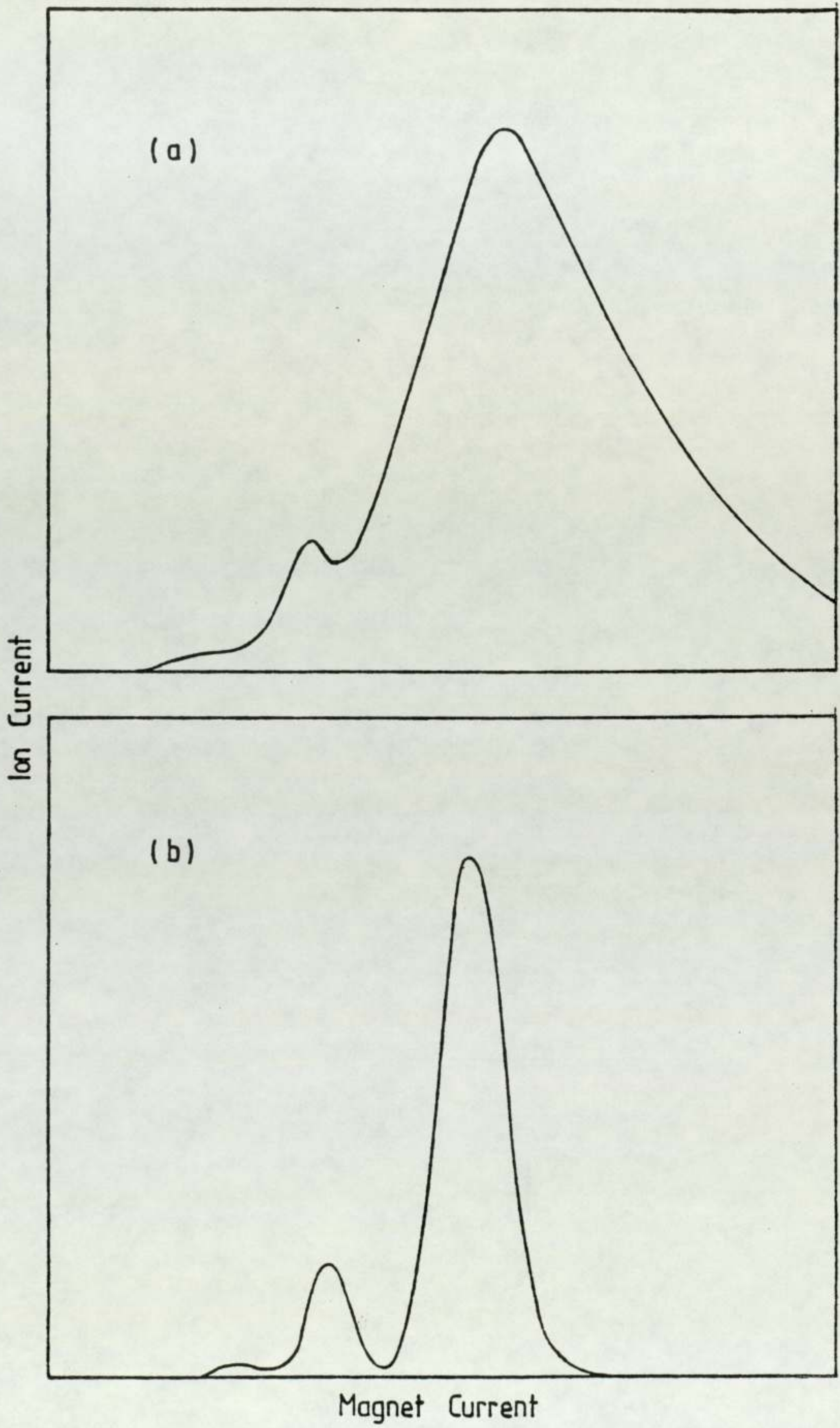

Figure 4.7 Spectra for argon (a) without the slit and (b) with the slit

4.2.4 Recording of the spectra

The ion beam, i_F, was monitored by an earthed Faraday cup placed at an angle of about 7° to the central axis with a screen electrode, biased at -14V, to suppress the secondary electrons. The spectra were taken on an X-Y recorder. The voltage developed by i_F across a 1 MΩ resistor controlled the Y deflection and the voltage developed by the magnetising current, i_m, across a 1Ω resistor controlled the X deflection. The spectra were taken by manually controlling the voltage on the magnet power supply and it was possible to record a complete spectrum in less than 10 seconds.

4.3 Calibration of the spectra

Although this ion source is mainly used with argon it was proposed to include the study of other gases which are sometimes used with this source, e.g. hydrogen, helium, neon, nitrogen, oxygen and argon. It is possible to calculate the deflection of any given ion in a known magnetic field. However this cannot be precise because we do not know the variation of the magnetic field outside the pole pieces. Thus it was necessary to calibrate the spectrometer.

If we assume that the ions are accelerated through a potential V, and are deflected in a magnetic field, B, then:

$$E = zeV = \frac{1}{2} mv^2$$

and $$Bzev = \frac{mv^2}{r}$$

where m = mass of the particle

v = velocity

e = electron charge

z = charge state

r = radius of curvature

From which it can be shown that

$$r^2 = \frac{2mV}{B^2 ze} \quad \text{or} \quad B^2 = \frac{2mV}{r^2 ze}$$

Therefore as the Faraday cup is positioned for a fixed value of r (7° to the axis), then a plot of B^2 against m/ze will yield a straight line. The x-coordinate on the spectrum is proportioned to the magnetizing current, i_m, and thus we required the relationship between i_m and B^2 which is shown in figure 4.8.

A typical spectrum for argon with the source operating conditions, I_A = 2.5 mA, V_A = 7 kV, P = 5.5 x 10^{-5} mbar is shown in figure 4.9 which shows peaks corresponding to the ions Ar^+ and Ar^{2+}. Similar spectrum were recorded for the other gases for V_A = 4, 5, 6 and 7 kV and the variation of $^m/_{ze}$ as a function of B^2 is shown in figure 4.10, which shows the ions, H_2^+, He^{2+}, Ne^{2+}, N^+, O^+, Ar^{2+}, Ne^+, N_2^+, O_2^+, Ar^+, although of course the N^+ peak may also include a proportion of N_2^{2+} ions.

The error bars show that the uncertainty in B^2 increases with increasing field but at all anode voltages there is a good linear relationship between $^m/_{ze}$ and B^2 and all lines pass through the origin indicating any absence of any systematic error.

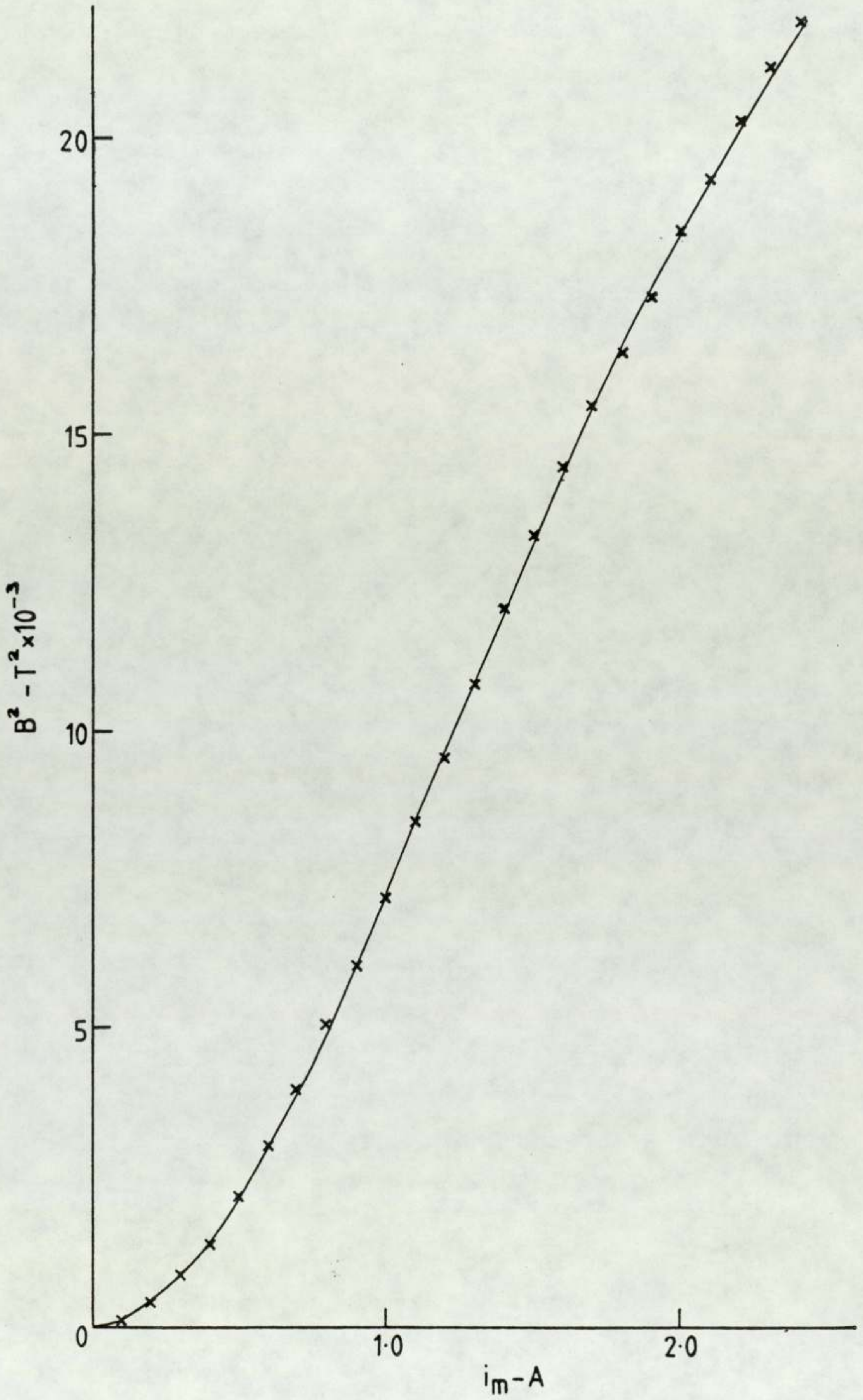

Figure 4.8 Relationship between i_m and B^2

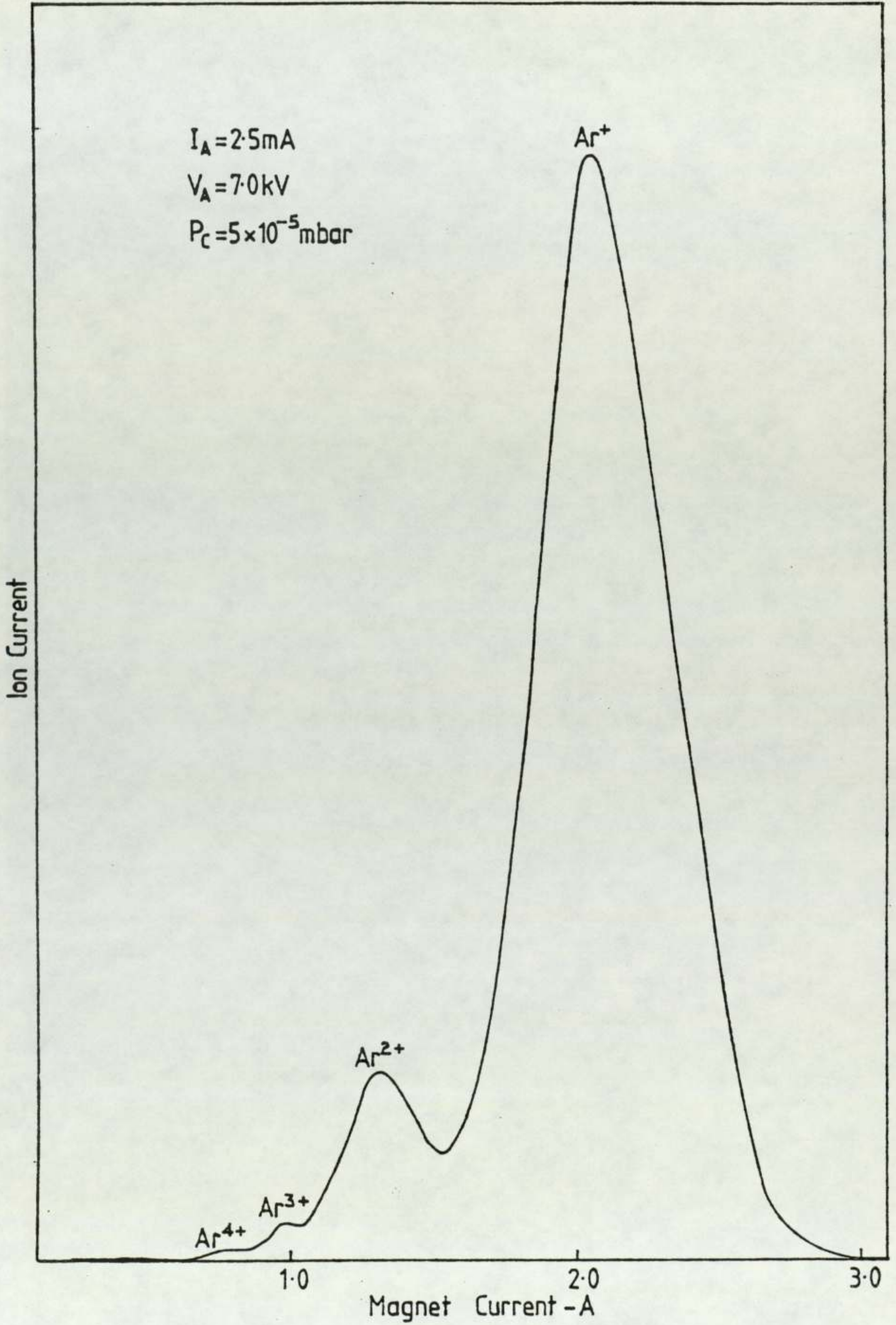

Figure 4.9 A typical spectrum for argon

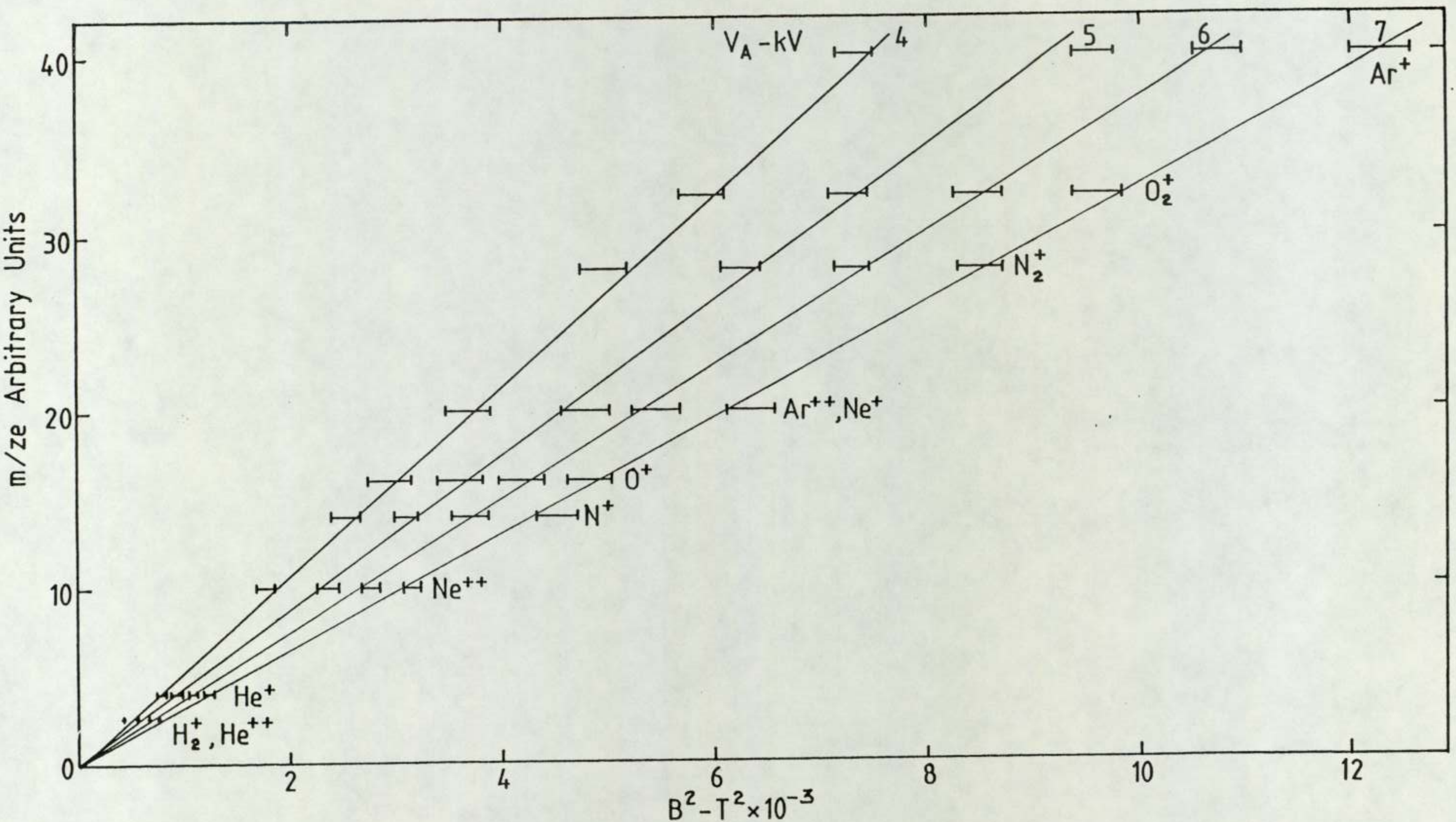

Figure 4.10 m/ze vs. B^2 for various gases at different voltages

4.4 Ion spectra for various gases

Figure 4.11 shows a number of spectra for argon for V_A = 6 kV and I_A = 2 mA with the Einzel lens voltage, V_i, varying from 0.8 to 4.5 kV. It is clear from this figure that the position of the two peaks corresponding to Ar^+ and Ar^{2+} is independent of the Einzel lens voltage, thus providing evidence that the energy of the ions is not changed by the focussing action of the lens. However the focal length of the lens is a function of V_i, and thus it was necessary to optimise this to give the maximum ion current i_F in the Faraday cup which was always placed at a constant distance from the lens.

Figure 4.12 shows the variation of i_F with V_i using argon with a 1.5 mm diameter aperture in the Faraday cup using an anode voltage of 7 kV and the cup positioned to receive the total ion beam with zero magnetic field. The figure shows that the maximum current occurs for a value of V_i = 3.4 kV. Thus during the recording of all spectra, when V_A was changed the Einzel lens voltage was adjusted to give the maximum ion beam current.

A large number of spectra have been taken for all gases although, as indicated earlier, a more detailed study was made with argon. Examples of spectra have been selected in order to illustrate the variation of the different charge state as a function of gas, anode voltage, anode current and chamber pressure. Figure 4.13(a), (b) and (c), show the spectra for argon at constant voltage, pressure and current respectively. In figure 4.13(a) the pressure varies from 6.5×10^{-5} to 1.4×10^{-4} mbar with the corresponding anode current varying from 1.7 to 3.0 mA, for V_A = 6 kV. The main peak corresponds to Ar^+ and there is clear evidence of the ion Ar^{2+}, but only very small proportions of Ar^{3+} and Ar^{4+} can be seen. The main peak occurs at a constant magnetising current, showing that the energy of the ions is constant. In figure 4.13(b), in which the pressure is constant,

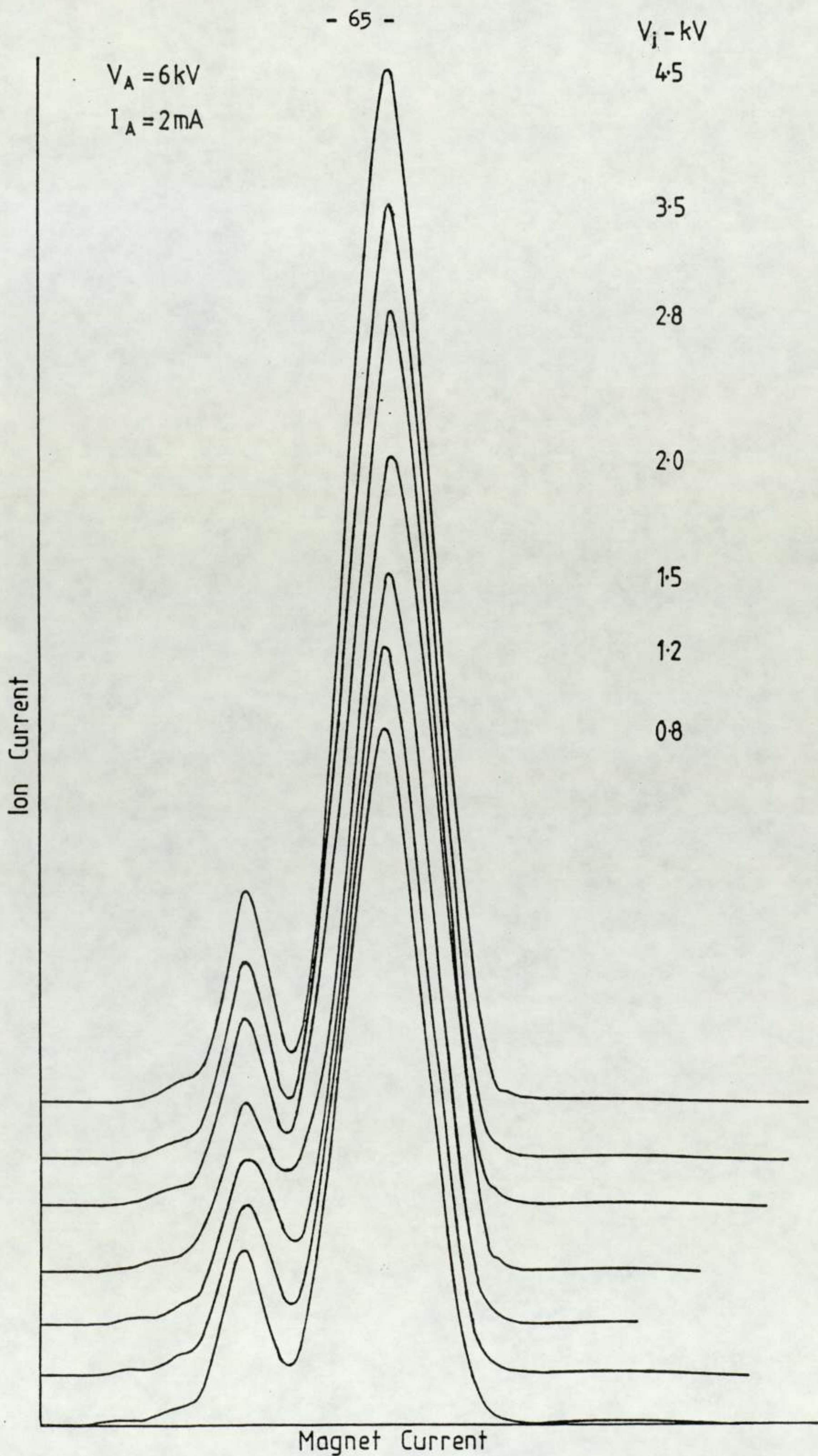

Figure 4.11 Argon spectra with the Einzel lens voltage varying from 0.8 to 4.5 kV

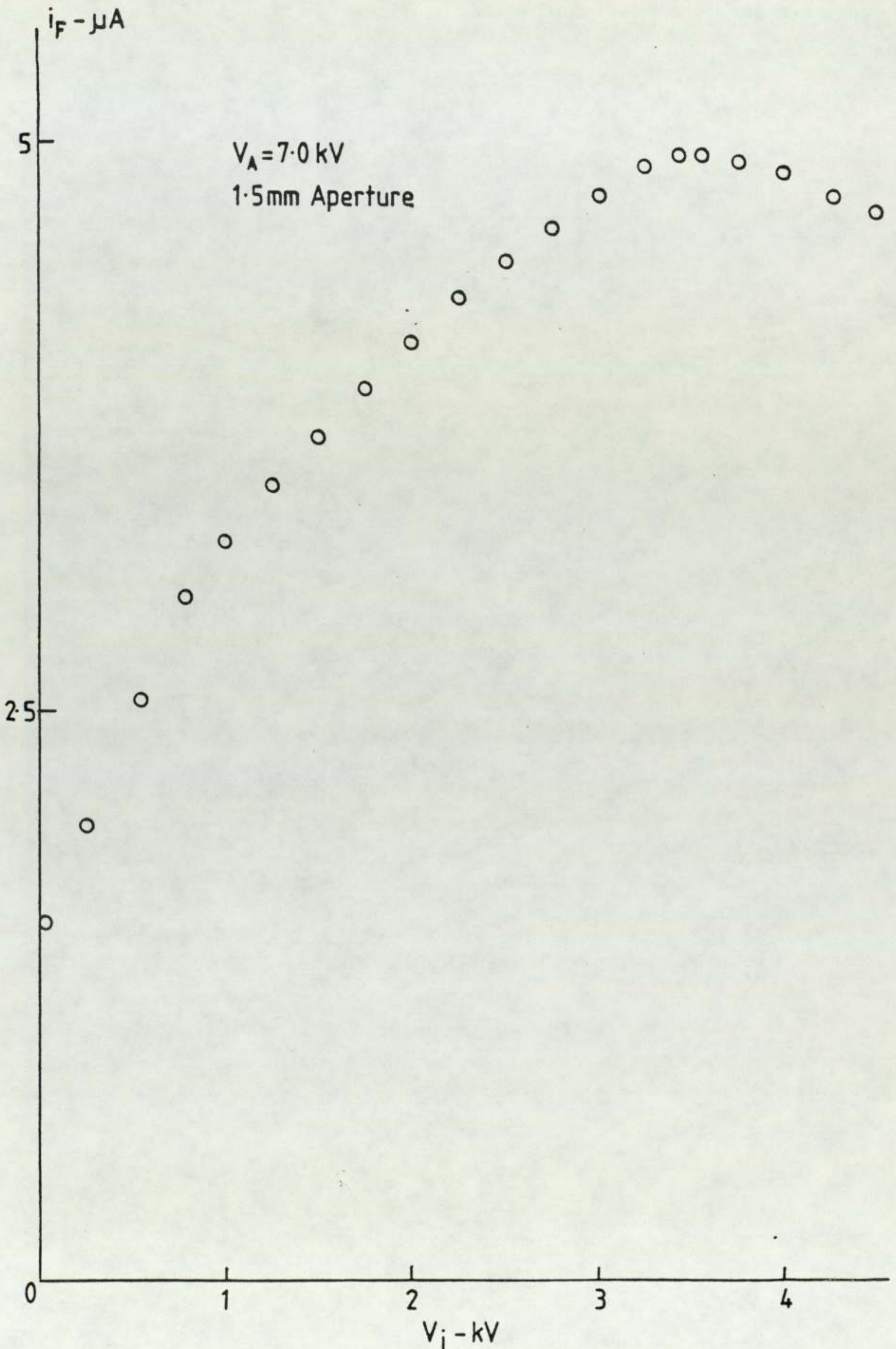

Figure 4.12 The variation of i_F with V_i using argon with a 1.5 mm diameter aperture in the Faraday cup

I_A-mA $V_A = 6{\cdot}0$ kV Pc-mbar $\times 10^{-5}$

Ar^{+}

I_A-mA	Pc-mbar $\times 10^{-5}$
1·7	6·5
1·8	7·0
1·9	7·5
2·0	8·0
2·1	8·5
2·2	9·5
2·3	10·0
2·6	12·5
3·0	14·0

Ion Current

Ar^{2+} Ar^{3+} Ar^{4+}

0 1·0 2·0

Magnet Current-A

ASTON UNIVERSITY LIBRARY

Figure 4.13(a)

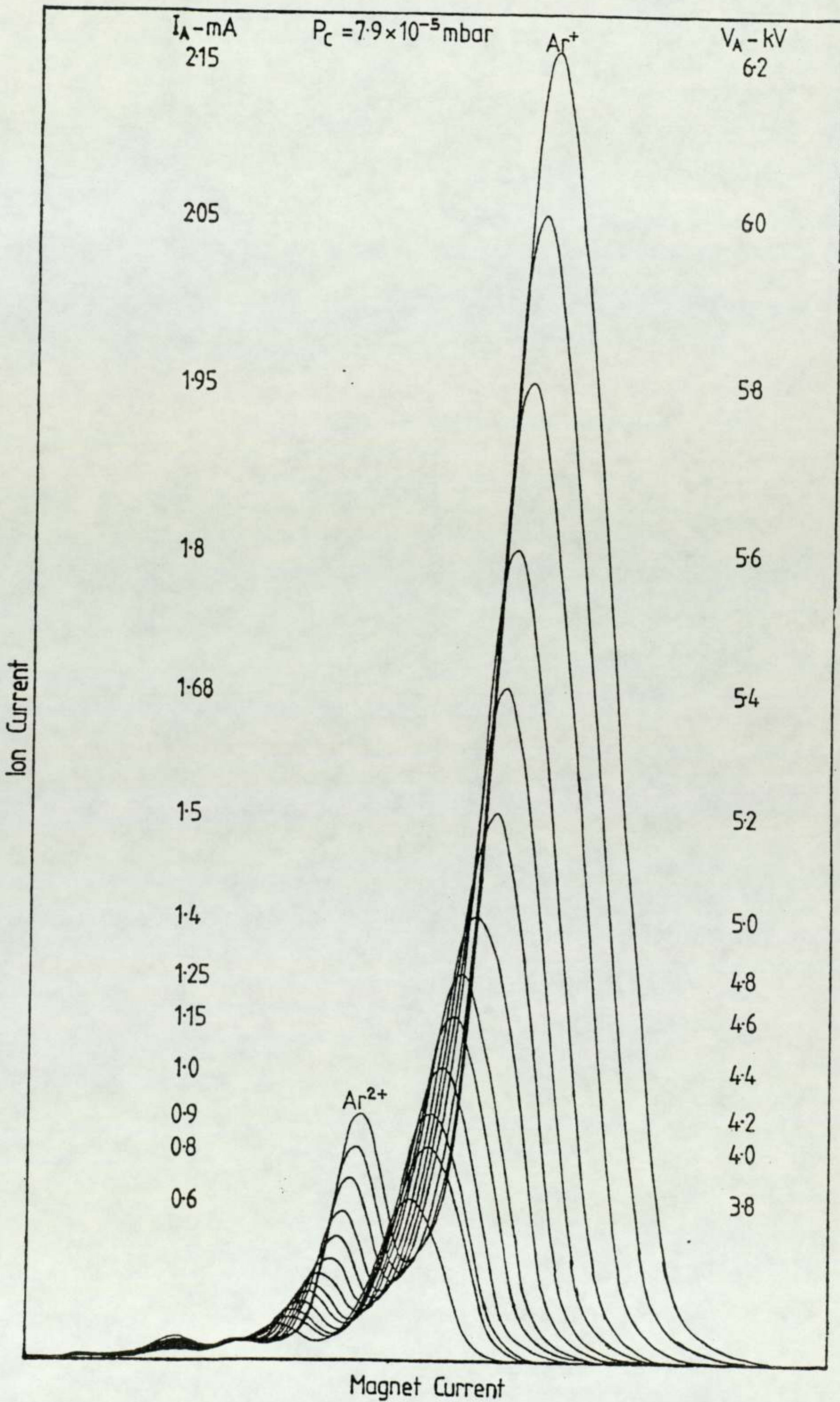

Figure 4.13(b)

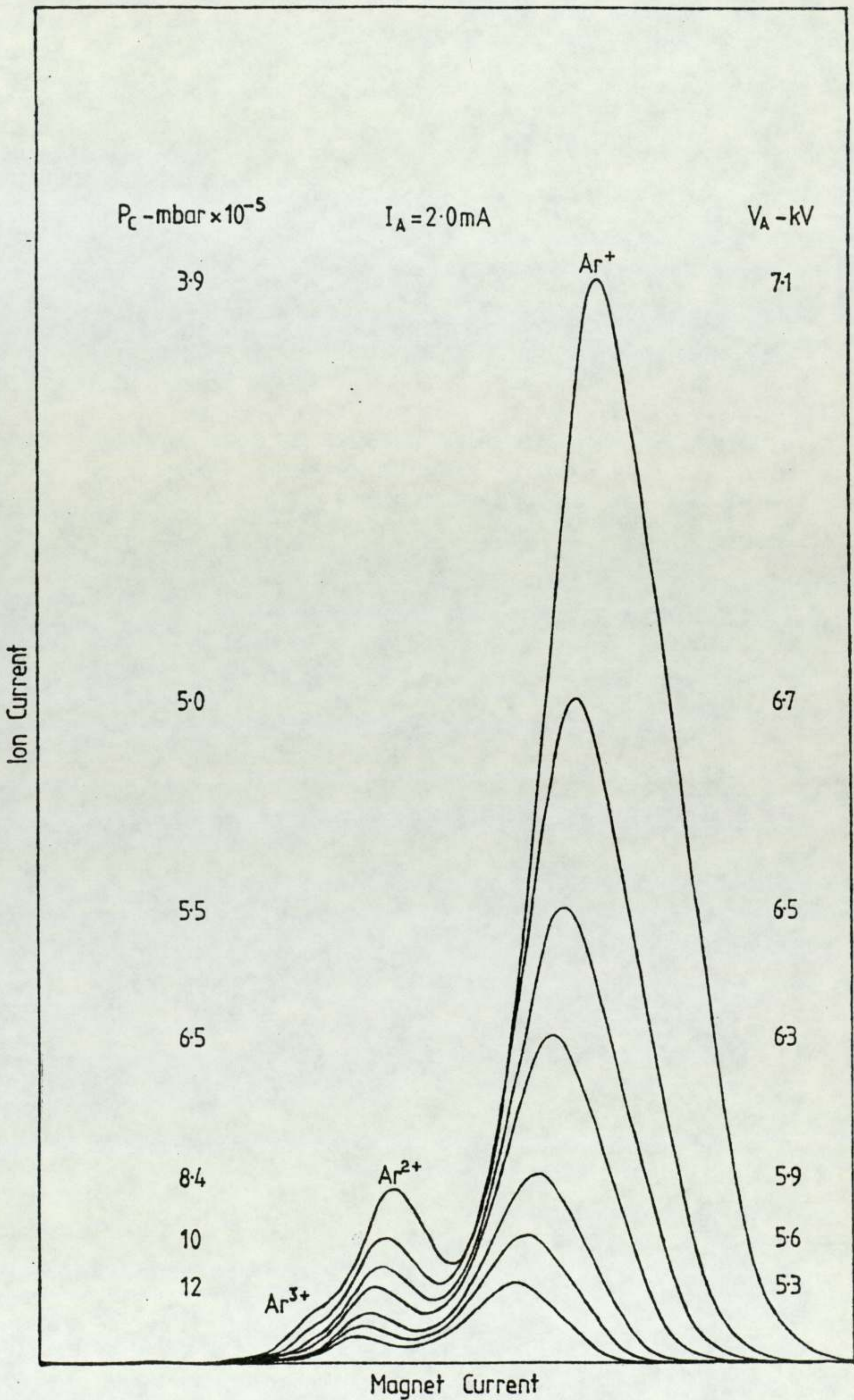

Figure 4.13(c)

all peaks are displaced to the right as the anode voltage and hence the ion energy increases. The combination of varying pressure and voltage is shown in figure 4.13(c) for a constant anode current of 2 mA.

Similar spectra are shown for nitrogen in figures 4.14(a), (b) and (c) at 6 kV, 2×10^{-5} mbar and 2 mA respectively. The main peak corresponds to N_2^+ and the second peak to either N_2^{2+} or N^+ and there is evidence of a small peak to the left of the spectrum indicating the presence of N_2^{3+}. In addition there is an unresolved peak at higher magnetic fields which is possibly an impurity oxygen peak although it may include the nitrogen isotope of mass 29 which is known to occur in significant proportions.

Spectra taken at constant pressure are illustrated in figure 4.15(a), (b), (c) and (d) for hydrogen, helium, neon and oxygen respectively. In the case of hydrogen the molecular and atomic ions can be seen, and for helium the main peak is He^+ with a very small proportion of He^{2+}. In the neon spectra a significant fraction of the Ne^{2+} ion can be seen but in addition there is evidence of the neon isotope of mass 22. In figure 4.15(d), the main peaks for oxygen are as expected O_2^+, and O^+ or O_2^{2+}.

Clark et al (79) measured the charge states for nitrogen, helium and hydrogen using the cylindrical source, and their spectra were similar to those reported in this work for hydrogen and helium. However they found that the dominant species for argon and nitrogen were Ar^{2+} and N^+, where as in the present work the dominant species were Ar^+ and N_2^+. Of course this could be due to the different source geometries, but this seems unlikely as the ionisation cross-sections for Ar^{2+} and N^+ are less than for Ar^+ and N_2^+. It is possible that they identified the peaks incorrectly because their calibration curve was not as satisfactory as in the present work.

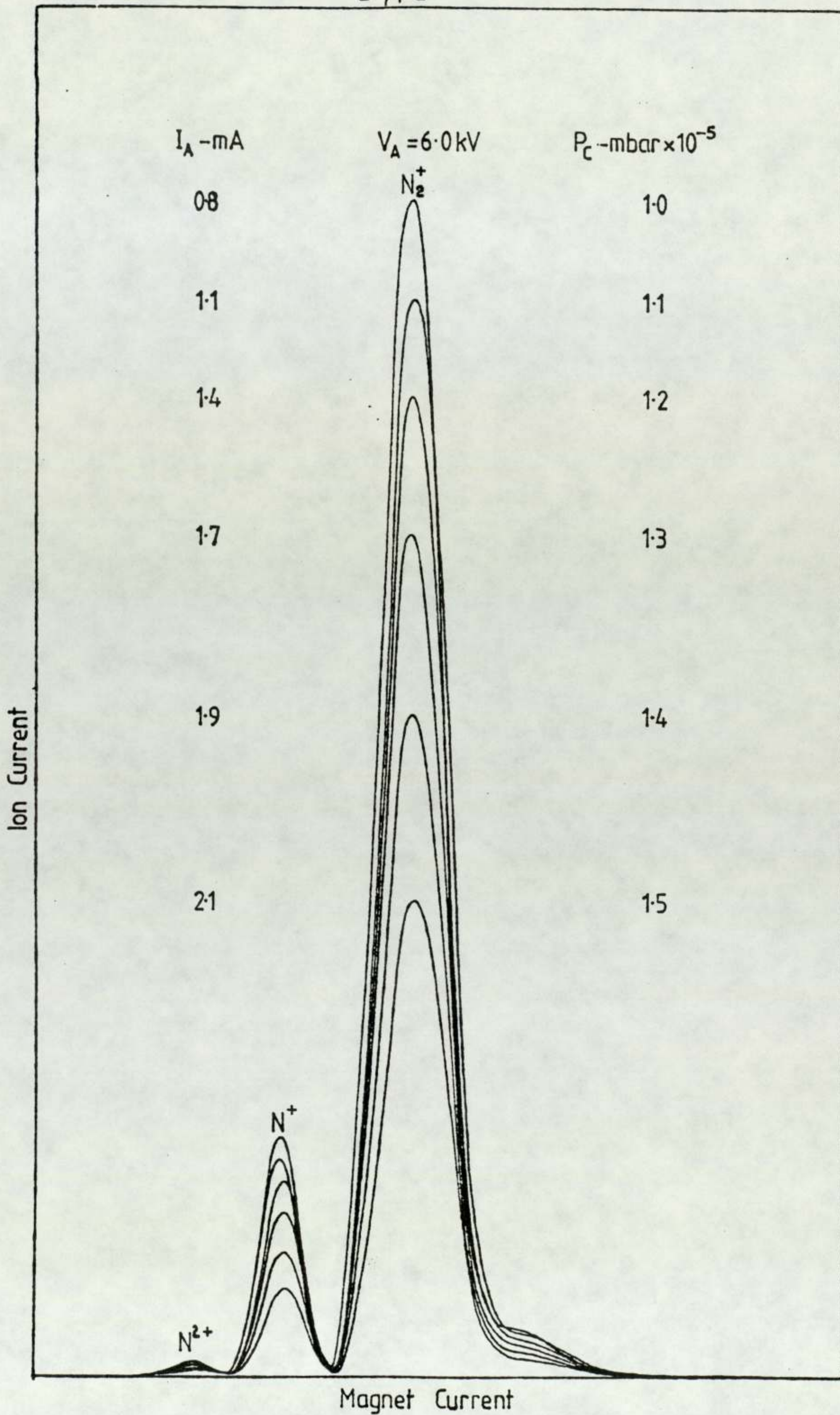

Figure 4.14(a)

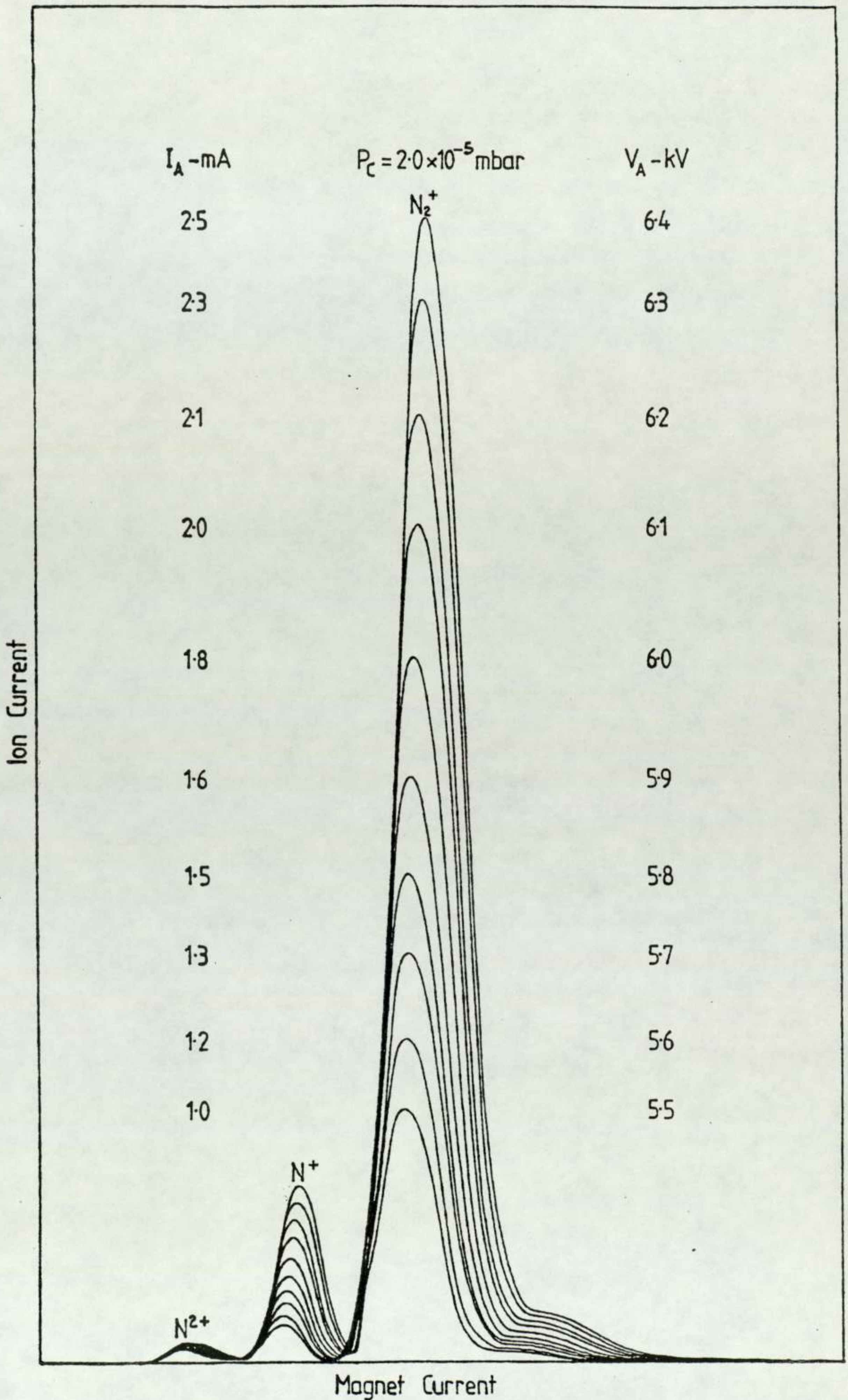

Figure 4.14(b)

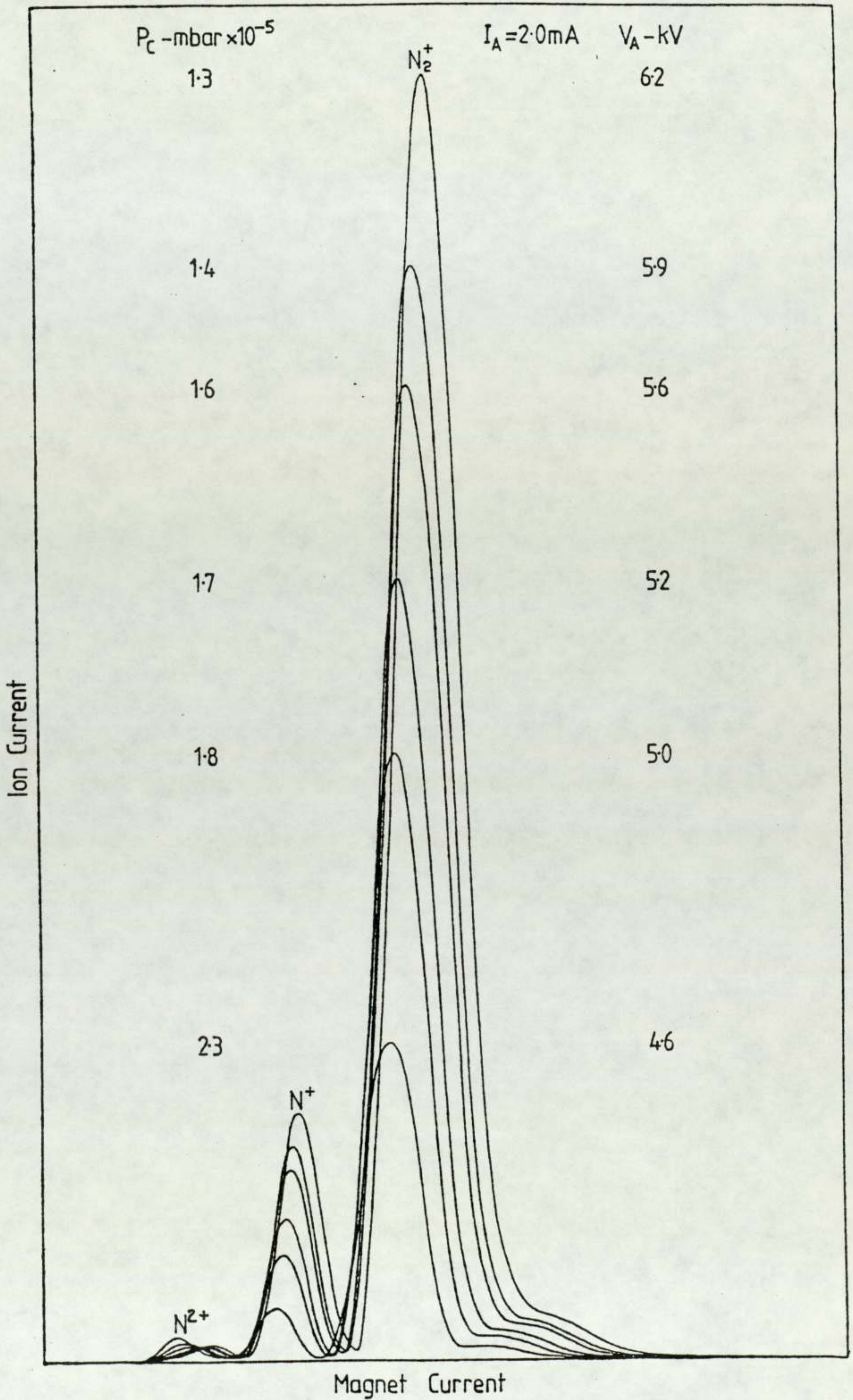

Figure 4.14(c)

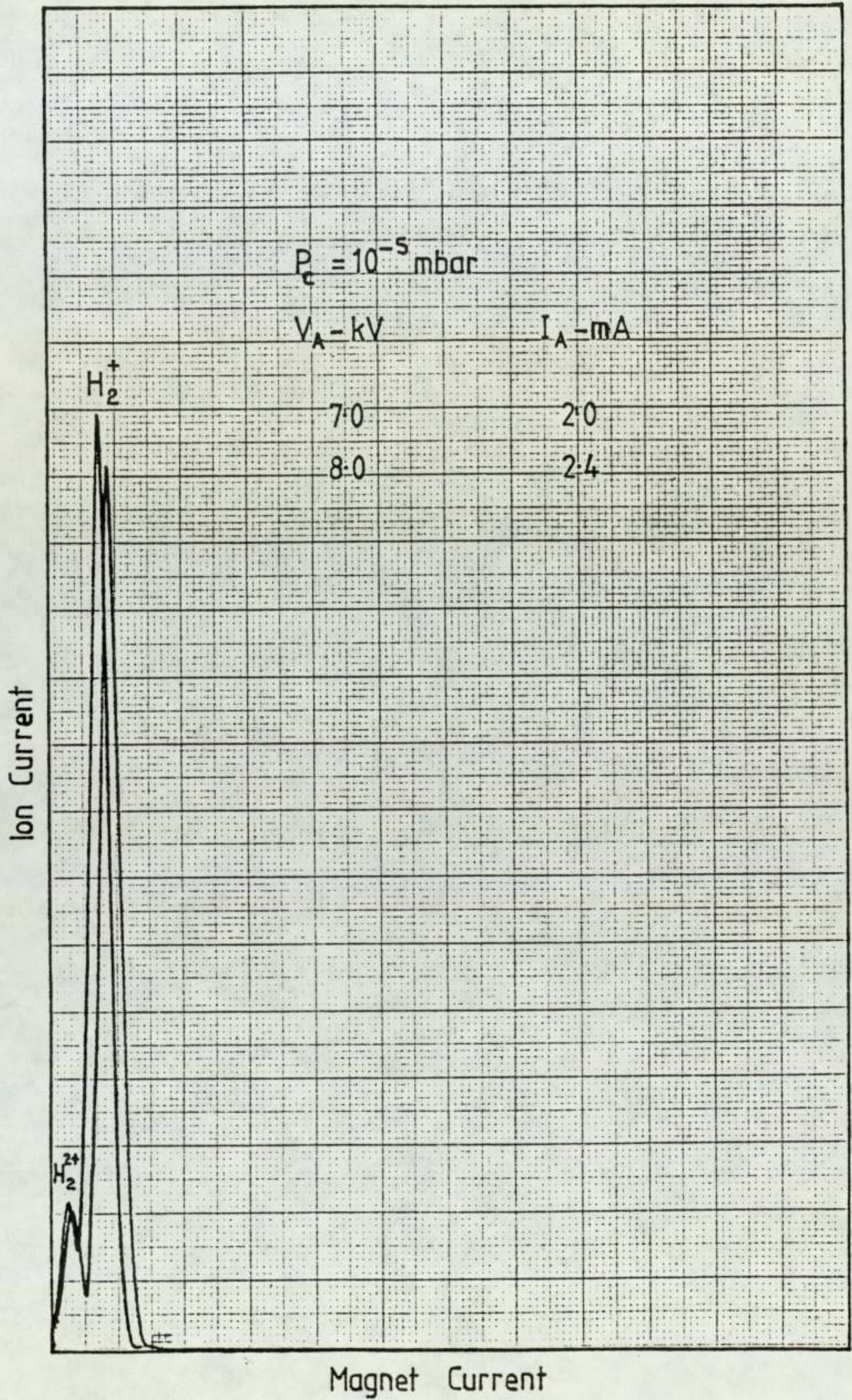

Figure 4.15(a)

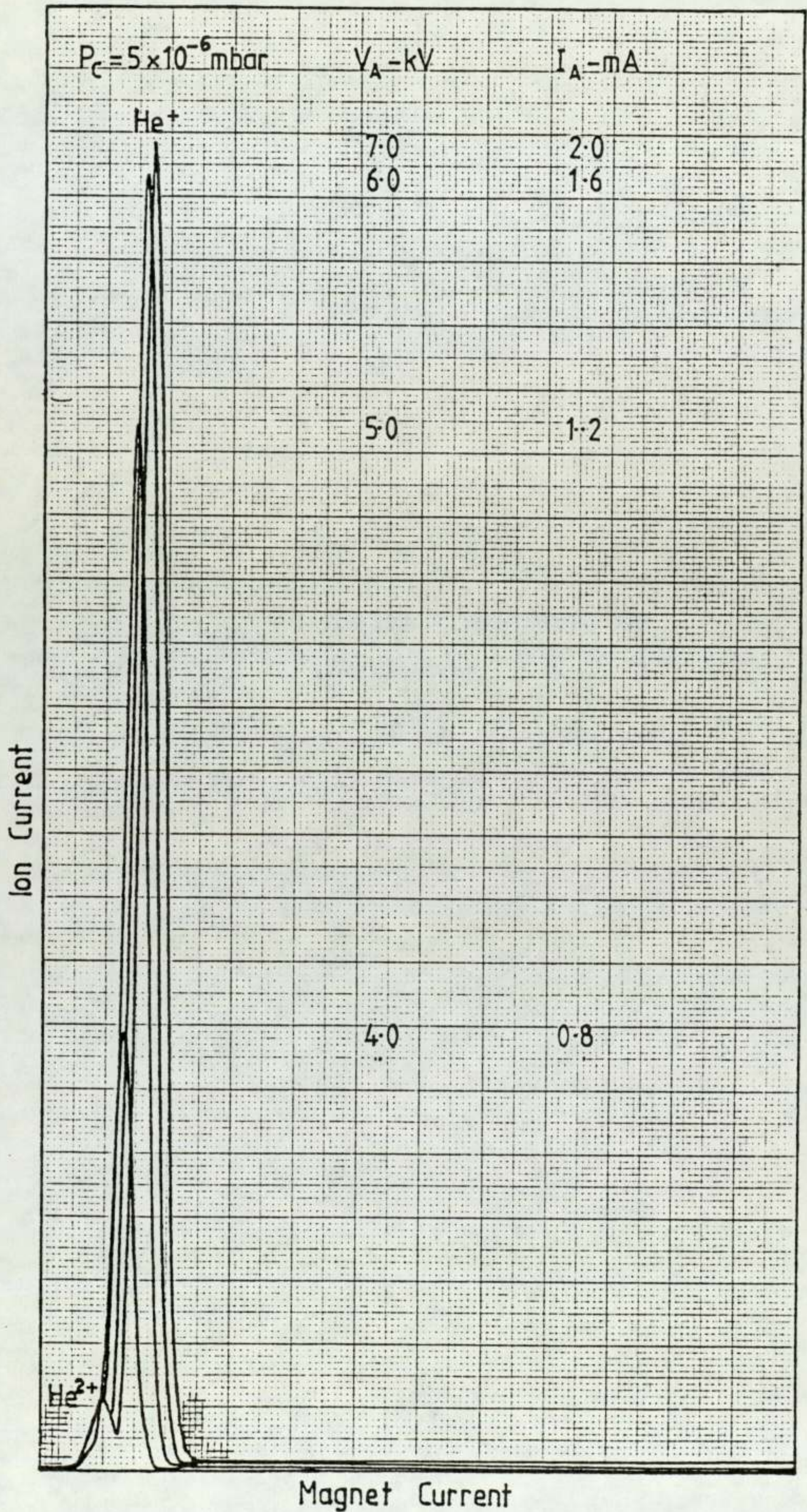

Figure 4.15(b)

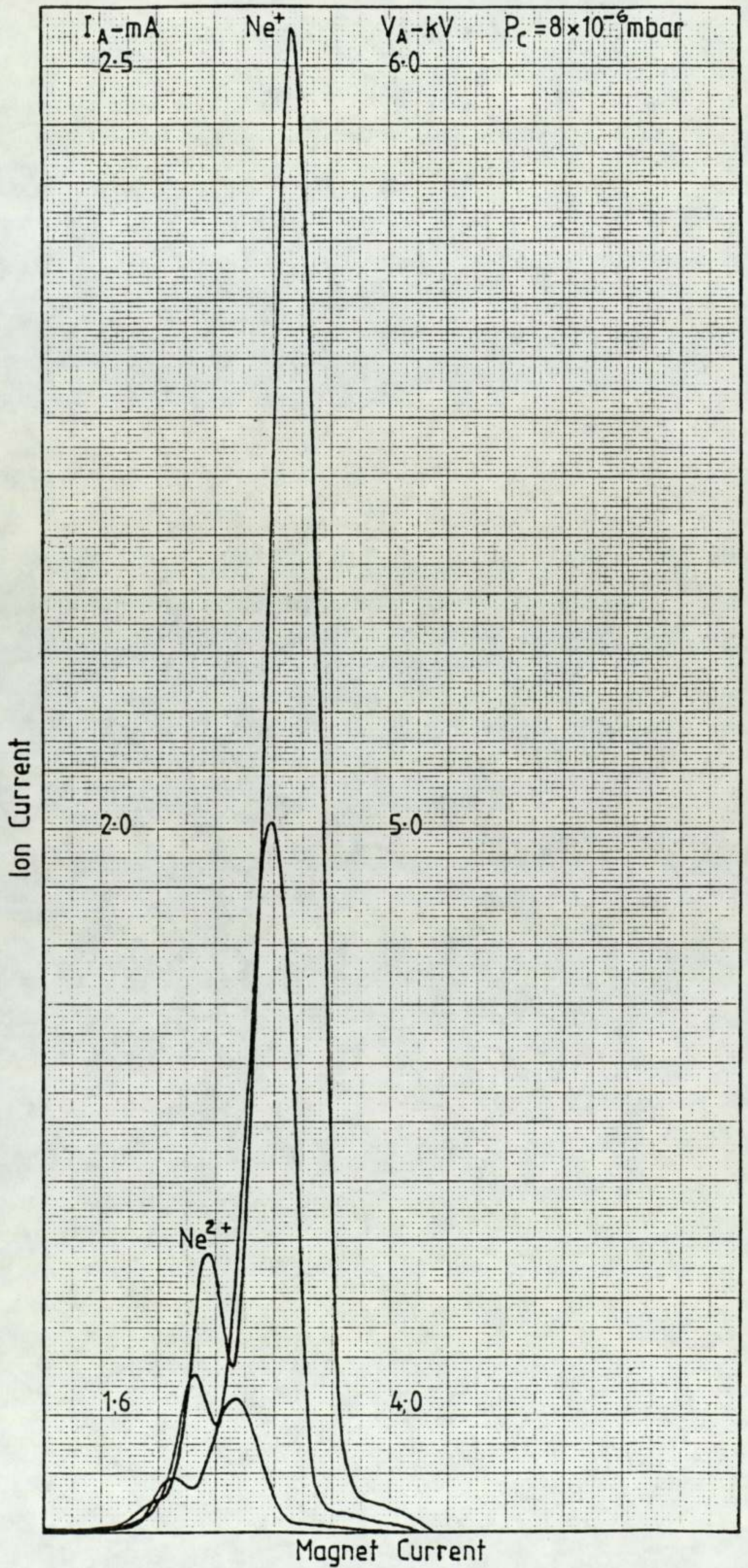

Figure 4.15(c)

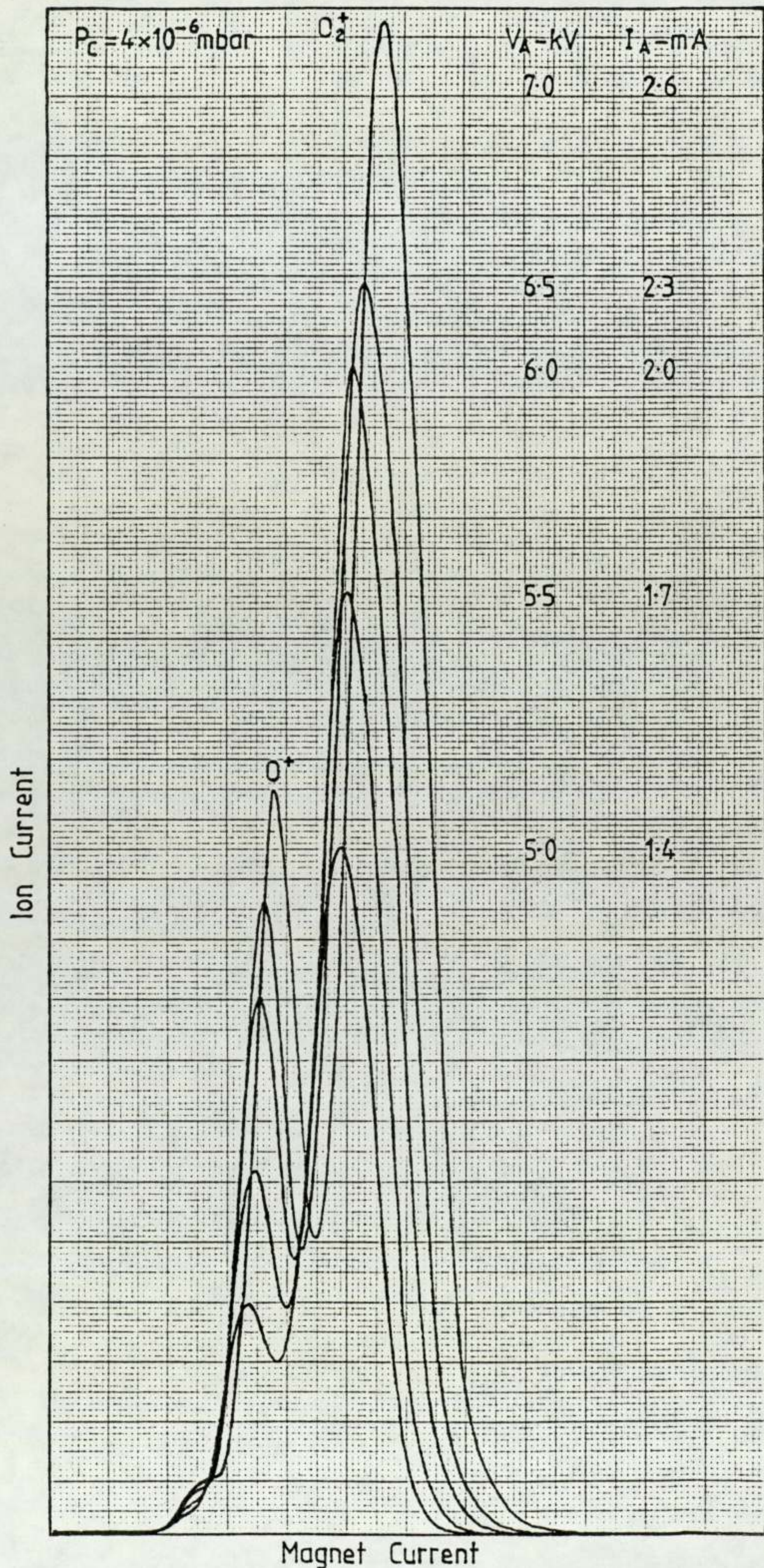

Figure 4.15(d)

4.5 Analysis of the spectra for argon

A large number of spectra have been recorded for argon for different operating conditions and an analysis of the spectra has been made to determine the percentage, P_{n1}, of the higher charge states for n = 2 and 3, in terms of the single charged ions.

This was done by assuming that the ion current was proportional to the height of the peak, and thus it was only necessary to measure the various peak heights. This was considered reasonable for the Ar^{2+} ion because it was clearly resolved from the single charged ion. However this was not the case with the Ar^{3+} ion and thus the uncertainty in P_{31} was much greater than for P_{21}. In both cases the uncertainty in P_{n1} increases as the pressure increases and the ion beam current decreases.

Of course in order to determine the actual number of the ions it was necessary to divide the peak height by 2 for the Ar^{2+} ions and by 3 for the Ar^{3+} ions.

A selection of the values of P_{n1} obtained from a number of the spectra are given in Tables 4.1 and 4.2. In each case the tables show a number which identifies the spectra, the chamber pressure, anode current, anode voltage and the values of P_{21} and P_{31}. It should be pointed out that values of P_{31} are not always included, when the pressure was high and the peak heights too small to make reliable measurements.

In Table 4.1, inspection of the values of P_{21} and P_{31} show that when the chamber pressure is constant, the percentage of high charge state is approximately constant for all values of anode voltage.

In contrast to this, Table 4.2 shows that when the voltage is kept constant, the values of P_{21} and P_{31} increase as the pressure increases. This is illustrated in figure 4.16, which shows the variation of P_{21} and P_{31} as a function of pressure. The figure also

shows that the error bars increase as the pressure increases. Over the pressure range $4x10^{-5}$ to $1.4x10^{-4}$ mbar, the percentage of doubly charged ions increases from 5 to 16% and for the Ar^{3+} ion the percentage increases from 0.5 to 1%.

These results will be discussed in more detail in the next Chapter when an attempt will be made to relate the charge state and the energy of the ions to the nature of the discharge and the fundamental processes involved.

Spectrum No.	P_c (mbarx10^{-5})	I_A (mA)	V_A (kV)	P_{21} %	P_{31} %
1	14	1.0	3.5	16.2	
		1.4	4.0	16.0	
		1.6	4.5	15.8	
		2.0	5.0	15.5	
		3.0	6.0	15.9	
2	12	1.0	3.5	14.8	1.1
		1.3	4.0	15.1	0.9
		1.8	5.0	14.6	0.9
		2.7	6.0	14.9	1.0
		3.0	6.7	14.2	1.0
3	10	1.2	4.0	12.3	0.8
		1.7	5.0	12.6	1.1
		2.0	5.5	12.9	0.9
		2.3	6.0	12.7	0.9
		3.0	7.0	13.0	0.8
		3.5	7.5	12.8	0.9
4	8.9	1.0	3.8	11.0	0.7
		1.4	4.4	10.9	0.8
		1.6	4.8	11.0	0.8
		1.8	5.2	11.3	0.8
		2.0	5.6	11.6	0.7
		2.2	6.0	11.9	0.7
		2.5	6.5	11.5	0.8
		2.8	7.0	11.2	0.9

Table 4.1

Spectrum No.	P_c (mbarx10^{-5})	I_A (mA)	V_A (kV)	P_{21} %	P_{31} %
5	7.9	0.7	3.8	9.8	0.6
		0.8	4.0	9.5	0.8
		0.9	4.2	9.4	0.8
		1.0	4.4	9.8	0.7
		1.2	4.6	10.0	0.9
		1.3	4.8	9.6	0.8
		1.4	5.0	9.5	0.8
		1.5	5.2	9.8	0.9
		1.7	5.4	9.6	0.8
		1.8	5.6	9.7	0.8
		1.9	5.8	9.7	0.9
		2.0	6.0	9.6	0.8
		2.2	6.2	9.7	0.9
6	6.5	0.9	4.6	7.3	0.7
		1.1	4.8	7.1	0.6
		1.2	5.0	7.6	0.6
		1.3	5.2	7.4	0.7
		1.5	5.4	7.9	0.6
		1.7	5.6	7.7	0.6
		1.8	5.8	8.0	0.6
		1.9	6.0	7.7	0.7
		2.1	6.2	7.9	0.5
		2.2	6.4	7.7	0.6
		2.3	6.6	7.9	0.7
		2.4	6.8	8.0	0.7
		2.6	7.0	8.1	0.7

Table 4.1 (Continued)

Spectrum No.	P_c (mbarx10^{-5})	I_A (mA)	V_A (kV)	P_{21} %	P_{31} %
7	5	0.8	5.0	6.6	0.5
		1.0	5.2	6.3	0.6
		1.1	5.4	6.1	0.6
		1,3	5.6	6.3	0.6
		1.4	5.8	6.3	0.5
		1.5	6.0	6.5	0.5
		1.6	6.2	6.3	0.5
		1.8	6.4	6.3	0.5
		1.9	6.6	6.5	0.6
		2.0	6.8	6.8	0.6
		2.3	7.0	6.6	0.5
8	3.8	0.5	5.0	6.0	0.4
		1.2	6.0	5.8	0.5
		1.5	6.5	5.1	0.5
		2.0	7.0	5.0	0.5
		2.8	8.0	5.2	0.4
		3.4	8.5	5.4	0.4

Table 4.1 (Continued)

Spectrum No.	V_A (kV)	I_A (mA)	P_c (mbarx10^{-5})	P_{21} %	P_{31} %
1	4.0	1.5	14.0	15.5	
		1.2	12.5	15.4	
		1.1	11.0	14.3	0.9
		1.0	10.0	13.1	0.8
		0.9	9.0	11.6	0.8
		0.8	8.0	10.0	0.6
2	5.0	2.1	14.0	15.8	
		1.9	12.0	14.1	0.8
		1.8	10.0	12.0	0.8
		1.6	9.0	11.2	0.9
		1.4	8.0	9.0	0.7
		1.3	7.5	9.1	0.7
		1.2	7.0	8.5	0.6
3	6.0	3.0	14.0	15.6	
		2.6	12.5	14.9	
		2.3	10.0	12.5	0.9
		2.2	9.5	12.0	0.9
		2.0	8.5	11.3	0.7
		1.9	8.0	9.4	0.8
		1.8	7.5	9.2	0.6
		1.7	7.0	8.5	0.6
		1.6	6.5	7.4	0.6

Table 4.2

Spectrum No.	V_A (kV)	I_A (mA)	P_c (mbarx10^{-5})	P_{21} %	P_{31} %
4	6.0	3.0	14.0	16.2	
		2.4	11.0	14.1	0.9
		2.2	9.5	12.0	0.8
		2.0	8.6	11.1	0.8
		1.9	7.6	9.3	0.7
		1.8	7.0	8.0	0.6
		1.7	6.4	7.6	0.6
		1.6	5.4	7.2	0.5
		1.5	5.0	6.5	0.5
5	7.0	3.2	12	16.1	1.1
		3.1	11.5	15.0	1.1
		3.0	10.0	13.2	0.9
		2.9	9.0	11.4	0.8
		2.8	8.5	11.5	0.8
6	8.0	3.8	9.0	11.5	0.8
		3.5	7.5	9.5	0.6
		3.1	5.5	7.4	0.5
		3.0	4.0	6.0	0.5

Table 4.2 (Continued)

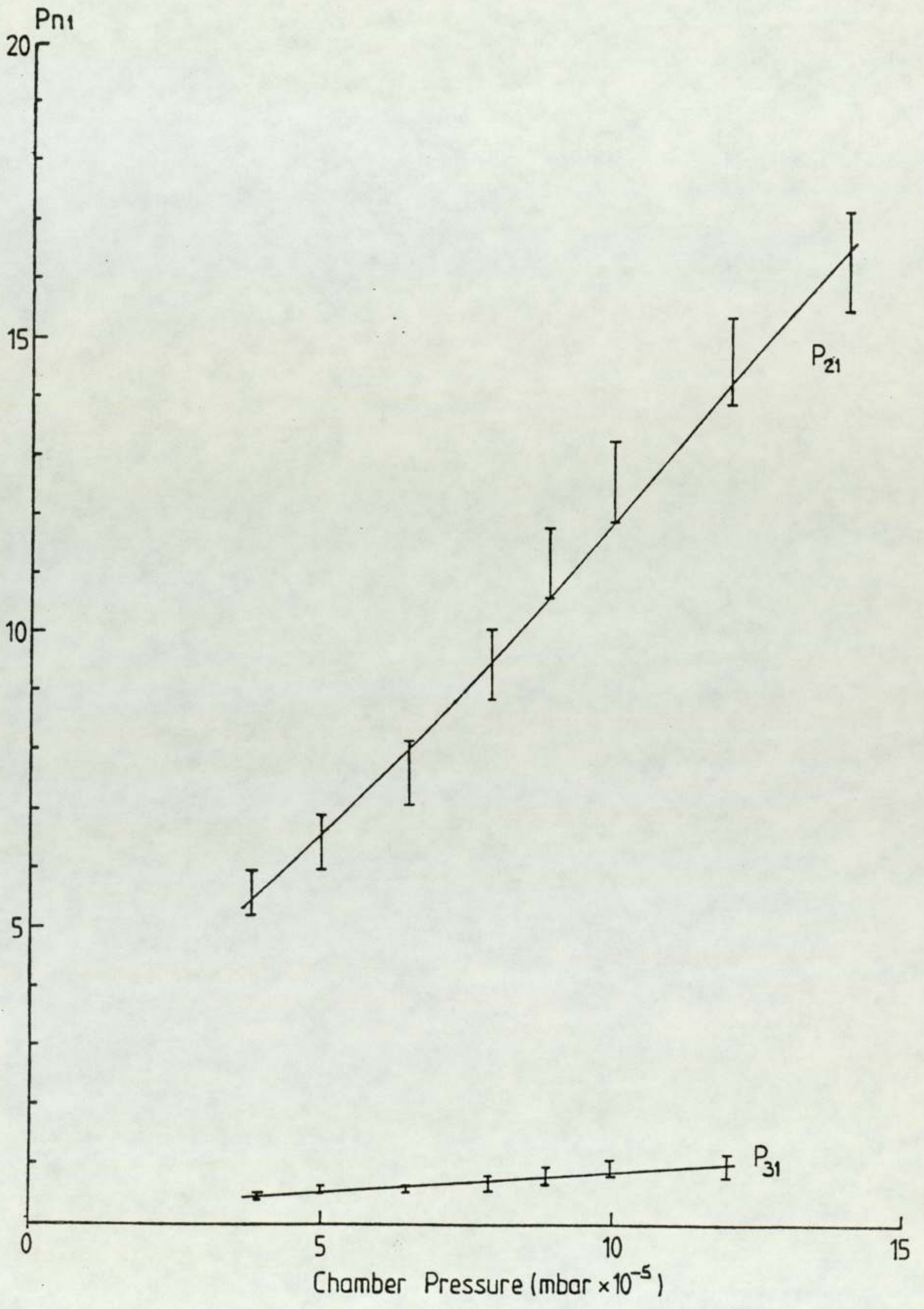

Figure 4.16 Variation of P_{21} and P_{31} as a function of chamber pressure

CHAPTER 5

MEASUREMENT OF THE ION ENERGY FOR ARGON

5.1 Introduction

It is important to have knowledge about the energy of the ions produced by this source, in ordèr to understand the possible mechanisms of the discharge and the processes occurring in the formation of multicharge ions. In addition, this information is essential in many of the applications of the source such as in the measurement of the sputtering yields or etching rates.

As stated previously, Khorrasany and Fitch (6), measured the energy of the ions for severl gases using a retarding field energy analyser, but this technique is unable to distinguish between different charge states when the ions are accelerated by the same potential.

It was decided to measure the energy for only the argon ions not only because this source is mostly used with argon but mainly because the argon spectra is less complex than for instance nitrogen.

The ion energy has been measured in two ways - indirectly using information obtained from the ion spectra and directly using a retarding field energy analyser in conjunction with the magnetic analyser.

5.2 Ion energy measurements

5.2.1 Indirect method

For the magnetic analyser, we have the following equations:-

$$E = \frac{1}{2} mv^2$$

$$Bzev = \frac{mv^2}{r}$$

Hence, $$E = \frac{B^2z^2e^2r^2}{2m}$$

Thus, as m, e and r are constant, we can write

$$E = KB^2z^2 \qquad \text{where} \qquad K = \frac{z^2r^2}{2m}$$

If we take, as an example, the spectrum for argon given in figure 4.13(a), we can obtain the information as shown in Table 5.1.

B (T)	$^E/_K$	z	$^{E_n}/_{E_1}$
0.132	17	1	1.0
0.098	38	2	2.2
0.078	54	3	3.1

TABLE 5.1

This shows approximately that the energy of the ions is proportional to z implying that the ions are accelerated through the same potential.

5.2.2 Direct method

A schematic diagram of the retarding field analyser is shown in figure 5.1. The analyser was positioned in front of the Faraday cup and normal to the ion beam which was again positioned 7° to the central axis. The retarding analyser consisted of two grids separated at distance of 4 mm. The first grid was the retarding grid and the second grid was a screen grid maintained at earth potential in order to shield the Faraday cup from the strong field

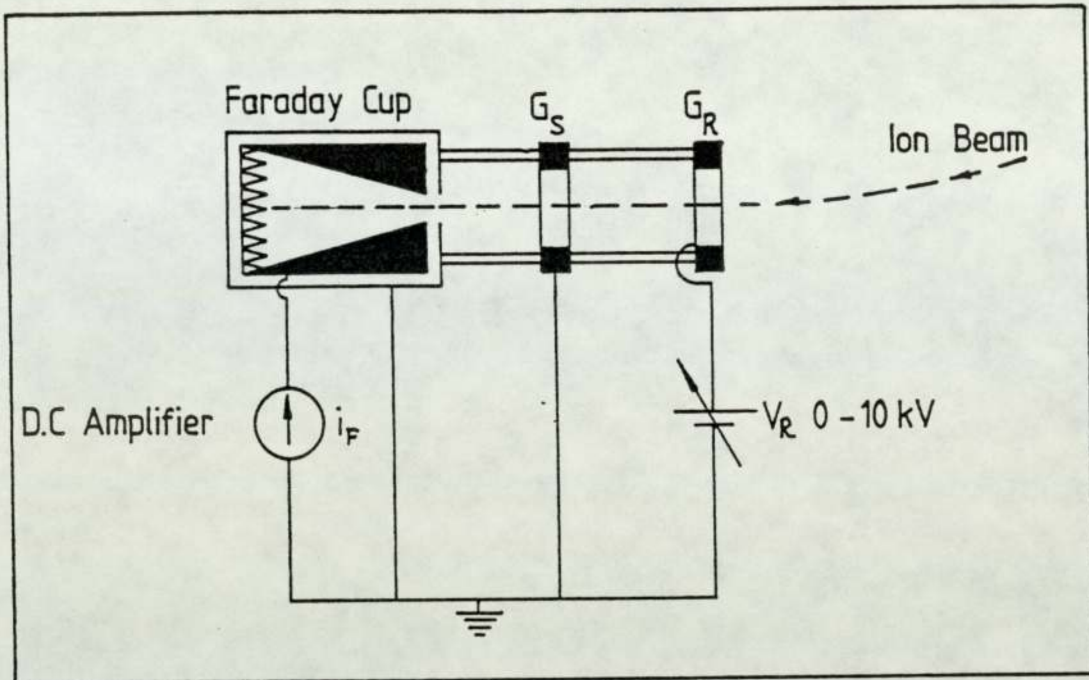

Figure 5.1 Schematic diagram of the retarding field energy analyser

produced by the retarding grid, thus avoiding the extraction of secondary electrons from the Faraday cup.

Both grids were made by winding 0.1 mm diameter tungsten wire around a stainless steel frame of 4 mm thickness such that the grids were 20 x 30 mm with the wires spaced at 1.6 mm. The double grid arrangement gives an optical transparency of about 95%. In practice, due to some misalignment of the grid wires, the transparency was found to be only about 90%. Double grids were used because it has been reported (Steckelmacher (93)) that such an arrangement produces a more uniform field and at the same time a high transparency. The current, i_F, to the Faraday cup was measured with a D.C. amplifier and recorded as a function of the retarding voltage and the energy spectrum was obtained by differentiating this curve.

Examples of the ion current to the Faraday cup as a function

of the positive retarding voltage on the grid are shown in figures 5.2 and 5.3 for anode voltages 5.3 and 8.0 kV respectively. Figures 5.2 and 5.3(a) show the curves for Ar^+ and figures 5.2 and 5.3(b) for Ar^{2+}.

There are three main features about these curves. As the retarding voltages increase from zero there is a gradual reduction of ion beam current. It is thought that this represents a low ion energy background similar to that reported by Khorrasany and Fitch (6) which was thought to be the low energy ions surrounding the main ion beam. The sudden fall of ion beam current at higher voltages shows that most of the ions are of high energy. The small residual current at even high voltages, which was also sometimes observed by Khorrasany and Fitch, is thought to be due to collection of low energy ions scattered in the chamber and collected by the Faraday cup independent of the retarding voltage.

The corresponding energy spectra are shown in figures 5.4(a) and (b) and 5.5(a) and (b), and the main peak occurs at energies 3.9, 4.0, 5.8 and 5.9 keV respectively. These values are in turn equivalent to 73, 75, 71 and 74% of the respective anode voltages. These figures are in reasonable agreement with Khorrasany and Fitch who found an average value of 75%. The full width half maximum (FWHM) for the main peak is about 500 and 600 V for V_A = 5.3 and 8 kV respectively.

The above results were recorded using the Einzel lens, but measurements taken without the Einzel lens gave a peak at the same value of retarding voltage, confirming that the Einzel lens does not change the ion energy.

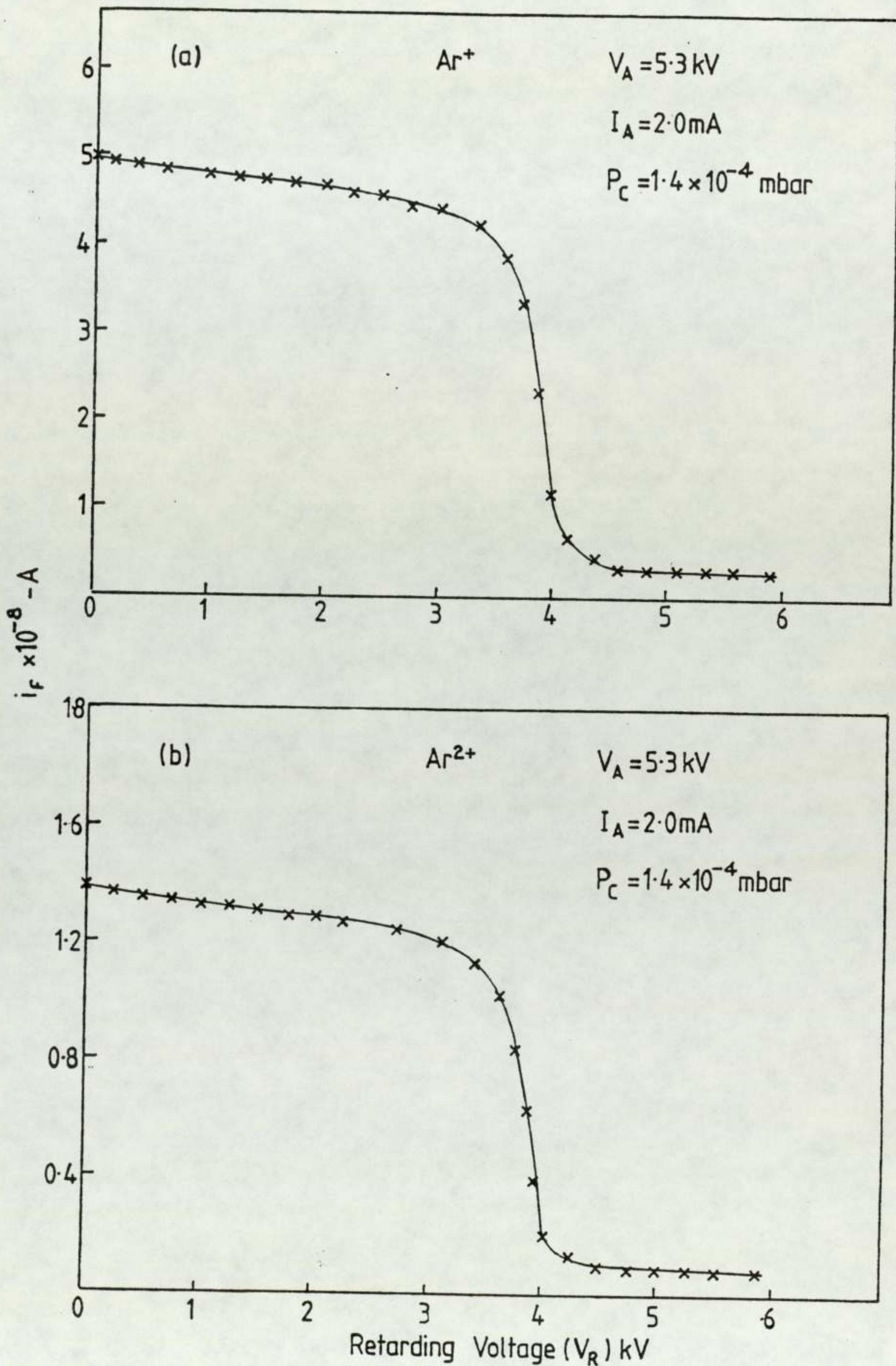

Figure 5.2 Ion current against the retarding voltage for (a) Ar^{+} and (b) Ar^{2+} for V_A = 5.3 kV.

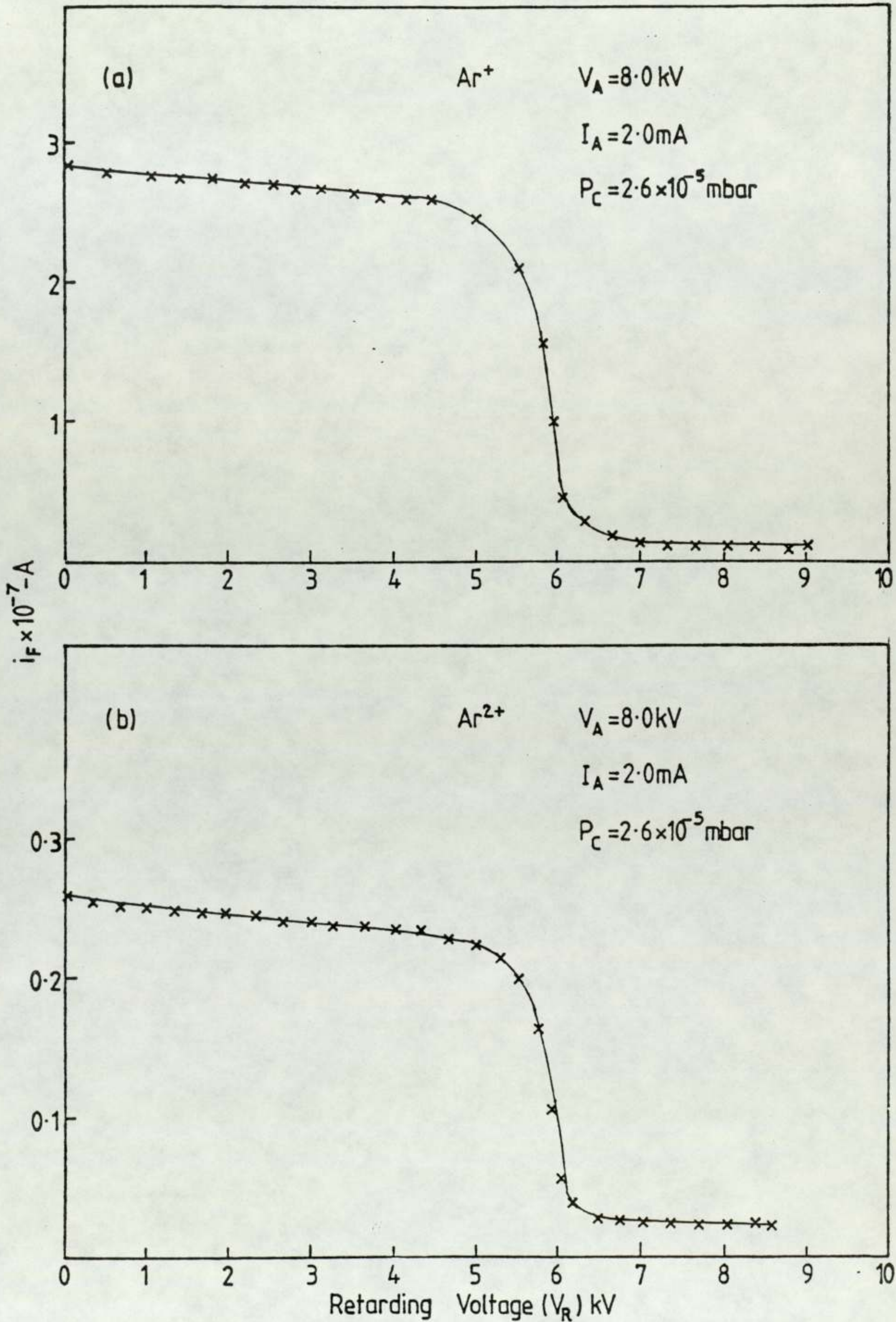

Figure 5.3 Ion current against the retarding voltage for (a) Ar^+ and (b) Ar^{2+} for V_A = 8 kV.

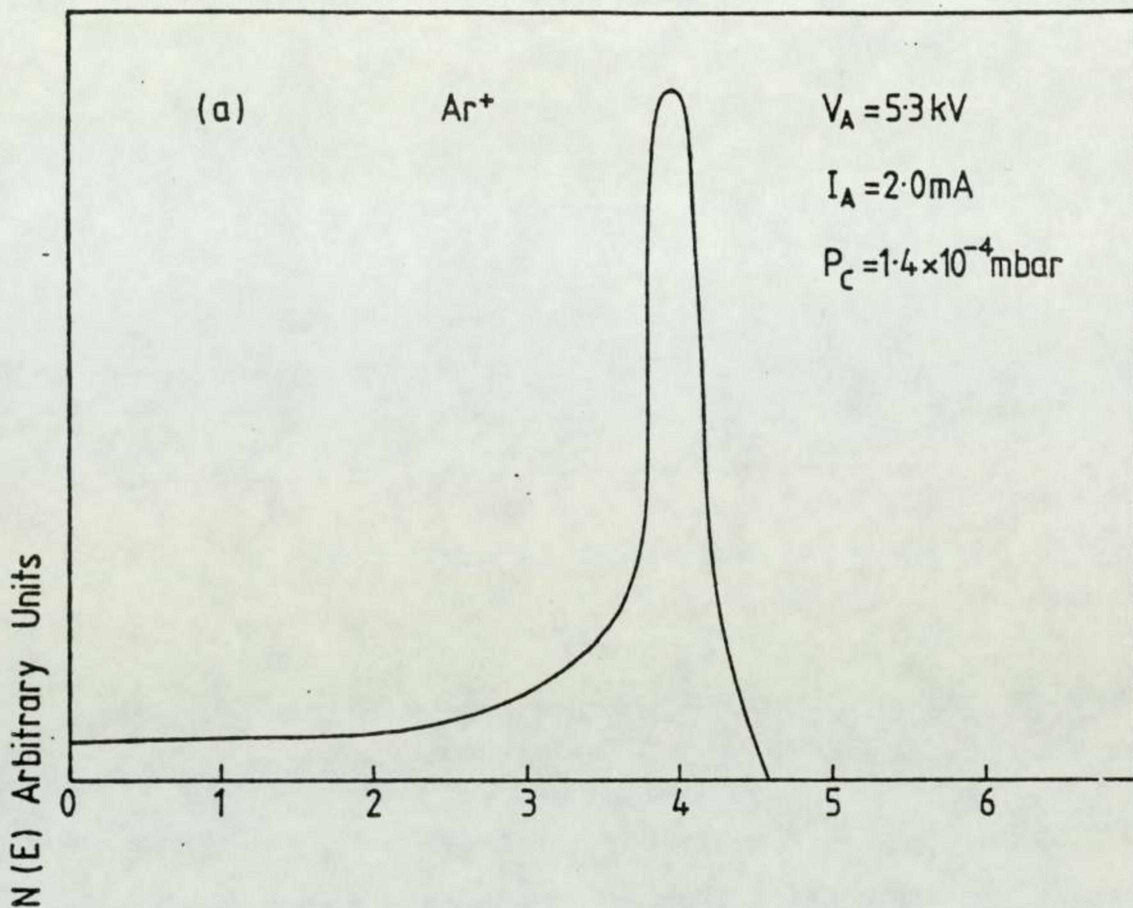

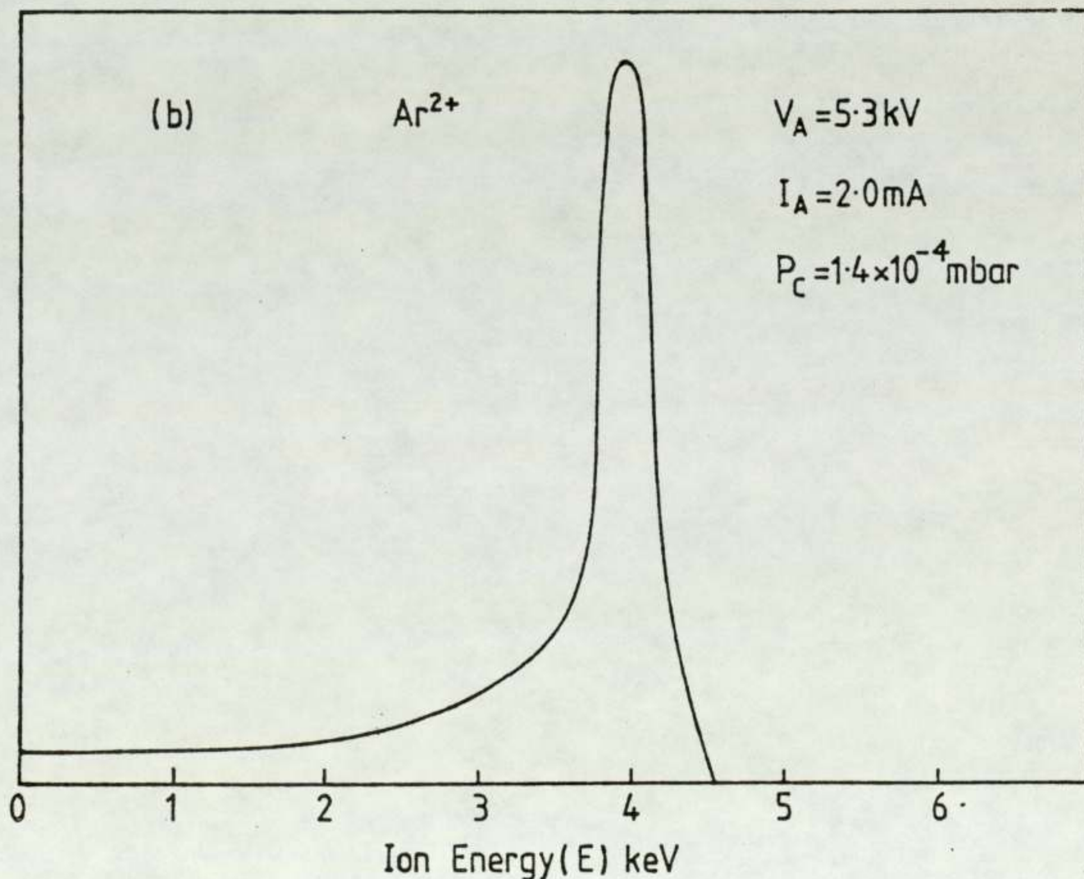

Figure 5.4 Ion energy spectra for (a) Ar^{+} and (b) Ar^{2+} for V_A = 5.3 kV

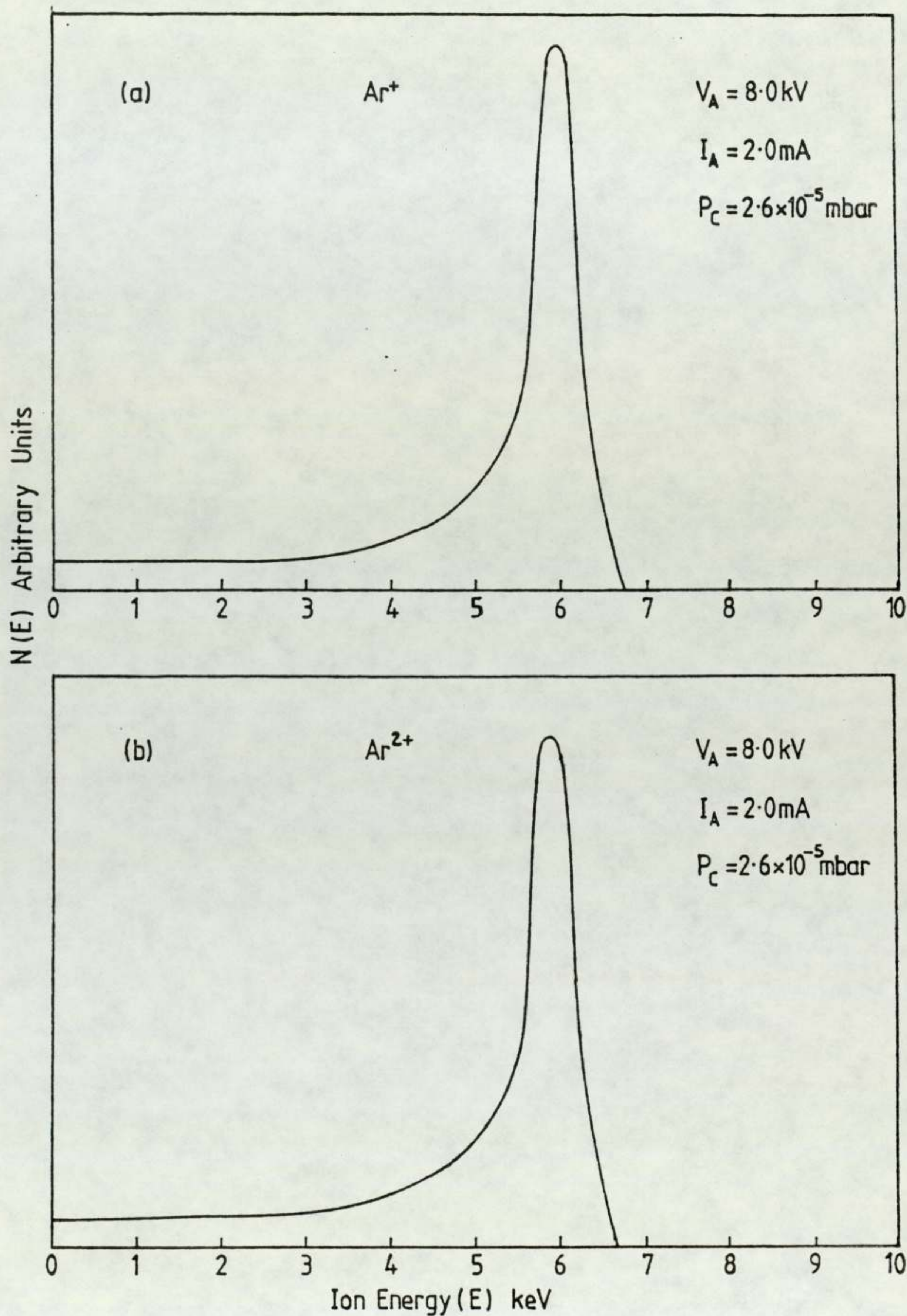

Figure 5.5 Ion energy spectrum for (a) Ar^+ and (b) Ar^{2+} for V_A = 8 kV.

5.3 Discussion

The fact that the main peak for a given anode voltage occurs at the same value of retarding voltage confirms that the energy of the doubly charged ions is twice that of the singly charged ion. Furthermore, this implies that the majority of the ions all experience the same value of accelerating voltage before they leave the source, and thus presumably originated from the same position inside the source. This is consistent with the model of a weak plasma existing inside the source at approximately 75% of the anode potential and the resulting cathode-fall being thus responsible for the ion acceleration.

As it seems probable that most of the ions are formed at the same position in the source, this suggests that the most likely process for the production of higher charge states is the single impact process which was discussed in Chapter 1. The maximum ionisation cross-sections for the production of Ar^{+}, Ar^{2+} and Ar^{3+} are given by Valyi (94) as $\sigma_1 = 3.5 \times 10^{-16}$, $\sigma_2 = 3.0 \times 10^{-17}$, $\sigma_3 = 1.0 \times 10^{-18}$ cm^2 respectively.

Thus theoretically at a given gas pressure we could expect P_{21} and P_{31} to be about 9% and 0.3% respectively. These values are in reasonable agreement with those found in the present work for argon, whose values varied from 5 to 16% for P_{21} and 0.5 to 1% for P_{31} over the pressure range 4×10^{-5} to 1.4×10^{-4} mbar.

These results are consistent with those referred to earlier for the cold cathode Penning ion source, when it was reported that the production of multiply charged ions is likely to be due to a single impact process.

This comparison is in many respects a good one because both the Penning ion source and the saddle field ion source are cold cathode devices operating at high voltages and low pressures. In both cases

the low pressure operation is a result of oscillating electrons and essentially they only differ in that one uses a magnetic field and the other an electrostatic field to achieve this.

In the final part of this work advantage has been taken of the existing facilities, comprising the ion source and magnetic analyser, to measure the sputtering yield as a function of the ionic charge state.

CHAPTER 6

MEASUREMENT OF THE SPUTTERING YIELD OF GOLD FOR Ar^{+} AND Ar^{2+} IONS

6.1 Introduction

Sputtering, which is the removal of surface atoms due to energetic particle bombardment, is caused by collisions between the incoming particles and the target atoms. Sputtering was first discovered in 1852 by Grove (95) who noticed the disintegration of cathodes in glow discharge tubes due to continuous bombardment by positive ions, but it took about 100 years until the physical processes involved and a quantitative description began to be developed. However since the appearance of the survey of this field in 1955 by Wehner (96) numerous studies under more controlled conditions have been conducted. This development is clearly reflected in recent reviews of Pollit et al (97), Kaminsky (98), Carter and Colligon (99) and the comprehensive review by McCracken (100) in which he covers most of the important developments in the field of ion bombardment of solids.

Today sputtering is no longer just an unwanted effect which destroys cathodes and grids and contaminates a plasma. It is now used for many applications and has become an indispensible process in modern technology. For instance, it can be used to produce thinning, surface cleaning or etching, for thin film deposition and for surface analysis, ion implantation and fabrications of integrated circuits (Melliar-Smith (101)).

The sputtering yield, S, is defined as the mean number of atoms removed from the surface of a solid per incident particle. The incident particles are usually energetic ions but can also be

energetic neutrals.

The process of kinetic ejection of the bombarded substrate, as a result of the momentum exchange between the impinging ion and the atoms of the target, have been advanced and treated extensively in the literature, e.g. Carter and Colligon (99). Various models based on this principle to explain the sputtering observations have been reported by Thompson (102), Sigmund (103) and Tsong and Barber (104). The energy and momentum are assumed to be transferred from the primary ion to the first target atom in a collision resembling elastic collisions between rigid spheres. This model was developed by Almen and Bruce (105). The energy transferred in an elastic collision between two atoms is limited by the conservation laws of energy and momentum. An atom 1 with initial energy E can at most transfer an energy,

$$T_m = \frac{4M_1M_2}{(M_1+M_2)^2} E$$

to an atom 2 with zero initial energy where M_1 and M_2 are the respective atomic masses.

Because of the complexity of the sputtering process this expression can only provide a guide to the variation of sputtering yield with such parameters as the masses of the particle and the target atoms, the particle energy, direction of incidence to the face of the target and the target temperature.

However there does not appear to be very much published work on the influence of the charge state of the ions. Wolsky and Zolanuk (106) studied this effect and measured the yields from silicon for Ar^+ and Ar^{2+} at energies up to 800 eV. They found that for ions of the same energy the yields for Ar^{2+} were four times those of Ar^+, whereas it might be expected that they would be the

same from simple momentum considerations. On the other hand, Weiss et al (107) found that the yields for neutral species of helium and hydrogen were larger than those of the corresponding singly charged ions.

Although it is clear that there has been extensive studies in this field, it is not always clear from the literature that any account has been taken of the charge states of the ions. The implications of this are twofold. Firstly, if allowance is not taken of higher charge states then the value of the ion dose will be too large, and secondly, the possibility that the yield is a function of the ionic charge state. Thus the sputtering yield for argon ions impinging on a gold film has been measured using single and double charged ions Ar^{+} and Ar^{2+}.

6.2 Measurement of the yield

6.2.1 Method

The method employed to measure the sputtering yield involved only minor modifications to the magnetic analyser used to measure the charge state and the slit previously introduced to increase the resolution was removed in order to increase the ion beam current. During the sputtering measurement the gold film supported on a glass substrate was positioned in the same place as the Faraday cup. A glass viewing window was used in place of the brass plate on the end of the analyser tube and the time was recorded to sputter a small area in the gold film as seen through the window, to produce a sputtered area for the single charge ions or the doubly charged ions. Of course, the sputtered area did not occur instantaneously because the ion current density was not uniform, thus an average of the initial time, when a very fine spot appeared, and the final time was used to calculate the ion dose. In all cases the magnetic field

was kept at zero until the source stabilized after which the magnetic field was switched on to reach appropriate value corresponding to Ar^+ and Ar^{2+}. The gold film was then removed and the sputtered area measured in a travelling optical microscope. Thus knowing the sputtered area, total ion dose and film thickness, it was possible to calculate the sputtering yield S in atoms per ion.

It was appreciated that the uncertainty involved in the measurement of S by this method is quite large. It was recognised that the uncertainty would be less by using a thin foil of known thickness, but this was found to be impracticable because the sputtering time was much too large for the small currents obtained for the doubly charged ions.

6.2.2 <u>Calibration of the ion beam</u>

In order to know the value of the ion beam current corresponding to a particular sputtered area, which slightly departed from the expected circular form due to the spherical aberration, it was necessary to calibrate the ion beam for a series of apertures from 1.0 to 3.0 mm diameter. The aperture was positioned in front of the Faraday cup and the maximum ion beam current obtained for each aperture was recorded as a function of anode voltage, V_A. During these measurements the value of I_A was kept constant at 2 mA and V_A was varied from 4 to 9 kV. Exact alignment for the beam was achieved by placing the film in front of the aperture to produce a fine sputtered spot on the film for a given magnetic field. This was repeated until the beam coincided with the centre of the aperture. The variation of ion beam current with aperture area at different values of V_A is shown in figures 6.1 and 6.2 for Ar^+ and Ar^{2+} respectively. Thus it was possible to determine the ion current corresponding to any particular sputtered area of gold film for a given value of anode voltage. It should be noted that initially the

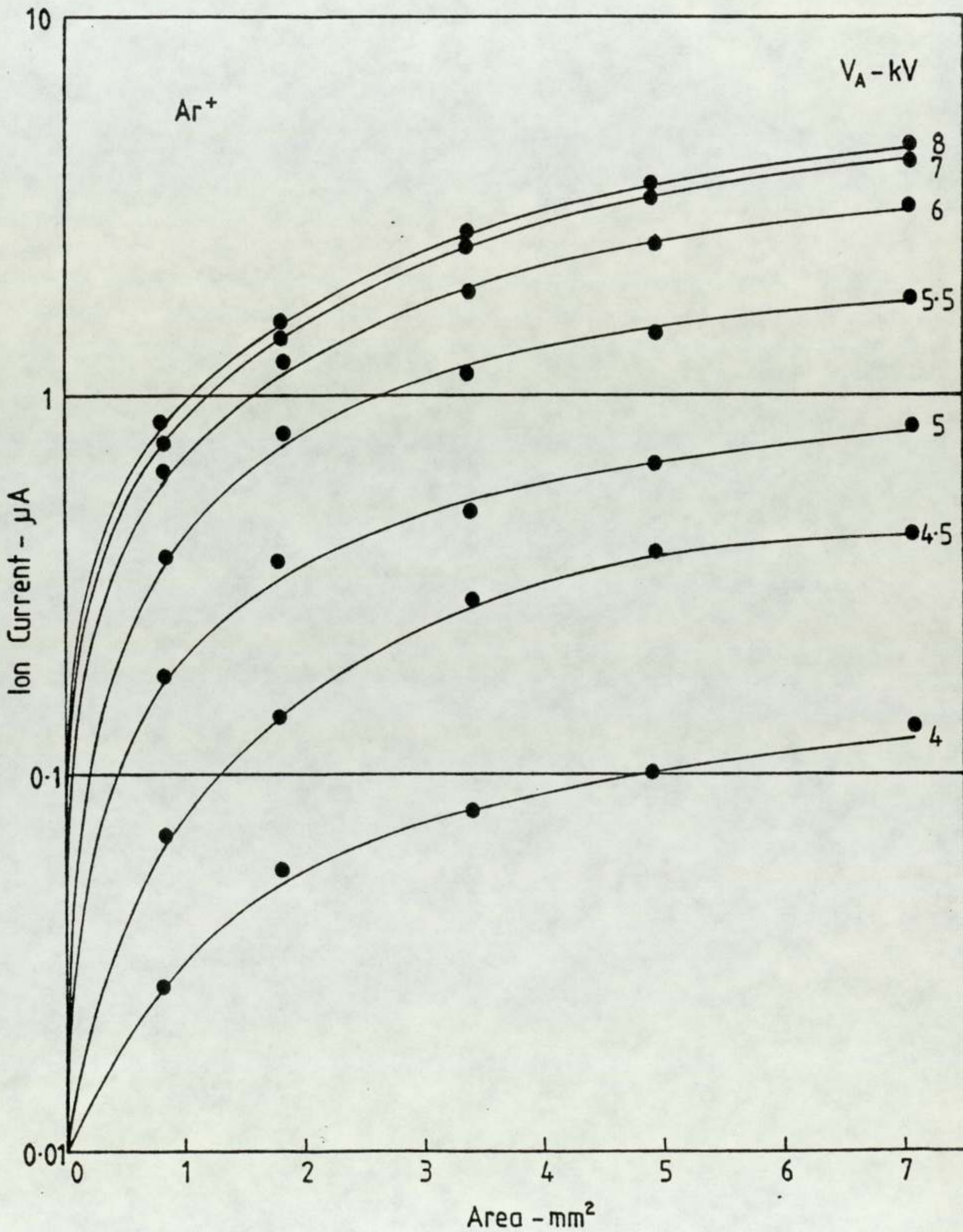

Figure 6.1 Variation of the ion current for Ar^+ with area for different anode voltages

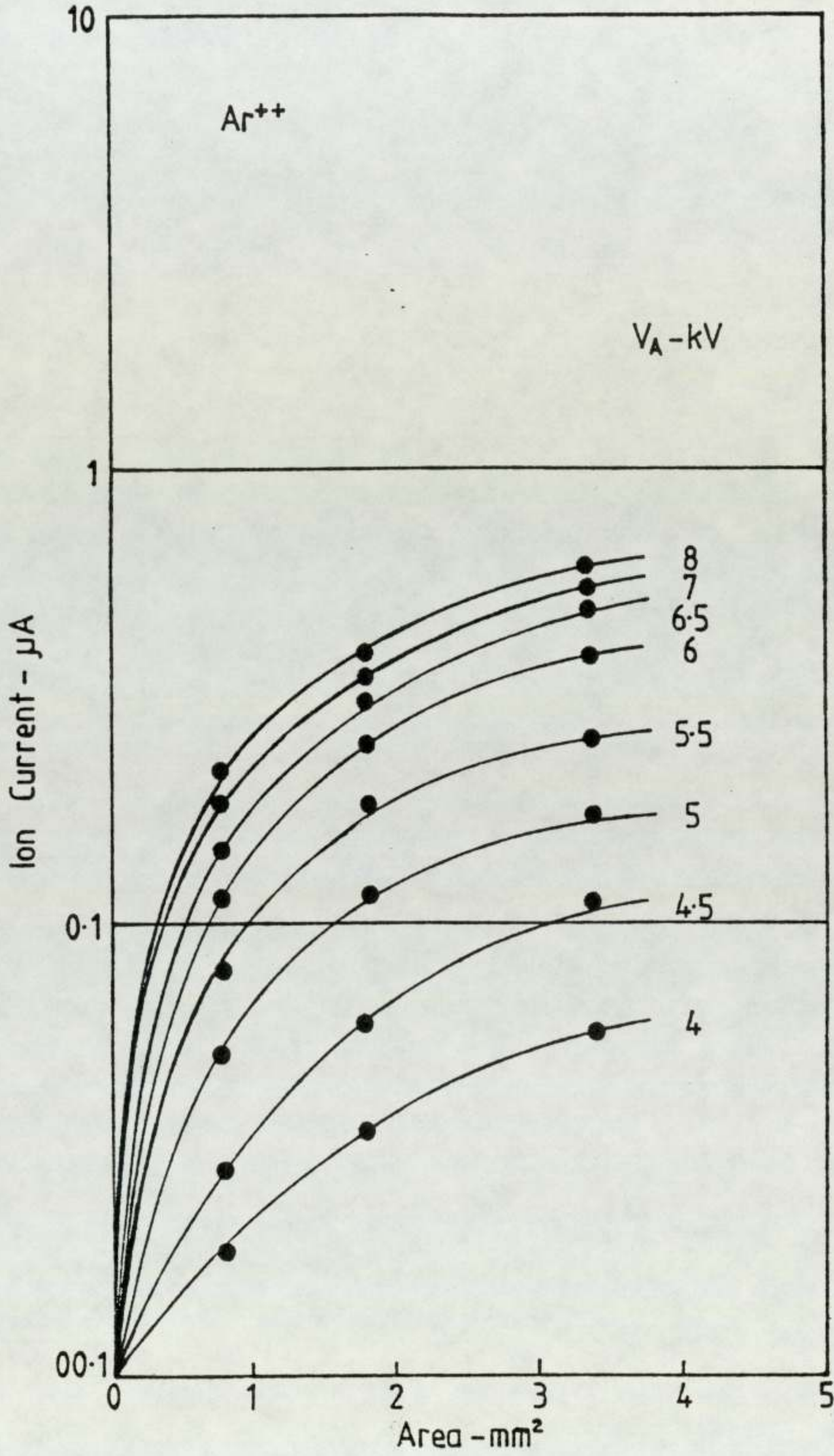

Figure 6.2 Variation of the ion current for Ar^{2+} with area for different anode voltages

current rises rapidly with increasing area and then much more slowly. Hence as the total current for large areas is not very dependent on the area, then the sputtering yield measurements were never recorded for areas greater than 3 mm^2.

6.2.3 Production of the films and measurement of their thickness

The films were produced by evaporating a small length of gold wire placed in molybdenum boat onto a clean glass slide using a conventional vacuum coating unit. A uniform thickness of film was ensured by placing the slide at a large distance from the boat. In all cases a razor blade was attached near to the end of the slide to produce a sharp edge on the gold film. Subsequently a small area of aluminium was evaporated over both this edge and the adjacent clear glass. The resulting step height on the aluminium film was thus equal to the thickness of the gold film and the height of the step was measured using a multiple beam interferometry technique. A semi-reflecting optical flat surface was placed over the step, thus producing an air gap between the two surfaces. A beam of white light incident normally to the surface produced an interference pattern between the light reflected either side of the step and the semi-reflecting surface. This is illustrated in figure 6.3 which shows that the film thickness is equal to $y_1 - y_2$. When the thickness of the air gap is equal to a multiple of half-wavelengths then destructive interference takes place. The interference pattern is viewed through a constant deviation spectrometer. Dark fringes appear in the field of view corresponding to wavelengths satisfying the above condition, but the fringes show a 'kink' due to the discontinuity in the air gap caused by the step. Thus it is possible to measure the change of wavelength corresponding to the discontinuity for a given fringe and hence find the film thickness.

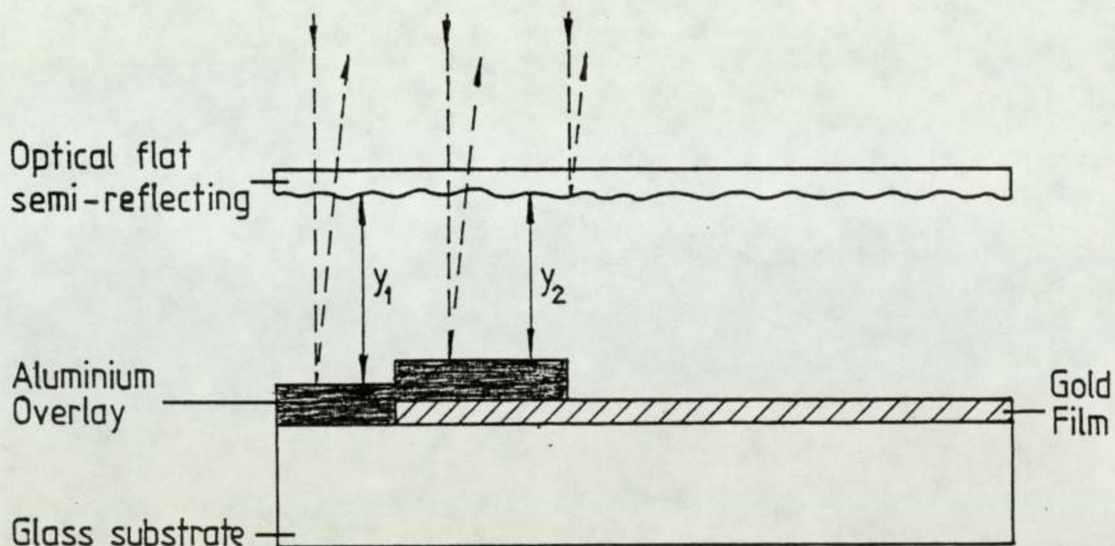

Figure 6.3 Illustration of the formation of the interference pattern

Films of thickness varying from 0.05 to 0.3 μm were produced in order to obtain suitable sputtering times for different ion beam currents and energies. The largest uncertainty in the film thickness occurred for the thinner films and was about ± 6%.

6.3 Results and discussion

The sputtering yield S, is given by:

$$S = \frac{Atd\ N_o ze}{iT\ m} \quad \text{atoms per ion}$$

Where,

A = sputtered area - mm^2

t = film thickness - mm

d = density of gold = 19.3×10^{-6} kg mm^{-3}

N_o = Avogadro's constant = 6.023×10^{23} mol^{-1}

z = charge state

e = electron charge = 1.6×10^{-19} C

i = total ion beam current - A

m = atomic weight of gold = 197

T = sputtering time-s

As an example, for $V_A = 4.0$ kV, and $z = 1$ then:

$$A = 3.0 \text{ mm}^2$$

$$t = 5.5 \times 10^{-5} \text{ mm}$$

$$i = 8.0 \times 10^{-8} \text{ A}$$

$$T = 74 \text{ mins.}$$

which gives: $S = 4.3 \pm 0.5$ atoms per ion

Forty measurements of the yield have been made using 28 gold films of different thickness and the appropriate values for the area, beam current, film thickness, sputtering time and yield are shown for different anode voltages for Ar^+ and Ar^{2+} in tables 6.1(a) and (b) respectively. The tables also show the corresponding ion energies which are equal to $0.75\ eV_A$ for Ar^+ and $1.5\ eV_A$ for Ar^{2+}. The uncertainty in S is of the order of 10% and takes into account not only the uncertainty in film thickness but also in the sputtered area, beam current and sputtering time. It can be seen that in the ion energy range 3 to 13.5 keV, the yield increases from about 4 to 11 atoms per ion. These values of the yield are in reasonable agreement with those published elsewhere as, for example, Carter and Colligon (99) give values of 8.2 and 8.8 for argon ions of energy equal to 10 keV.

Figure 6.4 also shows that the values of the yield for Ar^+ and Ar^{2+} follow a reasonably smooth curve, and the yield is the same for Ar^+ and Ar^{2+} at a given ion energy. It should be noted that the range of operating voltages of the source was limited from 4 to 9 kV and hence the yield could only be measured for Ar^+ in the range 3 to 6.75 keV and for Ar^{2+} in the range 6 to 13.5 keV. Thus the overlap of measurements for Ar^+ and Ar^{2+} only occurs in the relatively small range 6 to 6.75 keV.

These measurements have shown that the sputtering yield is the

V_A kV	E keV	Area mm^2	I µA	Thickness $x10^{-4}$ mm	Time Mins	S Atoms/Ion
4.0	3.0	3.0	0.08	0.55	74	4.3±0.5
		2.0	0.06	0.68	72	4.8±0.6
		2.7	0.07	0.49	57	5.1±0.6
5.0	3.75	3.2	0.55	1.40	29	4.5±0.5
		3.3	0.60	0.99	16.5	5.0±0.6
		3.1	0.50	1.26	21.5	5.3±0.6
6.0	4.5	3.4	2.1	0.56	2.7	5.2±0.5
		3.2	2.0	0.98	4.1	6.0±0.7
7.0	5.25	4.1	3.0	1.25	4.0	6.5±0.8
		3.5	2.7	0.79	2.3	6.7±0.8
8.0	6.0	4.8	3.7	2.10	6.1	6.9±0.7
		5.5	3.9	3.0	8.9	7.4±0.7
8.5	6.37	4.5	3.5	1.30	3.7	7.0±0.7
		3.2	2.9	3.1	7.2	7.3±0.7
9.0	6.75	2.1	2.1	2.95	6.5	7.0±0.7
		5.4	3.8	1.10	3.2	7.4±0.7

Table (6.1)a Values of the measured parameters and calculated yield of gold for Ar^+ ions in the energy range 3.0 to 6.75 keV

V_A kV	E keV	Area mm^2	I µA	Thickness $x10^{-4}$ mm	Time Mins.	S Atoms/Ion
4.0	6.0	1.5	0.030	0.75	163	7.1 ± 0.7
		2.0	0.038	0.55	118	7.6 ± 0.8
4.25	6.37	1.7	0.043	0.48	78	7.5 ± 0.8
		2.5	0.066	0.55	82	7.8 ± 0.8
4.5	6.75	1.7	0.055	1.48	191	7.4 ± 0.7
		2.0	0.070	0.60	66	8.0 ± 0.8
5.0	7.5	1.5	0.10	0.46	24.5	8.6 ± 0.9
		1.9	0.12	0.60	33	8.9 ± 0.9
5.5	8.25	2.3	0.14	0.48	28	8.8 ± 0.9
		2.5	0.22	1.54	60	9.0 ± 0.9
6.0	9.0	2.75	0.34	2.90	75	9.7 ± 1.0
		3.0	0.27	0.71	23.5	10.4 ± 1.0
6.5	9.75	2.5	0.38	0.65	15.5	8.5 ± 0.9
		1.8	0.30	1.57	27	9.0 ± 0.9
7.0	10.5	3.0	0.50	0.69	14	9.5 ± 1.0
		2.2	0.40	2.83	74	10.2 ± 0.9
		2.0	0.35	0.70	11.5	10.6 ± 0.9
7.5	11.25	2.3	0.45	0.92	16	9.0 ± 0.7
		1.6	0.35	3.05	43	10.0 ± 0.8
8.0	12.0	2.3	0.45	3.0	50	9.5 ± 0.8
		2.0	0.40	0.70	11	10.0 ± 0.8
8.5	12.75	1.8	0.40	1.25	18	9.5 ± 0.8
		2.5	0.50	2.95	47	9.7 ± 0.8
9.0	13.5	2.2	0.50	1.10	14	10.6 ± 0.8

Table (6.1)b Values of the measured parameters and calculated yield of gold for Ar^{2+} ions in the energy range 6.0 to 13.5 keV

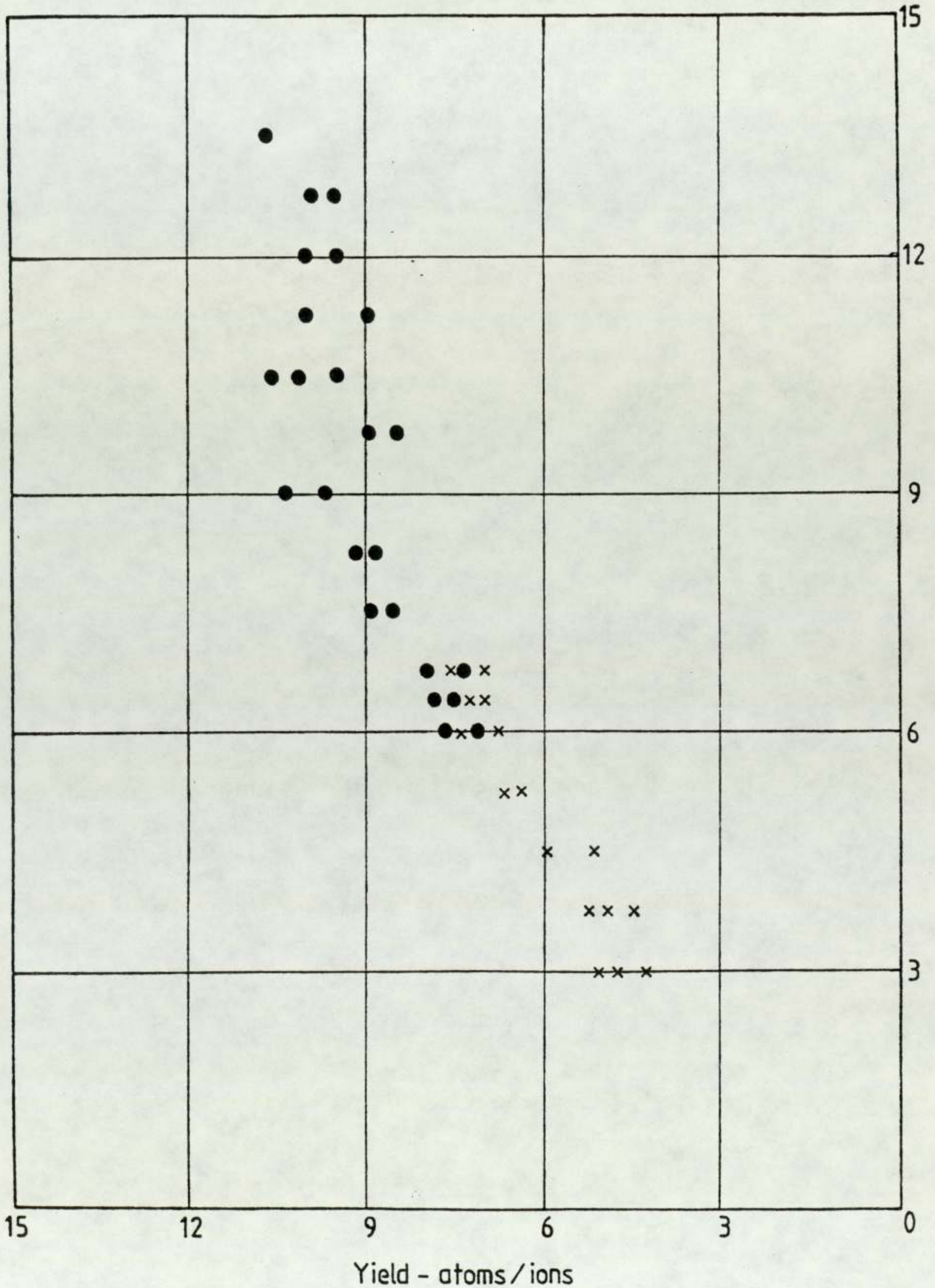

Figure 6.4 The sputtering yield for the argon ions Ar^{+} and Ar^{2+} as a function of ion energy

same for singly and doubly charged argon ions of the same energy. It is appreciated that the method used is not entirely satisfactory for measuring the absolute yield as it may involve a systematic error such as in the measurement of the sputtering time. It does however demonstrate quite clearly that the yield is independent of the charge on the ion. This is not in agreement with the measurement of the Wolsky and Zdank (106), but does support their remarks that the yield should be the same if one considers the "momentum transfer" theory for the sputtering process.

CHAPTER 7

CONCLUSIONS, DISCUSSION AND SUGGESTIONS FOR FURTHER WORK

It has been shown that when this source is operating in the normal oscillating mode, the most abundant ion for all the gases studied is the singly charged molecular ion. Higher charge states, which are believed to be formed by a single electron impact process, have never been observed in amounts greater than 20% of the singly charged ion. Thus this source is unlikely to make an important contribution in the fields of study where higher charge states are essential. On the other hand it is also clear that if the source is required to produce only the single charged ion then, in its present form, this source is also not appropriate.

Nevertheless, there are many applications which have already been used which do not require either of the above criteria. These include ion etching, cleaning and sputtering and thus this source should continue to be a useful instrument in these fields of research - its main advantages being the simplicity of design, freedom of magnetic field and thermionic source of electrons.

However, if the values of ion beam current are taken from the published work of this department and other establishments, it may be necessary to allow for the proportion of higher charge states. An example of some consequence in this respect is where experiments have been undertaken to determine the percentage of energetic neutrals in the beam. These experiments depend not only on the assumption that the secondary electron yield for energetic ions and neutrals is the same but also that the number of ions is directly

proportional to the ion current.

The energy measurements have shown that the energy of the ions is equal to the product of the ion charge and 0.75 of the anode potential, with a full width half maximum (FWHM) of about 10%. These results are only in partial agreement with the recent work of Pomathiod et al (108), who have studied the properties and discharge mechanism of a saddle field ion source which was to be used as a hydrogen ion injector in a space plasma experiment. They found that the energy spectrum contains not only the main peak as observed in the present work, but also two smaller peaks either side of the main one. It is unlikely that this difference is because they used hydrogen, but more likely due to the fact that their source is much larger - length 100 mm, diameter 90 mm and aperture 10 mm.diameter. There has not been any published work on the scaling factors with this source and it is possible that an increase in the dimensions by almost 10 times could affect the source characteristics. However, it is also recognized that the retarding field energy analyser may not be as satisfactory as the cylindrical sector analyser used by Pomathiod et al.

The present work on the energy measurements and the charge states have made it possible to produce a simple model of the discharge mechanism. It will only be possible to improve on this if more detailed and reliable information can be obtained about the distribution and energies of the ions, energetic neutrals and electrons produced by this source. It is unlikely that there could be a significant and useful improvement in the magnetic analyser used to measure the charge state. However, it could also be important to use this technique to study the beam profile to see if there is any variation in the proportion of different charge states. It is thought that no significant improvement could be made in the

retarding field energy analyser and more useful information could only be obtained by use of a cylindrical sector electrostatic analyser or a time of flight technique. The actual discharge characteristics could be directly studied using probe techniques to measure the ion and electron densities and energies. However it is likely that, because of the small size of the source, this may present considerable problems due to the disturbance of the discharge by the probes.

It is suggested that the work on sputtering should be extended to study the variation of yield with angle and energy for different materials and gas species. The accuracy could be improved by using a "punch technique" to produce a small hole through a thin foil rather than in a film as this makes it possible to measure the ion beam current directly, but this may be difficult with higher charge states.

At present this ion source has been the most useful of those devices which are based on the principle of McIlraith's charged particle oscillator. However other applications are still being considered, as demonstrated by (Chin et al (109)) who have recently used this idea to develop a mini-ionisation gauge and an electrostatic ion pump.

REFERENCES

(1) McIlraith, A.H. "A charged particle oscillator",
Nature, Vol.212, Page 1422, (1966)

(2) Fitch, R.K., Mulvey, T., Thatcher, W.J. and McIlraith, A.H.
"A new type of ion source"
J.Phys. D: Appl.Phys., Vol.3, page 1399 (1970)

(3) Fitch, R.K. and Rushton, G.J.
"Low pressure ion source"
J.Vac.Sci.Technol., Vol.9, Page 379 (1972)

(4) Rushton, G.J., O'Shea, K.R. and Fitch, R.K.
"Modes of operation of an electrostatic ion gun"
J.Phys.D: Appl.Phys., Vol.6, page 1167 (1973)

(5) Fitch, R.K., Ghander, A.M., Rushton, G.J. and Singh, R.
"Design and operating characteristics of a low pressure ion source"
Proc.6th Int.Vacuum Congr. 1974
Jap.J.Appl.Phys.Suppl. 2, pt.1, page 411 (1974)

(6) Khorossany, M. and Fitch R.K.
"Energy distribution of the ions produced by saddle field ion sources"
Vacuum, Vol.27, page 159, (1975)

(7) Frank, J.
"Ion Tech Ltd."
British Patent Appl.No. 44718/78 (1973)

(8) Frank, J. and Ghander, A.M.
"A saddle field ion source of spherical configuration for etching and thining application"
Vacuum, Vol.24, page 489 (1974)

(9) Ghander, A.M., Ph.D. thesis, Department of Physics, University of Aston in Birmingham (1974)

(10) Carlso, T.A., Nestor, C.W., Wasserman, N. and McDowell, J.D.
ORNL 4562 (1970)

(11) McGowan, J.W. and Kerwin, L.
"Metastable Ar^+ ions near the Ar^{++} Threshold"
Can.J. of Phys., Vol.41, page 1535 (1963)

(12) Okuno, Y., Okuno, K.K., Kaneko and Kanomata, I.,
"Absolute measurement of total ionization cross-section of Mg by electron impact"
J.Phys.Soc.Japan, Vol.29, page 164 (1970)

(13) Kieffer, L.J. and Dunn, G.H.
"Electron impact ionization cross-section data for atoms, atomic ions, and dia-atomic molecules"
Rev.Mod.Phys., Vol.38, page 1 (1966)

(14) Van der Wiel, M.J., Th.M.El-sherbini and Vriens, L.
"Multiple ionization of He, Ne and Ar by 2-16 keV electrons"
Physica, Vol.42, page 411 (1969)

(15) Abouaf, R.
"Effect auger dans l'ionisation multiple du manganèse et du cadmium par impact electronique"
J.Physque, Vol.31, page 277, (1970)

(16) Okudaira, S., Kaneko, Y., Kanomata, I.
"Multiple ionization of Ar and Mg by electron impact"
J.Phys.Soc.Japan, Vol.28, page 1536 (1970)

(17) Redhead, P.A.,
"Multiple ionization of the rare gases by successive electron impacts (0-250 eV)"
Can.J.Phys., Vol.45, page 1791 (1967)

(18) Redhead, P.A.,
"Multiple ionization in carbon monoxide by successive electron impacts"
Can.J.Phys., Vol.47, page 2449 (1969)

(19) Redhead, P.A.
Multiple ionization of cesium and barium by successive electron impacts"
Can.J.Phys., Vol.49, page 585 (1970)

(20) McFarland, R.H.
"Gryzinski electron-impact ionization cross-section computations for the alkali metals"
Phys.Rev., Vol.139, page 40 (1965)

(21) Thomas, B.K., Garcia, J.D.
"Ionization of positive ions"
Phys.Rev., Vol.179, page 94 (1969)

(22) Janes, G.S., Levy, R.H., Beth, H.A. and Feld, T.
"New type of accelerator for heavy ions"
Phys.Rev., Vol.145, page 925 (1966)

(23) Fuch, G.
Proc.Int.Conf. "Multiply-charged Ion Sources and Accelerating System"
I.E.E.E. Trans.Nucl.Sci. NS, Vol.19, page 160 (1972)

(24) Ardenne, M.V., Tabellen, zur. A.
Physik, Vol.1/2 Berlin (1964)

(25) Stuber, F.A.
"Multiple ionization in neon, argon, krypton and xenon"
J.Chem.Phys., Vol.42, page 2639 (1965)

(26) Moore, C.E.
Atomic energy levels, National Bureau of Standards (U.S.A.)
Circular No. 467, Vol.1 (1949)
Vol.2 (1952)
Vol.3 (1958)

(27) Carlson, T.A. and McDowel,
At Data, Vol.2, page 63 (1970)

(28) Schram, B.L.
"Partial ionization cross-sections of noble gases for electrons with energy 0.5-16 keV"
Physica, Vol.32, page 185 and 197 (1966)

(29) El-Sherbini, Th.M., Van der Wiel
"Multiple ionization of Kr and Xe by 2-14 keV electrons"
Physica, Vol.48, page 157 (1970)

(30) Drawin, H.W.
"Zur formelmöbigen darstellong der ionisierungsquershnitte gegenüber elecktronenstob"
Z. Physik, Vol 164, page 513, (1961)

(31) Muller, A.
"On the charge state distribution of multiply charged ions extracted from electron beam ion sources"
Nucl.Inst. and Meth., Vol.140, page 181-188 (1977)

(32) Dontes, E.D.
"Proc.1st Conf.des Sources et Ions", page 635, Paris (1969)

(33) Rose P.H.

"Proc.Conf.la Physique et la production des ions"

Lourdes, IV 2.1. (La Pharigne, 1969)

(34) Burhop, E.H.S.

The Auger effect, Cambridge Univ.Press, 49 (1952)

(35) Carlson, T.A. and Krausa, M.O.

"Electron shake-off resulting from k-shell ionization in neon measured as a function of photoelectron velocity"

Phys.Rev., Vol.140A, page 1057 (1965)

(36) Carlson, T.A.

"Electron shake-off following the Beta decay of Ne^{23}"

Phys.Rev., Vol.130, page 2361 (1963)

(37) Pleasontaon, F. and Shell, A.H.

"Ionization following internal conversion in xenon"

Proc.Roy.Soc., Vol.241A, page 141 (1957)

(38) Okudaira, S.

"Multiple ionization of Ca, Sr and Ba by electron impact"

J.Phys.Soc. Japan, Vol.29, page 409, (1970)

(39) Carlson, T.A., Moddeman, W.E., Krause, M.O.

"Electron shake-off in neon and argon as a function of energy of the impact electron"

Phys.Rev.A, 1, page 1406 (1970)

(40) Levinger, J.S.

"Effects of radioactive disintegrations on inner electrons of the atom"

Phys.Rev., Vol.90, page 11 (1953)

(41) Von Ardenne, M.
"Tabellen zur angewandren physik"
Part 1, VEB Verlag der Wissen Schaften, Berlin 1962

(42) Frohlich, H.
Nat.Leonik, Vol.1, page 183, (1959)

(43) Demirchanov, R.A.
Report BNL, 767, 12, 224, Brookhaven 1952

(44) Slaytek, M.
Report JINR, page 7-757- Dubna 1972

(45) Braams, C.M.
"Composition of noble gas ion beams produced with a duoplasmatron"
Rev.Sci.Inst., Vol.36, page 1411 (1965)

(46) Arminen, E.
"Performance measurements of the Scandinavian type isotope separator with a duoplasmatron ion source"
Nucl.Instr.Meth., Vol.85, page 109, (1970)

(47) Lejeune, C.
Thesis, University de Paris, Sud.Orsay (1971)

(48) Lejeune, C.
"Theoretical and experimental study of the duoplasmatron ion source"
Nucl.Instr.Meth., Vol.116, page 417, 429 (1974)

(49) Illgen, T.
"Multiply-charged ion sources and accelerating system"
I.E.E.E., Tran.Nucl.Sci., NS-Vol. 19/2, page 35 (1972)

(50) Green, T.S.
"Intense ion beams"
Rep.Prog.Phys., Vol.37, page 1257-1344 (1974)

(51) Lejeune, C.
"Symp.Ion Sources", Brookhaven, BNL 50310, page 27 (1971)

(52) Morgan, O.B.
"Symp. Ion Sources", Brookhaven, BNL 50310, page 29 (1971)

(53) Winter, H.
GSI-report PB-1-74, Darmstadt (1974)

(54) Dow, D.G.
"Electron-beam probing of a Penning discharge"
J.Appl.Phys., Vol.34, page 2395, (1963)

(55) Schuurman, W.
"Investigation of a low pressure Penning discharge"
Physica, Vol.36, page 136 (1967)

(56) Bethge, K.
"Eine Penning-Ionenquelle fur Negative Lithium-Ionen"
Nucl.Inst.Meth., Vol.30, page 283 (1964)

(57) Bennet, J.R.T.
"Multiply-charged ion source and accelerating system"
I.E.E.E., Trans.Nuc.Sci., NS, Vol.19/2, page 49 (1972)

(58) Green, T.M. and Goble, C.
"Power and particle flux balance in a P.I.G. discharge ion source"
Nucl.Inst.Meth., Vol.116, page 157-165 (1974)

(59) Lapolstolle, P. and Septier, A.
Linear accelerators (North-Holland Publ.Co., Amsterdam, 1970)

(60) Cobic, B.

"Low-power ion source for multi-charged ions of krypton and xenon"

Int.J.Mass.Spectm.Ion Phys., Vol.7, page 269 (1971)

(61) Thonemann, P.C.

"The performance of a new radio-frequency ion source"

Proc.Phys.Soc., London, Vol.61, page 483, (1948)

(62) Eubank, H.P.

"Operating characteristics of a high yield RF ion source"

Rev.Sci.Instr., Vol.25, page 989 (1954)

(63) Valyi, L.

"Investigation of a source of He^{++} ions"

Nucl.Inst.Meth., Vol.79, page 315 (1970)

(64) Rushton, G.J. and Fitch, R.K.

"The performance of the twin wire electrostatic charged particle oscillator"

Vacuum, Vol.21, Number 10, page (449-452), (1971)

(65) Fitch, R.K., Khorassany, M. and Mawlood, T.N.

"The production of energetic neutrals by saddle field ion sources"

Proc.7th Int.Vac.Cong. and 3rd Int.Conf.Solid Surface, (1977)

(66) Rushton, G.J. and Fitch, R.K.

"The twin anode electrostatic ion gun with thermionic electron injection"

J.of Phys.E., Sci.Instr., Vol.7, page 313 (1974)

(67) Khorrasany, M.

Ph.D. Thesis, Physics Dept., University of Aston in Birmingham, page 94 (1977)

(68) Barnes, P., Fonseka, G.M., Ghose, A., Moor, N.T.
"Ion beam etching in the study of Cementations materials"
J.Mat.Sci., Vol.14, page 2831 (1979)

(69) Christopher, S.C., Geoffery, W.P.
"Ion beam sputtering: an improved method of metal coating SEM samples and shadowing CTEM samples
J.Microscopy, Vol.123, Pt.1., page 25 (1981)

(70) Walls, J.M., Southworth, H.N., Rushton, G.J.
"The preparation of field electron/field ion emitters by ion etching"
Vacuum, Vol.24, page 475, (1974)

(71) Lewis, G.W., Colligon, J.S., Paton, F., Nobes, M.J., Carter, G. and Whitton, J.L.
"The life cycle of copper cones"
Rad.Effects Letters, Vol.43, page 49 (1979)

(72) Burger, F. and Maier, J.P.
"Vacuum ultraviolet of the line radiation of the rare gas ion suitable for photoelectron spectroscopy"
J.Phys.E: Sci.Instr., Vol.8, page 420 (1975)

(73) Ghander, A.M. and Fitch, R.K.
"A saddle field ion source of spherical configuration for etching and thining application"
Vacuum, Vol.24, page 101 (1974)

(74) Franks, J., Clay, C.C., Peace, G.W.
"Ion beam thin film deposition"
Scanning electron microscopy
(Ed. by Johari, O), Vol.1, page 155, SEM Inc.Chicago, U.S.A.

(75) Dhariwal, R.S. and Fitch, R.K.
"In situ ion etching in a scanning electron microscope"
J.Mater Sci., Vol.12, page 1225 (1977)

(76) Ghafouri, S.N., Fitch, R.K. and Ball, P.C.
"Application of ion etching to the study of dental restorative materials"
Vacuum, Vol.31, page 33 (1981)

(77) Mohindra, S.
Ph.D. Thesis, Physics Dept., University of Aston in Birmingham (1981)

(78) Rehal, A.S.
Ph.D. Thesis, Physics Dept., University of Aston in Birmingham (1978)

(79) Clark, R.B., Fitch, R.K., Ghander, A.M. and Smith, A.G.
"The ionic charge states produced by the oscillating electron electrostatic ion source"
J.Phys.E: Sci.Instr., Vol.7, page 566-568 (1974)

(80) Mahmoud, E.A.
M.Sc. report, Physics Dept., University of Aston in Birmingham (1978)

(81) Perrin, J.
An.Chim.Phys., Vol.7, page 503 (1897) (English Transl.)

(82) Tate, J.T.
"The effect of angle of incidence on the reflection and secondary emission of slow moving electrons from platinum"
Phys.Rev., Vol.17, page 394 (1921)

(83) Hasted, J.B.
"Physics of Atomic Collisions", page 130, Butterworth, London and Washington, D.C., (1964)

(84) Bronshtein, I.M. and Denisov, S.S.
Soviet Phys. - Solid State, (EnglTransl.)
Vol.7, page 1819, (1966)

(85) Khorassany, M.
Ph.D. Thesis, Physics Dept., University of Aston in Birmingham, page 56, 106, (1977)

(86) Plass, G.N.
"Electrostatic electron lenses with a minimum of spherical aberration"
J.Appl.Phys., Vol.13, page 49 (1942)

(87) Ramberg, E.G.
"Variation of the axial aberrations of electron lenses with lens strength"
J.Appl.Phys., Vol.13, page 582 (1942)

(88) Bachman, C.H. and Ramo, S.
"Electrostatic Electron Microscopy"
J.Appl.Phys., Vol.14, page 8 (1943)

(89) Harting, E and Read, F.H.
"Electrostatic lenses", Amsterdam, Elsevior (1976)

(90) Liebmann, G.
"Measured properties of strong unipotential electron lenses"
Proc.Phys.Soc., Vol.62B, page 213 (1949)

(91) Gobrecht, R.
Arch Electrotech, Vol.36, page 484 (1942)

(92) Klemperer, O.

"On a new test method for spherical aberration of electron lenses"

Proc.Phys.Soc., Vol.64B, page 790 (1951)

(93) Steckelmacher, W.

"Energy analysers for charged particle beams"

J.of Physics E: Scientific Instruments, Volume 6, page 1061 (1973)

(94) Valyi, L.

"Atom and ion sources"

Wiley, page 378 (1977)

(95) Grove, W.R.

"On the electro-chemical polarity of gases"

Phil.Trans.Royal Soc., Vol.142, page 87 (1852)

(96) Wehner, G.K.

"Sputtering by ion bombardment"

Advance in electronics and electron physics, Vol.7, page 239 (1955)

(97) Pollitt, K.R., Robb, J.C. and Thomas, D.W.

"Mechenism of sputtering of solid surface by ion-impact"

Nature, Vol. 272, page 436 (1978)

(98) Kaminsky, M.

Atomic and ionic impact phenomena on metal surface, Springer-Verlag (1965)

(99) Carter, G. and Colligon, J.S.

Ion bombardment of solids, Heinemann Educational Books, London (1968)

(100) McCraken, G.M.

"The behaviour of surfaces under ion bombardment"

Reports on Progress in Physics, Vol.38, page 241 (1975)

(101) Melliar-Smith, C.M.

"Ion etching for pattern delineation"

J.Vac.Sci and Technol. Vol.13, page 1008 (1976)

(102) Thompson, M.W.

"The energy spectrum of ejected atoms during the high energy sputtering of gold"

Phil.Mag., Vol.18, page 377 (1968)

(103) Sigmund, P.

"Theory of sputtering 1. Sputtering yield of amorphous and polycrystalline targets"

Phys.Rev., Vol.184, page 383 (1969)

(104) Tsong, I.S.T. and Barber, D.J.

"Review: Sputtering mechanisms for amorphous and polycrystalline solids"

J.Mater Sci., Vol.8, page 123 (1973)

(105) Almen, C. and Bruce, G.

"Collection and sputtering experiments with noble gas ions"

Nucl.Instrum.Meth., Vol.11, page 257 (1961)

(106) Wolsky, S.P. and Zdanuk, J.S.

"Ion bombardment of solids"

Page 318, Heinemann, London (1968)

(107) Weiss, A., Hedlt, A. and Morr, W.J.

"Sputtering of silver by neutral beams of hydrogen and helium"

J.Chem.Phys., Vol.29, page 7 (1958)

(108) Pomathiod, L., Henry, D., Aral, Y., Boswell, R.
"Properties and discharge mechanism of a saddle-field ion source"
Inst.Phys.Ser. No. 54: Chapter 7, page 309 (1980)

(109) Chen, P.C., - Tsinghua University, Peking - Private Communication (1982)

PUBLICATIONS

(1) "The charge state of the ions produced by a saddle field ion source and its application to the measurement of sputtering yields"

R.K. Fitch, E.A. Mahmoud and S.N. Ghafouri
Proc.4th Intern.Conf. on Solid Surfaces
and 3rd Europ.Conf. on Surface Science
Vol. II, Page 1084, (Cannes 1980)

(2) "Temperature limitation of a saddle field ion source"

R.K. Fitch, S.N. Ghafouri and E.A. Mahmoud
Vacuum, Vol.31, Page 19, (1981)

(3) "Measurement of the sputtering yield for Ar^{+} and Ar^{2+} ions on gold films

R.K. Fitch and E.A. Mahmoud

Presented at 3rd Intern.Conf. on Ion and Plasma Assisted Techniques, Amsterdam, the Netherlands, June 30th - July 2nd (1981), to be published in Thin Solid Films

THE CHARGE STATE OF THE IONS PRODUCED BY A SADDLE FIELD ION SOURCE AND ITS APPLICATION TO THE MEASUREMENT OF SPUTTERING YIELDS

R. K. Fitch, E. A. Mahmoud* and S. N. Ghafouri*

Physics Department, University of Aston in Birmingham, B4 7ET, England.

Abstract

A magnetic analyser has been developed to measure the charge state of the ions produced by a saddle field ion source in the pressure range 8×10^{-6} to 5×10^{-3} mbar. The source is water cooled and an Einzel lens was used to focus the ion beam into a Faraday collector. Measurements have been made for Hydrogen, Helium, Neon, Nitrogen, Oxygen and Argon and the ionic species, H_2^+, H^+, He^+, He^{2+}, Ne^+, Ne^{2+}, N_2^+, N^+, N^{2+}, O_2^+, O^+, O^{2+}, Ar^+, Ar^{2+}, and Ar^{3+} have been observed with the percentage of higher charge states varying with pressure. The source has been used to develop a novel method of measuring the sputtering yield and has been successfully applied to aluminium and various dental materials. The yield has been determined directly from a knowledge of (a) the ion bombardment rate taking into account the presence of multi-charged ions and energetic neutrals (b) the sample thickness and (c) the area of the material sputtered using a scanning electron microscope. The method has also been used to measure the yield with incident ion angle and energy and has the advantage that once calibrated it is not necessary to measure the sputtered area.

1. Introduction

During the last decade there has been a considerable expansion in the application of energetic ion beams as, for example, in ion etching, Glöersen {1}, and ion thinning of specimens for transmission electron microscopy, Franks {2}. Of course one important aspect of this technology is the ion source and recently the saddle field ion sources, based on the idea of McIlraith {3}, are finding increasing use particularly where low pressure operation and freedom from magnetic fields is required. Two forms of this source are now available and both are cold cathode devices, one is of cylindrical geometry producing a wide ion beam of fairly broad energy spread whereas the other is of spherical geometry and produces a fine ion beam with a narrower energy spread. The properties of these sources have been reported by, for example, Fitch et al {4} and Franks and Ghander {5} and their application to in-situ ion etching by Dhariwal and Fitch {6} and Dhariwal et al {7}. The energy distribution of the ions and the percentage of energetic neutrals have been measured for both sources by Khorassany and Fitch {8} and Fitch et al {9}. However the charge state of the ions has only been briefly studied in the case of the cylindrical source,Clark et al {10}, and the purpose of the work described in section 2 is to report the measurements recently undertaken to determine the ionic charge state with the spherical ion source using a magnetic analyser. In section 3 a novel method of measuring the sputtering yield is described which has been applied to aluminium and various dental materials and takes into account the fraction of higher ion charge states and energetic neutrals.

2. Measurement of the charge state of the ions

The spherical ion source is water cooled and produces ions in the range 3 to

*Supported by the Ministry of Education, Baghdad, Iraq.

6 keV when the source is used at anode voltages 4 to 8kV {8}. The energy spread is about ± 10% so that it was considered that adequate resolution would be obtained without the need for further acceleration of the ions. A schematic diagram of the analyser and ion source is shown in figure (1).The source contains two ion exit apertures of diameter 1.5mm thus producing two identical ion beams, one of which falls on a flat plate collector to record the monitor current, I_M. The voltage stabilized D.C. power supply provides the anode voltage, V_A, which is variable from 0 to 10kV and also records the anode current, I_A. The other ion beam passes through a small stainless steel collimating tube, length 15mm and internal diameter 1.5mm, before entering the Einzel lens. The electrodes of this lens are made of stainless steel and are placed 4.5mm apart and the apertures of the two outer negative electrodes are each 1.5mm in diameter, whereas the positive central electrode contains a 3.0mm diameter aperture. The focussed ion beam then enters the uniform magnetic field, B, which is provided by an electro-magnet and is variable from 0 to 0.3T and is uniform within the rectangular polepieces, 6 x 8cm, being 2.5cm apart. The ion source is very sensitive to stray magnetic fields and thus it was necessary to place a μ-metal screen between the electro-magnet and the source. A slit aperture, width 1.4mm, is placed near the centre of the field to improve the resolution. The ion beam, i_F, is monitored by an earthed Faraday cup placed at an angle of about 7° to the central axis and a screen electrode biased at - 40V suppresses the secondary electrons. The spectra is traced on an X-Y recorder which plots the voltage developed by i_F across a 1MΩ resistor on the Y-axis and the voltage developed by the magnetising current, i_m, across a 1Ω resistor on the X-axis. The complete analyser is contained in a brass tube attached to a conventional stainless steel high vacuum system using "Santovac 5" fluid in the diffusion pump. The pressure is recorded by a Penning gauge and various gases can be admitted into the source through a needle valve.

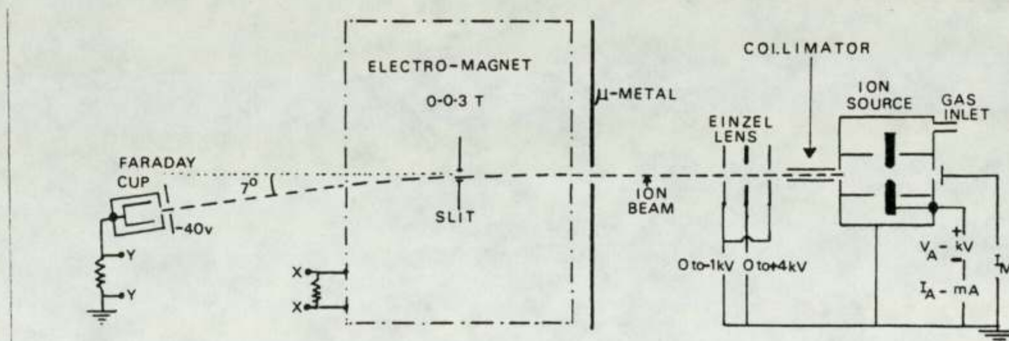

Fig.1 - Schematic diagram of the analyser

The variation of m/Ze with B^2 for various gases at V_A = 4, 5, 6 and 7kV is given in figure 2. The figure shows that at a constant value of V_A, Ar^+ and Ar^{2+} are on the same line and therefore Ar^{2+} has twice the energy of Ar^+. Thus both ions must have been accelerated through the same potential, indicating that they were both formed in the same position in the source. Examples of the spectra for nitrogen and argon are given in figure 3. Figures 3a and 3b are at constant voltage and the ions N_2^+, N^+ and N^{2+}can be seen in figure 3a whereas in figure 3b there is evidence of A^{3+} as well as Ar^{2+} and Ar^+. The ratio, R, of the ion currents for Ar^{2+} to Ar^+ varies with pressure similarly to that reported by Kornelsen[11] and Abe et al[12]. The largest value of R is 0.2 at 9.1 x 10^{-5} mbar, indicating the presence of about 10% of Ar^{2+} ions. Figure 3c gives the spectra for argon at constant

pressure for different values of V_A and it was found that R is approximately constant as V_A is increased from 5.6 to 6.8kV. The increase in width of the Ar^+ peak compared to the N_2^+ peak is due to the lack of proportionality between the magnet current and B when the current exceeds 2A.

3. Measurement of sputtering yields and etching rates

The source has been used to measure the sputtering yields and etching rates of various materials of thickness 20-200μm. The specimens were polished when necessary with a 1μm diamond paste and were supported in a stainless steel holder attached to the ion source. The angle of the specimen with respect to the ion beam could be varied from 0° to 80°. The time to etch through the specimen was taken when the ion current in a Faraday cup, placed on the other side of the specimen, reached 1.0μA. The etched area was measured in a scanning electron microscope and was found to be $0.109mm^2$ with the beam at 75°. It was found that if the specimen-source distance and angle were kept constant this area only varied by $0.002mm^2$ and it was therefore not necessary to repeat this measurement. The accuracy of the method thus only depends on the etching time and sample thickness.

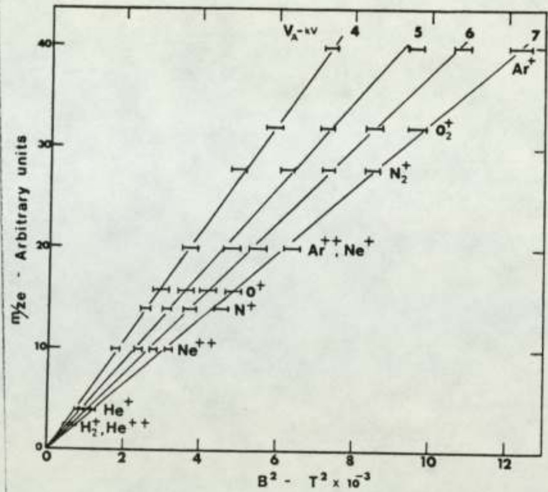

Fig.2 - m/Ze vs. B^2 for various gases at different voltages

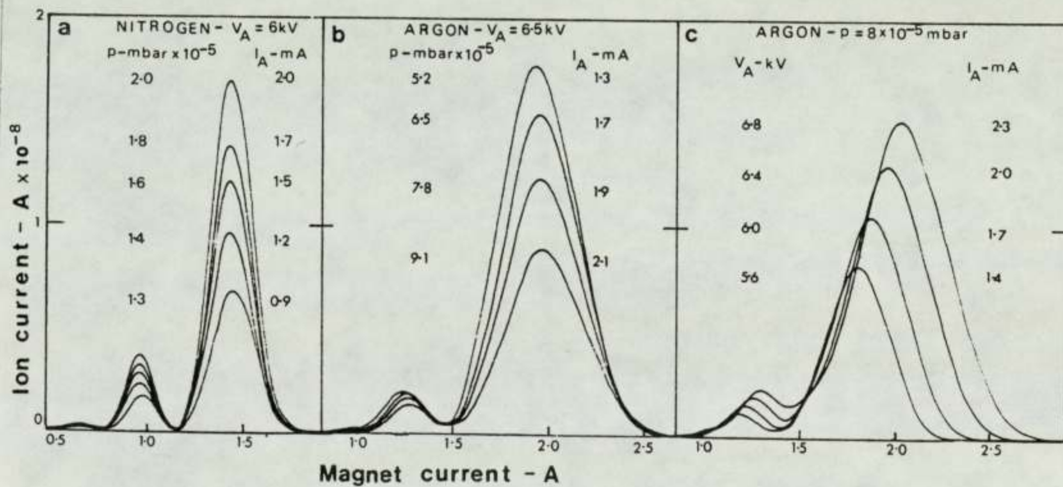

Fig.3 - Ion current vs. magnetic current for (a) Nitrogen and (b) Argon at constant voltage and (c) Argon at constant pressure

Figure 4 shows the value of the yield and etching rates for various materials using argon with V_A varying from 4 to 9kV which is equivalent to ion energies of 3 to 6.75 keV{8}. In calculating these values allowance has been made for the fraction of energetic neutrals and doubly charged argon ions. Figures 4a and 4b show the yields for aluminium with ion angle and ion energy respectively. The maximum yield of 5.4 atoms/ion occurred at 60° which is in good agreement with the literature eg. Wilson and Brewer[13] and Al-Rawi[14]. Figure 4c shows the etching rates with incident angle for aluminium and some dental materials. The maximum etching rate occurs at

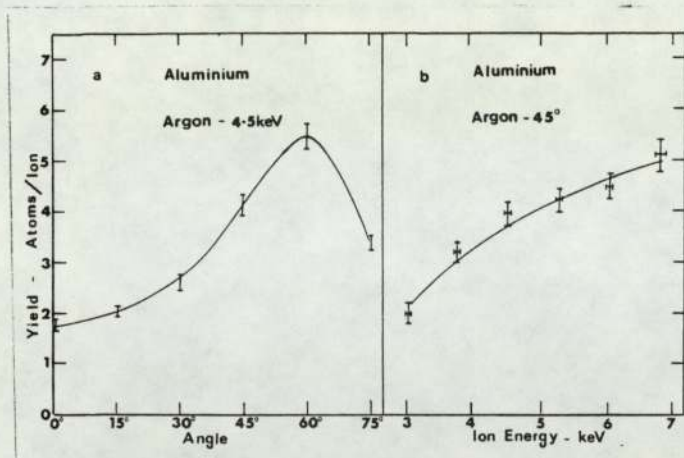

Fig.4 Variation of yield with (a) angle and (b) energy for argon on aluminium

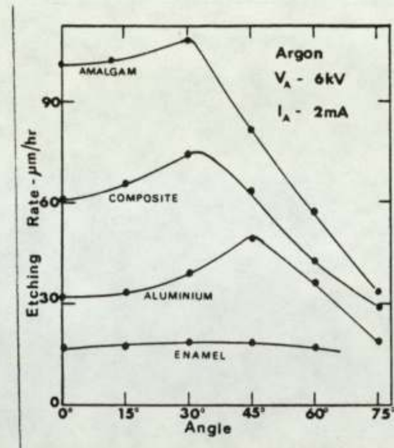

Fig.5 Etching rates vs angle for various materials

about 45° for aluminium which is in good agreement with Lee[15] and the rates vary from 16µm hr^{-1} for enamel to 100µm hr^{-1} for amalgam.

4. Discussion

The results of this work have shown that the percentage of multi-charged ions produced by the spherical source is small and similar to that found for the cylindrical source {10}. This work is still in progress and it is hoped to be able to provide a theoretical model to explain the formation of these various ion states. The work on the etching rates has already been used in conjunction with an in-situ ion etching study in a scanning electron microscope which is part of a research programme attempting to explain the failure of dental restorations.

5. References

{1} Glöersen, P.G. J.Vac.Sci.Technol. 12, 28, 1975
{2} Franks, J. Adv. in Electronics and Electron Physics, 47, 1, 1978
{3} McIlraith, A.H. Nature, Lond. 212, 1422, 1966
{4} Fitch, R.K., Ghander, A.M., Rushton, G.J. and Singh, R. Jpn.J.App.Phys.Supp.2. 1, 411, 1974
{5} Franks, J. and Ghander, A.M. Vacuum, 24, 489, 1974
{6} Dhariwal, R.S. and Fitch, R.K. J.Mater.Sci. 12, 1225, 1977
{7} Dhariwal, R.S., Ball, P.C., Marsland, E.A. and Fitch, R.K. Inst.Phys.Conf.Ser.No.38, 3, 151, 1978
{8} Khorrasany, M. and Fitch, R.K. Vacuum, 27, 153, 1977
{9} Fitch, R.K., Khorassany, M. and Mawlood, T.N. Proc.VIIth Int.Vac.Congr. 1, 285, 1977
{10} Clark, R.B., Fitch, R.K., Ghander, A.M. and Smith, A.G. J.Phys.E. 7, 566, 1974
{11} Kornelsen, E.V. J.Vac.Sci.Technol. 13, 716, 1976
{12} Abe, N., Yamamoto, T., Oda, K., and Kawanishi, M. Jpn.J.App.Phys. 19, 149, 1980
{13} Wilson, R.G. and Brewer, G.R. 'Ion beams', John Wiley, New York, 333, 1973
{14} Al-Rawi, H.Y. M.Sc. Thesis, University of Aston in Birmingham, 1979
{15} Lee, R.E. J.Vac.Sci.Technol. 16, 164, 1979

Vacuum/volume 31/pages 19 to 21. 0042-207X/81/0101-0019$02.00/0
Pergamon Press Ltd, 1981/Printed in Great Britain

Temperature limitation of a saddle field ion source

R K Fitch, S N Ghafouri and E A Mahmood, *Department of Physics, University of Aston in Birmingham, Birmingham, B4 7ET, UK*

received 8 August 1980; in revised form 18 September 1980

It has been found that the fine beam saddle field ion source will not operate satisfactorily if the temperatures of the cathode and anode exceed 265 ± 15°C and 460 ± 20°C respectively. Experiments have shown that the most likely cause of failure is due to electrical breakdown of the Sintox alumina insulators at high temperatures.*

During the last four or five years there has been a considerable amount of research in this laboratory into the properties[1,2] and applications[3,4] of the fine beam saddle field ion source described by Ghander and Franks[5] and manufactured by Ion Tech Ltd, Teddington. This source is a cold cathode electrostatic device which can operate at low pressures due to the very long paths attained by the electrons oscillating through a circular anode positioned between two aluminium cathodes. The ions are self-extracted through a small hole in the cathode producing an ion beam of typically 60 μA of energy 4.5 keV at a chamber pressure of 2×10^{-5} mbar when the source is operated with argon at an anode voltage, V_A, of 6 kV and an anode current, I_A, of 2 mA.

In one particular application[4] this source has been incorporated into the specimen stage of a Vacuum Generators 'Miniscan' scanning electron microscope for *in situ* ion etching of various dental materials to study the margin between the tooth enamel and the amalgam or composite filling. This work has now been in progress for about four years and the source has been quite reliable apart from the need to remove it for cleaning after about 40 hours of operation due to contamination of the insulators from the aluminium sputtered from the cathodes. Recently, however, when the source was replaced after a routine cleaning a leakage resistance of about 1 MΩ developed between the anode and cathode after about an hour and since the normal dc impedance of the source is in the region of 3 MΩ the discharge ceased. Repeated cleaning of the source and replacement of the ceramic insulators failed to correct this and the source continued to breakdown after about one hour. The internal dimensions of the source, particularly the anode–cathode separation, were checked and compared with another source and were found to be correct. The source was then mounted in another vacuum system and it operated normally for many hours. It was therefore assumed that some fault had developed in some part of the electron microscope such as breakdown of the diffusion pump fluid (Santovac 5), a leak in the specimen chamber or a fault in the gas inlet system. However all possible causes of trouble were checked including replacement of the diffusion pump fluid but the source continued to fail after only one hour of operation.

Previous work in this laboratory[6] had shown that if the cathode of the source is water cooled there is no improvement in the characteristics and operation of the source apart from the fact that the source is more stable and can be operated at higher values of V_A even up to 12 kV. It had therefore been assumed during the previous two years that the risk of a water leak in the electron microscope was not worth the marginal advantage of using a water cooled source. Finally, in an attempt to overcome this problem of breakdown a water cooling jacket was added to the source and fitted into the specimen stage of the microscope, and it was found that the source operated quite normally for several hours. Thus the breakdown of the source must have been due to some temperature effect and the purpose of this letter is to report briefly the investigations that have taken place to explain this effect.

A copper–constantan thermocouple was attached to the cathode of the source in the electron microscope and the cathode temperature was recorded as a function of time for various source powers. The results of these measurements are shown in Figure 1. Curve A shows that with the source operating at 8.4 W ($V_A = 6$ kV, $I_A = 1.4$ mA) the cathode temperature increased quickly and eventually reached a maximum of 215°C after about 100 minutes and the source continued to operate satisfactorily for several hours. Curve B shows the temperature increasing as the source power was increased from 5 W and it operated quite satisfactorily until the power had reached 12 W (6 kV, 2 mA) when electrical breakdown of the source was observed. The latter condition was, of course, the same as that used in the microscope when the source first failed after one hour and the results shown in Curve B indicate that the original condition was quite critically dependent upon the temperature. Curve C shows that the cathode only reached 40°C with a source power of 12 W when water cooling was employed.

The source was then operated in the other vacuum system and the mechanical supports to the source were varied in order

* The authors would like to point out that the failure of this source at high temperatures has also been observed by G W Lewis, J S Colligon and N J Nobes, *J Mater Sci*, **15**, 1980, 681.

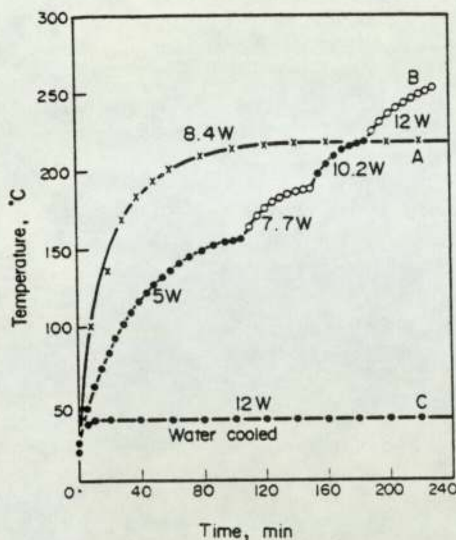

re 1. Variation of cathode temperature with time for (a) stable ration at 8.4 W, (b) increase of power from 5 W to eventual kdown at 12 W and (c) stable operation at 12 W using water ling.

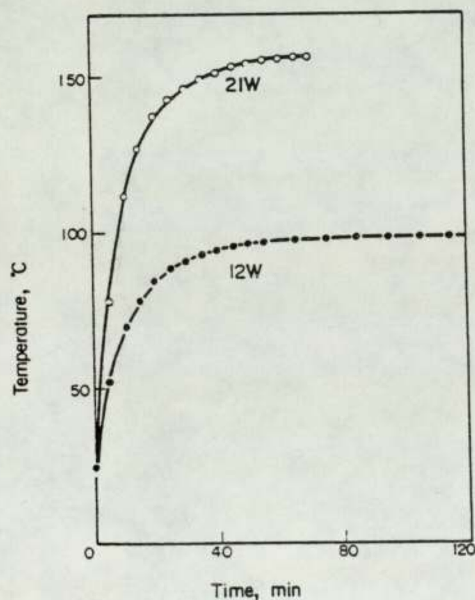

gure 2. Variation of cathode temperature with time for stable eration at 12 W and 21 W using a good heat sink without water oling.

change the heat 'sink' on the source. Figure 2 shows the sults of two such experiments using a "good" heat sink for the rmal source power of 12 W and a much higher one of 21 W. both cases the cathode reached temperatures of 100°C and 5°C respectively, and no breakdown occurred. It was, wever, possible to adjust the heat sink for a power of 12 W d still achieve breakdown after one hour as found in the ctron microscope.

An additional thermocouple was then attached to the anode d, using the heat sink that had previously given breakdown 12 W, the temperatures of the cathode and anode were corded as shown in Figure 3. Breakdown occurred after one our when the anode had reached 460°C and the cathode 275°C. his demonstrated that the critical maximum operating

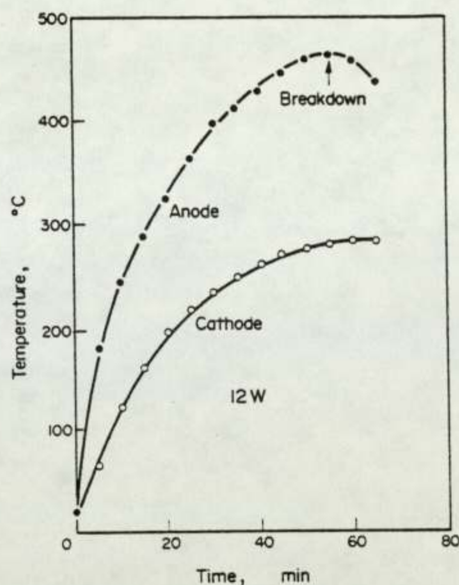

Figure 3. Variation of cathode and anode temperature at 12 W using a poor heat sink showing breakdown occurring after 1 hour when the anode had reached 460°C.

temperatures of the cathode and anode are 265 ± 15°C and 460 ± 20°C.

It seemed unlikely that these effects could be explained by breakdown of the diffusion pump fluid by ion or electron bombardment as 'Santovac 5' was used in the microscope and 'Silicone 704' in the other vacuum system. Thus breakdown across the ceramic insulators was suspected. In order to demonstrate this, one of the insulators was mounted in a vacuum system and electrical leads were connected to its inner and outer surfaces. The insulators were tested at room temperature under vacuum with a dc test meter at 1 kV and the resistance was found to be greater than 2×10^9 Ω. The insulator was then indirectly heated by a molybdenum boat and the temperature of the insulator was measured by means of a thermocouple attached to its surface. It was found that the resistance remained greater than 2×10^9 Ω until the temperature had reached about 500°C when its resistance fell to about 10^7 Ω. When the insulator was allowed to cool its resistance recovered to its original value of more than 2×10^9 Ω.

The temperature of 500°C is, of course, somewhat higher than the anode temperature of 460°C at which the source breaks down but the conditions in the source and in the test procedure with the ceramics are far from identical. In the test procedure the applied voltage is much less and is free of the additional problems of ion bombardment.

The water cooled source has been operated for up to 70 h without any cleaning being necessary. It is possible that this time could be extended by incorporating a suitable cylindrical shield to capture the sputtered material and thus protect the insulator. This shield would also suppress any discharge in the region of the insulator[7]. However, it should be noted that after operating the source for a long time it is usually necessary to replace the aluminium cathodes, as the apertures become widened by ion bombardment resulting in a change in the source characteristics.

This work has shown quite clearly that the source will not operate satisfactorily if the anode reaches a temperature of

about 460°C. The most likely cause of failure appears to be electrical breakdown across the insulators which are glazed 'Sintox' alumina. This remark is supported by the data given by Espe[8], which shows that the resistivity of glazed ceramic materials decreases with increase of temperature and can be as low as 10^5 Ω cm at 350°C.

It still remains an unsolved problem as to why this source has been successfully operated in the electron microscope for several years without any problem. It can only be assumed that at the time of the original failure some small adjustment may have been made to the mounting assembly of the source which reduced its effectiveness as a heat 'sink', resulting in a small increase of the anode temperature above the critical value of 460°C.

Two of the authors of this letter, S N Ghafouri and E A Mahmood, would like to thank the Ministry of Education in Iraq for their financial support during the course of this work.

References

[1] M Khorassany and R K Fitch, *Vacuum*, **27**, 1977, 159.
[2] R K Fitch, M Khorassany and T N Mawlood, Proc. 7th Int. Vacuum Congress, Vienna, p 285 (1977).
[3] R S Dhariwal and R K Fitch, *J. Mater Sci*, **12**, 1977, 1225.
[4] R S Dhariwal, R K Fitch, C L B Lavelle and G A Johnson, *J Anat*, **122**, 1976, 133.
[5] J Franks and A M Ghander, *Vacuum*, **24**, 1974, 489.
[6] E A Mahmood, M.Sc. Thesis, University of Aston in Birmingham, 1978.
[7] L Holland, *Vacuum Deposition of Thin Films*. Chapman and Hall, London, p 90 (1966).
[8] W Espe, *Materials of High Vacuum Technology*. Pergamon Press, Oxford, Vol. 2, p 478 (1968).

Measurement of the sputtering yield for Ar^{+} and Ar^{2+} ions on gold films

R.K.FITCH and E.A.MAHMOUD*

Department of Physics, University of Aston
in Birmingham, Birmingham B4 7ET, U.K.

ABSTRACT

The sputtering yield for gold has been measured for the Argon Ions, Ar^{+} and Ar^{2+}. The ions were produced by a fine beam saddle field ion source and a magnetic analyser was used to separate the ions which were focussed by an Einzel lens onto an evaporated film of gold on a glass substrate. It was found that at normal incidence the yield increased from about 4 to 11 atoms per ion as the ion energy increased from 3 to 13.5 keV, but the yield was independent of the charge state of the ions.

1) Introduction

The process of sputter ion etching for the controlled removal of material from surfaces is now a widely accepted technique in many branches of physics and materials science. In some applications for instance, fabrications of integrated circuits (Melliar-Smith)[1], it is necessary to be able to predict the actual amount of material removed by a given ion dose. This requires a knowledge of the sputtering yield and this varies with the nature and energy of the ions, angle of incidence and material being bombarded, (Carter and Colligon)[2]. However there does not appear to be very much published work on the influence of the charge state of the ions. Wolsky and Zdanuk [3] studied this

*Supported by the Ministry of Education, Baghdad, Iraq.

effect and measured the yields from silicon for Ar^{+} and Ar^{2+} at energies up to 800eV. They found that for ions of the same energy the yields for Ar^{2+} were four times those of Ar^{+}, whereas it might be expected that they would be the same for simple momentum considerations. On the other hand, Weiss et al[4] found that the yields for neutral species of helium and hydrogen were larger than those of the corresponding singly charged ions.

The purpose of this paper is therefore to report the results of an investigation in which the yield has been measured for argon ions on gold films using the single and double charged states Ar^{+} and Ar^{2+}.

2) Description of experimental techniques

A schematic diagram of the experimental arrangement is shown in Figure 1 in which the complete system was pumped by a conventional high vacuum system, using "Santovac 5" fluid in the diffusion pump. The ion source is the fine beam ion source (Franks and Ghander)[5] with an additional water cooling facility to improve the stability, (Mahmoud)[6]. Collimation of the ion beam has also been improved by positioning a small stainless cylinder close to the ion exit aperture. The performance of the source was monitored by the current, I_m, to a flat plate collector at the back of the source. The ions were focussed by an Einzel lens in which the central electrode could be varied from 2 to 4 kV. An electromagnet provides the required field (0 to 0.3T) to separate the ions and a μ-metal shield was placed behind the magnet in order to screen the ion source from the magnetic field. The ion beam is deflected into a Faraday cup positioned at an angle of 7° to the central axis.

A similar arrangement to the above has been used by Fitch et al[7], to study the charge state of the ions for various gases, but a slit of

width 1.4mm was introduced between the magnet polepieces to improve the resolution. The variation of the ion current against magnet current

for argon is shown in Figure 2 for various values of anode voltage, V_A, at a constant anode current I_A of 2mA. It can be seen that the ratio of the peak heights Ar^{2+}/Ar^{+} varies from a few per cent up to about 20% and the position of the peaks shift as the anode voltage increases from 5.3kV to 7.1kV and the corresponding chamber pressure decreases from 10^{-4} to 4×10^{-5} torr.

During the measurement of the sputtering yields the slit was removed to increase the ion current. The ion current to the Faraday cup was then recorded for both Ar^{+} and Ar^{2+} ions, in which a series of apertures of areas varying from 1.0 to $7mm^2$ were positioned in front of the Faraday cup. During these measurements the value of I_A was kept constant at 2mA and V_A was varied from 4 to 9kV. The variation of ion current with area at different values of V_A is shown in Figures 3a and 3b for Ar^{+} and Ar^{2+} respectively.

A gold film evaporated onto a glass substrate was then placed into the same position as the Faraday cup. The film was viewed through a glass window in the vacuum chamber and the time was recorded to sputter the film to expose an etched area which was subsequently measured with an optical microscope. However, because the ion current density was not uniform the time taken was the mean time between the appearance of a small spot and the final sputtered area. Films of thickness varying from 0.05 to 0.3µm were used in order to obtain suitable sputtering times for different ion beam currents and energies. The thickness of the films was measured by the "Tolansky" method, using multiple beam interferometry. Thus knowing the film thickness, sputtering time,

sputtered area and corresponding value of ion current from Figures 3a, or 3b, it was possible to calculate the yield in atoms per ion.

3) Results and discussion

Forty measurements of the yield have been made using 28 gold films of different thickness and the yield for Ar^{+} and Ar^{2+} is shown as a function of ion energy in Figure 4. During each measurement the anode voltage, V_A, was constant and with this source it is known that the ion energy is approximately 0.75 eV_A for Ar^{+} and 1.5 eV_A for Ar^{2+}, (Khorassany and Fitch)[8]. It can be seen that in the energy range studied, 3 to 13.5 keV, the yield increases from about 4 to 11 atoms per ion. The values of the yield for Ar^{+} are in reasonable agreement with those published elsewhere (eg Patterson and Tomlin)[9] although the present values are about 10% higher. This is perhaps not surprising as the main purpose of the present work was to make a comparison of the yields at the same energy using Ar^{+} and Ar^{2+} rather than aim for a precise measurement with Ar^{+} only. Taking into account the uncertainties in measuring the film thickness, sputtered area and ion dose, it is estimated that the uncertainties in the yield were about ±9%. This does not exclude, of course, the possibility of a systematic error that may have been present, for example in measuring the total ion dose.

However, Figure 4 shows that the values of the yield for Ar^{+} and Ar^{2+} follow a reasonably smooth curve over the energy range studied, and the yield is the same for Ar^{+} and Ar^{2+} at a given ion energy. It should, however, be noted that the range of operating voltages of the source were limited from 4 to 9kV and hence the yield could only be measured for Ar^{+} in the energy range 3 to 6.75 keV and for Ar^{2+} in the

range 6 to 13.5 keV. Thus the overlap of measurements for Ar^{+} and Ar^{2+} only occurs in the relatively small range 6 to 6.75 keV.

4) Conclusions

The use of the magnetic analyser has ensured that there was no possibility of any sputtering of the films due to energetic neutrals in the beam. The investigation has shown that the sputtering yield is the same for singly and doubly charged argon ions of the same energy. It is appreciated that the method used is not entirely satisfactory for measuring the absolute yields but it does demonstrate quite clearly that the yield is independent of the charge of the ion. This is not in agreement with the measurements of Wolsky and Zdanuk, but does support their remarks that the yields should be the same if one considers the "momentum transfer" theory for the sputtering process. However, due to the different charge on the ion it may be useful to consider the new theory of sputtering proposed by Pollit et al[10] who suggest that the bombarding species electronically excite the surface atoms of the target.

It is hoped to be able to extend the present work to other bombarding species and targets and to improve its accuracy by applying the technique to thin foils of material.

References

(1) C.M.Melliar-Smith, J.Vac.Sci. and Technol. 13, (1976), 1008.

(2) G.Carter and J.S.Colligon "Ion bombardment of solids". Heinemann London (1968).

(3) S.P.Wolsky and E.J.Zdanuk, Phys.Rev.121, (1961), 374.

(4) A.Weiss, A.Hedlt and W.J.Moore, J.Chem.Phys.29, (1958),7.

(5) J.Franks, and A.M.Ghander. Vacuum 24, (1974), 489.

(6) E.A.Mahmoud, M.Sc., Thesis, University of Aston in Birmingham (1978).

(7) R.K.Fitch, E.Mahmoud and S.N.Ghafouri, Proc. of lVth Int.Conf. on Solid Surfaces and 3rd European Conference on Surface Science, 11, (1980), 1085.

(8) M.Khorassany and R.K.Fitch. Vacuum 27, (1977) 153.

(9) H.Patterson and D.H.Tomlin, Proc.Roy.Soc., A265, (1962), 474.

(10) K.R.Pollit, J.C.Robb and D.W.Thomas. Nature 272, (1978), 436.

Captions for the Figures

Figure 1. Schematic diagram of the experimental arrangement showing the ion source, einzel lens, magnetic analyser and ion detector.

Figure 2. Variation of the ion current with magnet current for different values of anode voltage.

Figure 3a. Variation of the current for Ar^{+} with area for different anode voltages.

Figure 3b. Variation of the current for Ar^{2+} with area for different anode voltages.

Figure 4. The sputtering yield for the argon ions Ar^{+} and Ar^{2+} as a function of ion energy.

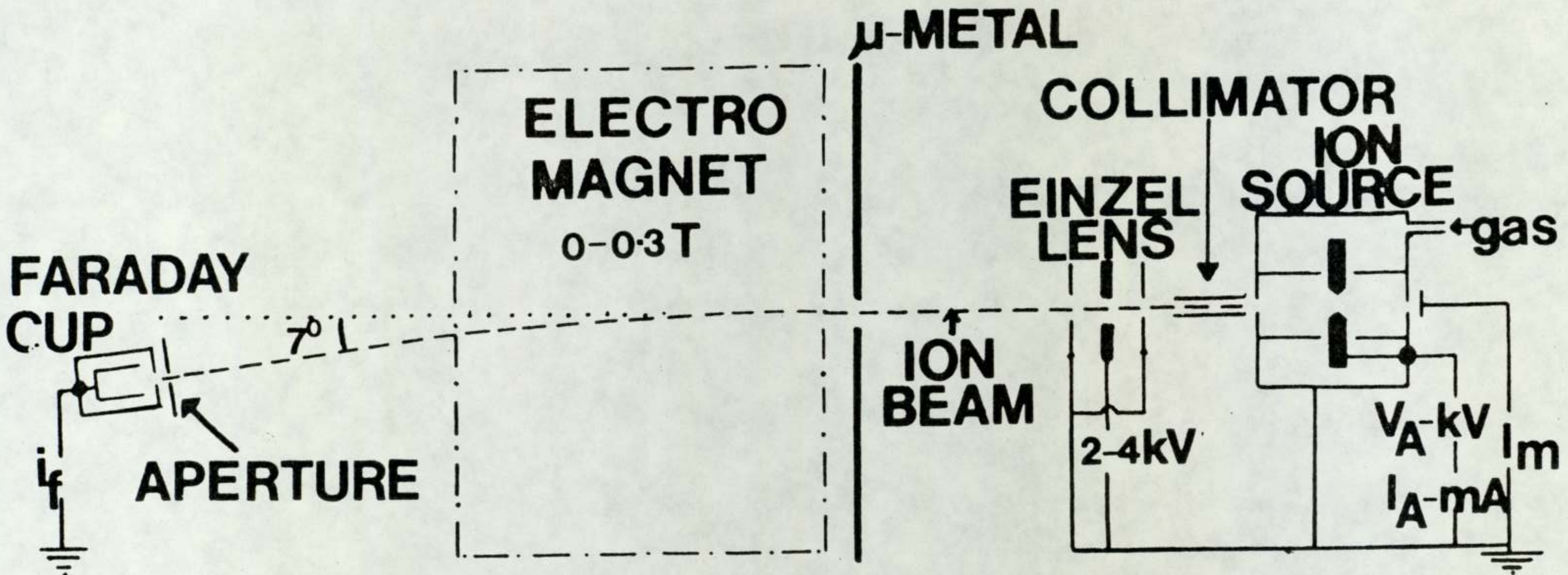

FIGURE 1

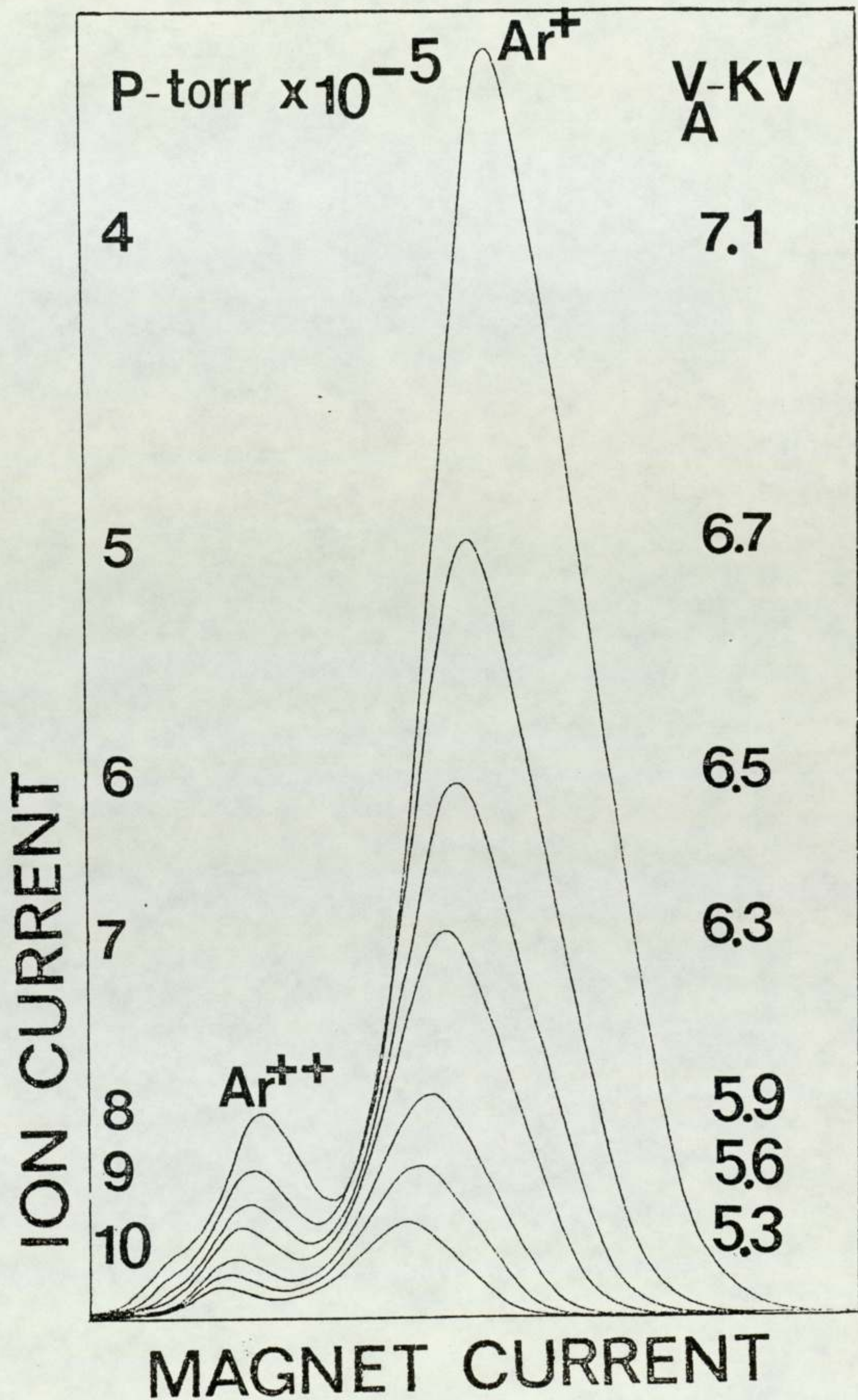

FIGURE 2

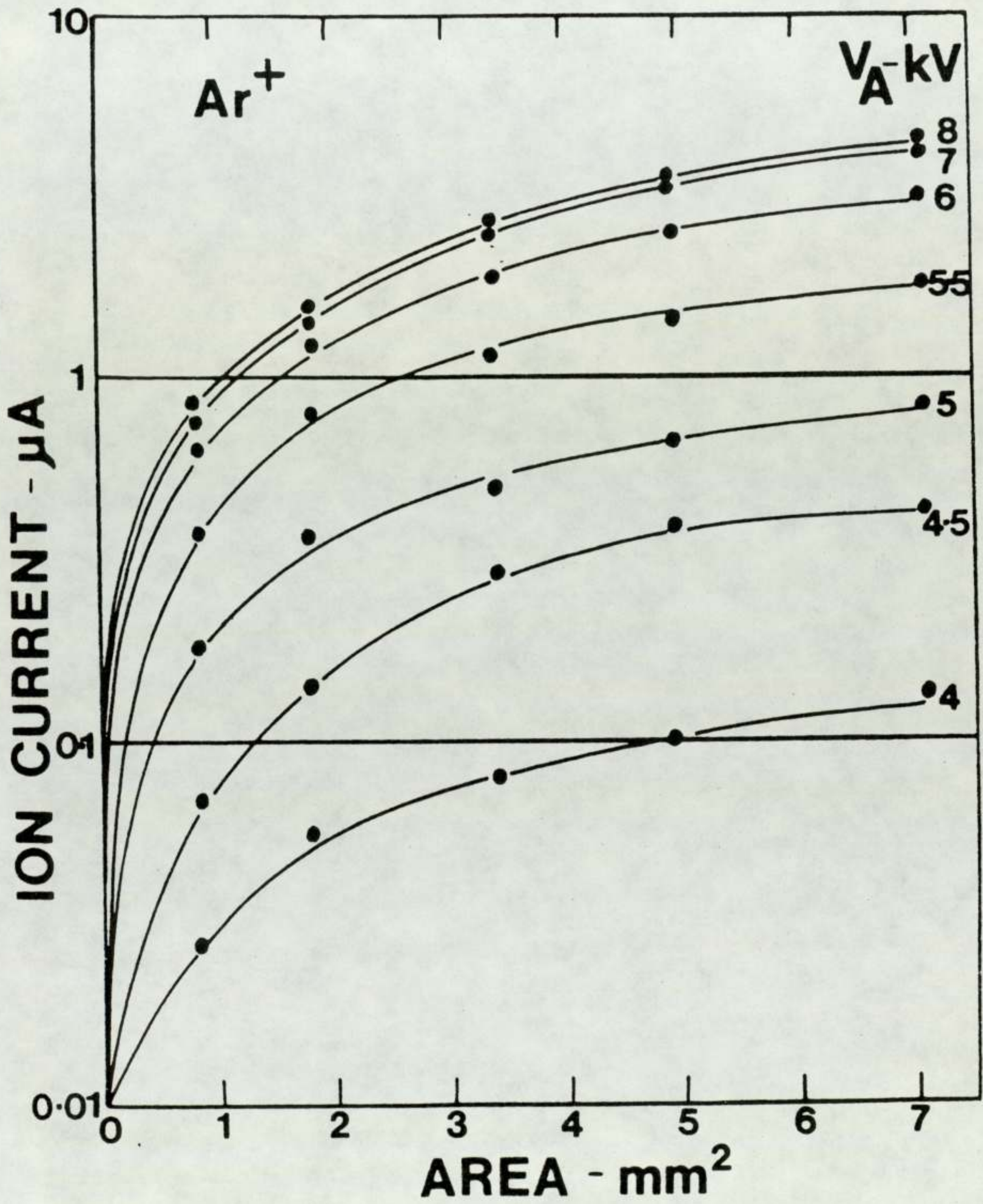

FIGURE 3a

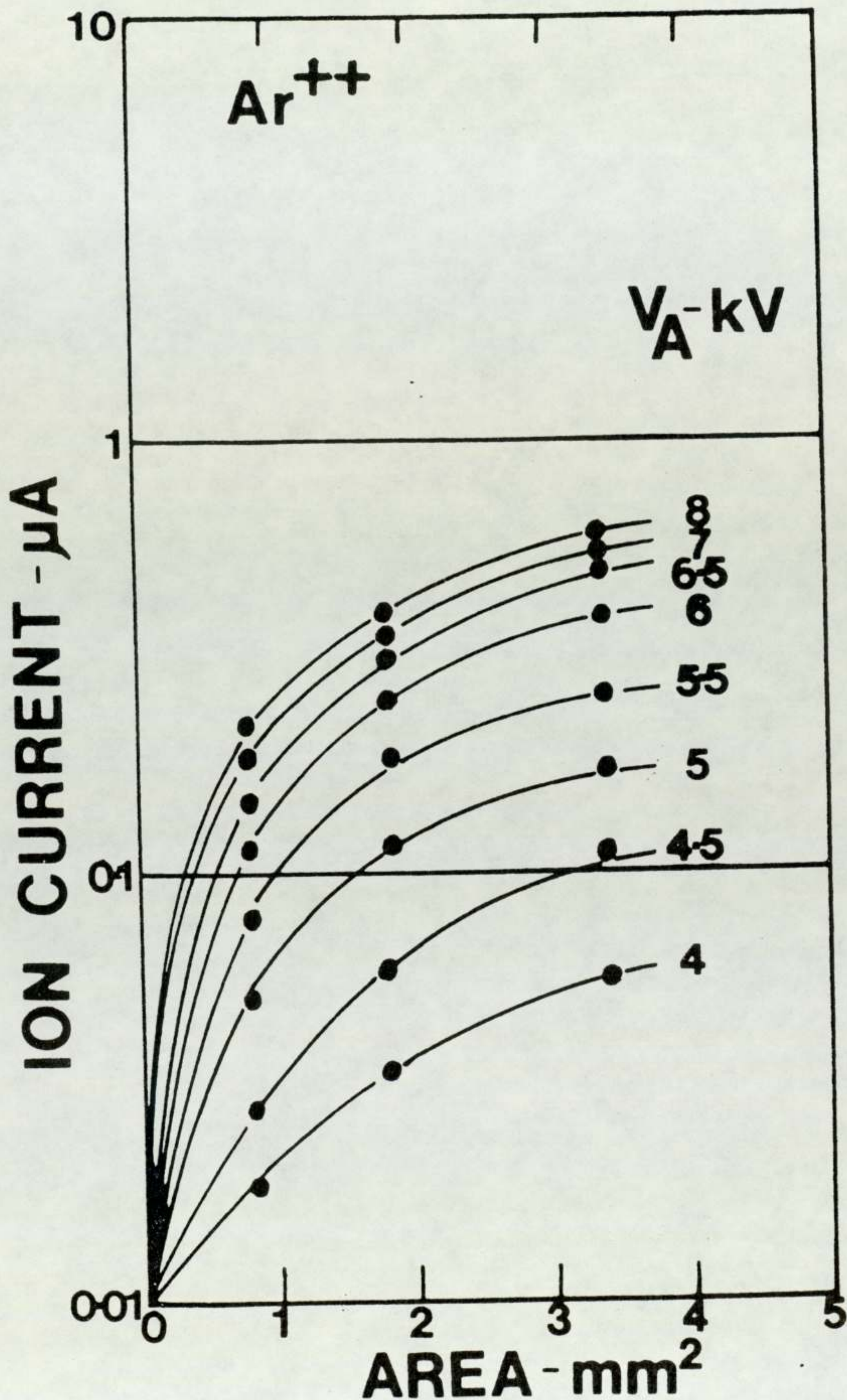

FIGURE 3b

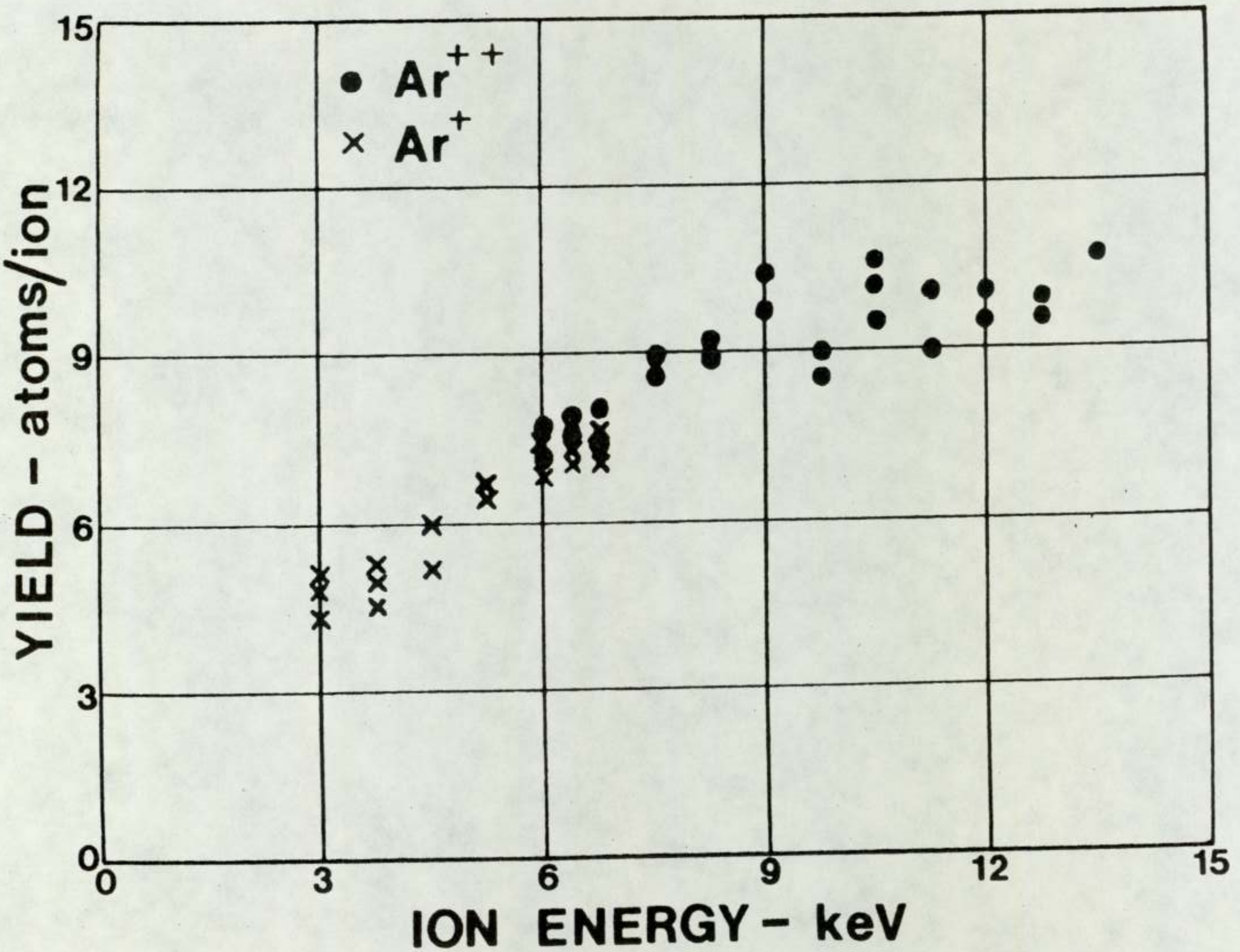

FIGURE 4